APPLICATION OF THE HOMOGENEOUS OXIDATION OF ALKANES AND THE SYNTHESIS AND CHARACTERIZATION OF METAL COMPLEXES OF A LINKED ARYLOXIDE

By

BENJAMIN W. F. GORDON

A DISSERTATION PRESENTED TO THE GRADUATE SCHOOL
OF THE UNIVERSITY OF FLORIDA IN PARTIAL FULFILLMENT
OF THE REQUIREMENTS FOR THE DEGREE OF
DOCTOR OF PHILOSOPHY

UNIVERSITY OF FLORIDA

1999

Dedicated to my parents, Frank and Suzanne Gordon.

ACKNOWLEDGEMENTS

Several people deserve mention for providing me with direction, and support during my time at the University of Florida. The most important person is Dr. Russell S. Drago, whose relationship with me went beyond mutual academic interests and developed into a friendship. He was a good friend who believed that encouragement was the means to better science and people.

My current advisor, Dr. Michael J. Scott, is a trusted friend and generous person. I feel lucky to have been given the opportunity to work for him. Without that opportunity, I would never have realized my love for organometallic chemistry.

I must also thank the Drago and Scott research groups who's cult of personality made life entertaining. Particular mention should be made of Dr. Edwin Webster and Dr. Maarten Dinger for conversations and advice that proved to be invaluable at times and always insightful. Other individuals worth mentioning are Dr. John Osegovic, Matt Peterson and Nermeen Aboelella. All three people have contributed to my personal and professional life, which is intangible.

Finally I must thank my wife Sheryl Gordon. Four drops of water in a pool of dreams. Already the ripples of uncertainty are fading away to reveal a placid surface of the future. It is a resplendent site. We have dreamed of many things, but the one embodying the most truth is the vision of ourselves striding forward with confidence to embrace the future. That vision is ours.

PREFACE

This dissertation combines two distinct areas of chemistry. The first part, chapters 1-4, covers applications of homogeneous oxidation. This work was performed under the guidance of Russell S. Drago until his death in December 1997 and continued until late 1998.

The second part, chapters 5-6, covers the synthesis and characterization of the metal complexes of a partial calix[n]arene. This work was performed under the guidance of Michael J. Scott from the fall of 1998 until present.

TABLE OF CONTENTS

page

ACKNOWLEDGEMENTS ii

PREFACE iv

LIST OF TABLES ix

LIST OF FIGURES xi

ABSTRACT xv

CHAPTERS

1 INTRODUCING THE HOMOGENEOUS OXIDATION CHEMISTRY OF LIGHTWEIGHT ALKANES 1

Direct Oxidation of Methane 4
Autoxidation 5
Homogeneous Metal Oxo Reactions 10
Trapping Reactive Intermediates 13
Green Catalytic Systems 16
Summary 17

2 MILD ALKANE OXIDATION WITH DIOXYGEN ACTIVATION IN AQUEOUS ACIDIC MEDIA USING A STERICALLY HINDERED RUTHENIUM COMPLEX 18

Introduction 18
Methods 20
Materials 20
Physical Measurements for Catalyst Characterization 20
Synthesis of Compounds 20
Oxidation Procedure 21
Safety Precautions 22
Results and Discussion 22
Hydroxylation of Alkanes in Aqueous Solution 22
Spectral Changes 36

Conclusions 43

3 PEROXY ACID MEDIA AS AN EFFECTIVE TRAP OF TRANSITIONAL PRODUCTS FROM THE MILD OXIDATION OF METHANE 45

Introduction 45
Experimental 49
Materials and Methods 49
Synthesis of Compounds 49
Oxidation Procedure 49
Safety Precautions 50
Results and Discussion 51
Reactions Using Acetic Acid and Acetic Anhydride 51
Reactions Using Propionic Acid and Propionic Anhydride 58
Reactions in Carboxylic Media with O_2 as Oxidant 63
Conclusions 70

4 HOMOGENEOUS SELECTIVE OXIDATION OF ETHANE, PROPANE, BUTANE, ISO-BUTANE AND PENTANE 71

Introduction 71
Experimental 75
Reagents 75
Analyses 75
Oxidation Procedure 76
Safety Precautions 76
Results and Discussion 77
$[Ru(dmp)_2(H_2O)_2](CF_3SO_3)_2$ Catalyzed Oxidation of Selected Alkanes with H_2O_2 77
$[Ru(dmp)_2(H_2O)_2](CF_3SO_3)_2$ Catalyzed Oxidation of Selected Alkanes with $CuCl_2$ and H_2O_2 82
$[Ru(dmp)_2(H_2O)_2](CF_3SO_3)_2$ Catalyzed Oxidation of Propane 87
Temperature Effects on the Oxidation of Propane 90
Conclusions 94

5 LINKED ARYLOXIDES LIGANDS: SYNTHESIS AND CHARACTERIZATION OF ALKALI METAL CLUSTERS OF A PARTIAL CALIX[N]ARENE 95

Introduction 95
Experimental 97
General Procedure 97
Synthesis of Linked Aryloxide Ligands 97
2,6-bis(3-t-butyl-5-methyl-2-hydroxy benzyl)-4-methyl phenol (L) 97
2,6-bis(3,5-di-t-butyl-2-hydroxy benzyl)-4-methyl phenol (L′) 98
Synthesis of Lithium Salts of L and L′ 99

Lithium 2,6-bis(3-t-butyl-5-methyl-2-hydroxy benzyl)-4-methyl phenolate **(1,2)** ... 99
Lithium 2,6-bis(3,5-di-t-butyl-2-hydroxy benzyl)-4-methyl phenolate **(3)** ... 100
Synthesis of Sodium Complexes ... 101
Sodium 2,6-bis(3-t-butyl-5-methyl-2-hydroxy benzyl)-4-methyl phenolate **(4)** ... 101
Sodium 2,6-bis(3,5-di-t-butyl-2-hydroxy benzyl)-4-methyl phenolate **(5)** ... 101
Collection and Reduction of X-ray Diffraction Data ... 102
Results and Discussion ... 103
Synthesis of 2,6-Bis(3-t-Butyl-5-Methyl-2-Hydroxybenzyl)-4-Methyl Phenol and 2,6-Bis(3,5-di-t-Butyl-2-Hydroxybenzyl)-4-Methyl Phenol ... 103
Structure of H_3L and H_3L' ... 104
Synthesis and Structure of the Lithium Salts of L and L′ ... 109
Synthesis and Structure of the Sodium Salts of L and L′ ... 118
Conclusions ... 125

6 SYNTHESIS AND CHARACTERIZATION OF TANTALUM AND NIOBIUM COMPLEXES OF A TRIMER OF LINKED ARYLOXIDES ... 127

Introduction ... 127
Experimental ... 131
General Procedure ... 131
Synthesis of Chloride Structures ... 131
Synthesis of [[2,6-bis(3,5-di-t-butyl-2-hydroxy benzyl)-4-methyl-phenolato]-tantalum dichloride]$_2$ **(1)** ... 131
Alternative synthesis ... 132
Synthesis of [[2,6-bis(3,5-di-t-butyl-2-hydroxy benzyl)-4-methyl-phenolato]-niobium dichloride]$_2$ **(2)** ... 133
Synthesis of pyridine adduct [2,6-bis(3,5-di-t-butyl-2-hydroxy benzyl)-4-methyl phenolato]-tantalum dichloride **(3)** ... 133
Synthesis of Dimethyl Structures ... 134
Synthesis of [[2,6-bis(3,5-di-tbutyl-2-hydroxy benzyl)-4-methyl phenolato]-dimethyl-tantalum]$_2$ **(4)** ... 134
Synthesis of [[2,6-bis(3,5-di-tbutyl-2-hydroxy benzyl)-4-methyl phenolato]-dimethyl-niobium]$_2$ **(5)** ... 135
Synthesis of [2,6-bis(3,5-di-tbutyl-2-hydroxy benzyl)-4-methyl phenolato]-dibenzyl- tantalum **(6)** ... 135
Results and Discussion ... 136
Synthesis of Ta, Nb Chloride Complexes ... 136
Synthesis of Ta, Nb Dimethyl Complexes ... 146
Synthesis of Tantalum Benzyl Complex ... 148
Conclusions ... 153

LIST OF REFERENCES 155

BIOGRAPHICAL SKETCH 161

LIST OF TABLES

Table page

1-1 Selected Bond Dissociation Energies. 3

1-2 Selected initiators for autoxidation. 7

2-1 Alkane oxidations using O_2 and $Ru(dmp)_2(H_2O)_2[CF_3SO_3]_2$ in aqueous acidic media. 25

2-2 Alkane oxidations using O_2 and $Ru(dmp)_2(H_2O)_2[PF_6]_2$ in aqueous acidic media. 25

2-3 SUR screen reactions for methane oxidation using O_2. 26

3-1. Screen reactions of **1** with methane in acetic acid/anhydride mixed media. 52

3-2. Oxidation of **1** with methane in acetic acid/anhydride. 54

3-3 The oxidation of methane in propionic acid/propionic anhydride[a] 62

3-4 The oxidation of methane in the propionic acid/propionic ahydride: system adjusted for decomposition of perpropionic acid. 62

3-5 Oxidation of methane in acetic acid and anhydride using O_2. 67

3-6 Oxidation of methane in propionic acid and anhydride using O_2. 68

4-1 Oxidation of C_2-C_5 alkanes using **1** with H_2O_2. 78

4-2 Oxidation of C_2-C_5 alkanes using **1** with H_2O_2 in the presence of $CuCl_2$. 83

5-1 Crystallographic and Selected Parameters for 2,6-bis(3-*t*-butyl-5-methyl-2-hydroxy benzyl)-4-methyl phenol (H_3**L**) and 2,6-bis(3,5-di-*t*-butyl-2-hydroxy benzyl)-4-methyl phenol (H_3**L′**). 105

5-2 Selected Hydrogen Bonding for 2,6-bis(3-*t*-butyl-5-methyl-2-hydroxy benzyl)-4-methyl phenol (H_3**L**) and 2,6-bis(3,5-di-*t*-butyl-2-hydroxy benzyl)-4-methyl phenol (H_3**L′**). 108

5-3 Crystallographic and selected parameters for $Li_3L(THF)_4$ (**1**), $Li_6L_2(THF)_2$ (**2**), $Li_6L'_2(CH_2Cl_2)_2$ (**3**). 110

5-4 Selected Bond Distances (Å) and Angles (°) for $Li_3L(THF)_4$ (**1**), $Li_6L_2(THF)_2$ (**2**), $Li_6L'_2(CH_2Cl_2)_2$ (**3**). 111

5-5 Crystallographic and selected parameters for $Na_6L_2(Me_2CO)_4$ (**4**), $[Na_6L'_2(CH_2Cl_2)_3]_x$ (**5**). 120

5-6 Selected Bond distances (Å) and Angles (°) for $Na_6L_2(Me_2CO)_4$ (**4**), $[Na_6L'_2(CH_2Cl_2)_3]_x$ (**5**). 121

6-1 Crystallographic and selected parameters for $L'_2Ta_2Cl_4$ (**1**), $L'_2Nb_2Cl_4$ (**2**), and $L'TaCl_2(py)$ (**3**). 139

6-2 Selected bond distances (Å) and angles (°) for $L'_2Ta_2Cl_4$ (**1**), $L'_2Nb_2Cl_4$ (**2**), and $L'TaCl_2(py)$ (**3**). 140

6-3 Crystallographic and selected parameters for $L'Ta(CH_2Ph)_2$ (**6**). 150

6-4 Selected bond distances (Å) and angles (°) for $L'Ta(CH_2Ph)_2$ (**6**). 151

LIST OF FIGURES

Figure page

1-1 Simplified molecular orbital diagrams for dioxygen and methane with graphical orbital representations........2

1-2 A general scheme describing the initiation, propagation, and termination steps of a simplified autoxidation of a hydrocarbon........6

1-3 Selected steps from the proposed mechanism of the Amoco Mid-Century process........9

1-4 Modes of dioxygen activation and metal oxo formation with the corresponding class designation........12

1-5 Reaction diagram for the product cascade of methane........14

1-6 Schematic diagram of 2,9-dimethyl-1,10-phenanthroline and $Ru(dmp)_2(H_2O)_2^{2+}$........17

2-1 Trends in the effect of counter ion on the distribution of primary and secondary oxidation products of methane, propane, and cyclohexane at pH 1 for complexes **1** and **2**........26

2-2 Product distribution for the oxidation of methane using 5 x 10^{-5} mol $[Ru(dmp)_2(H_2O)_2](CF_3SO_3)_2$ at pH 1 in the presence of 1 mol equivalent H_2O_2 at 70 °C........29

2-3 Product distribution for the oxidation of propane using 5 x 10^{-5} mol $[Ru(dmp)_2(H_2O)_2](CF_3SO_3)_2$ at pH 1 in the presence of 1 mol equivalent H_2O_2 at 70 °C........30

2-4 Oxidation of methane in water pH = 1 using 5 x 10^{-5} mol $[Ru(dmp)_2(H_2O)_2](CF_3SO_3)_2$ at 70 °C; typical catalyst turnovers over 24 hours........31

2-5 Cyclic voltamogram of 2.4 x 10^{-3} M $[Ru^{II}(dmp)_2(H_2O)_2](CF_3SO_3)_2$ in 0.1 M $LiClO_4$ at pH 7........33

2-6 Porbait plot [29]of the potentials for: (a) O_2; (b) $Ru^{II}(dmp)_2^{2+}$; (c) $Ru^{IV}(dmp)_2^{2+}$; (d) H_2O_2. 35

2.7 UV-VIS spectra of 4.7 x 10^{-5} M $[Ru^{II}(dmp)_2(H_2O)_2](CF_3SO_3)_2$ in H_2O at 25 °C and pH 7. 37

2-8 UV-VIS spectra of 4.7 x 10^{-5} M $[Ru^{II}(dmp)_2(H_2O)_2](CF_3SO_3)_2$ in H_2O at 70 °C and pH 1. 38

2-9 Frontier orbital splitting diagrams with the aid of the angular overlap model (AOM) for *cis*-$Ru(dmp)_2(H_2O)_2^{2+}$ and *cis*-$Ru(dmp)_2(O)(OH)^{2+}$ [26]. 40

2-10 Proposed catalytic cycle for the O_2 oxidation of alkanes by $Ru(dmp)_2^{2+}$ in aqueous media. 42

3-1 Mass balance of methanol trap and peroxyacetic acid formation for acetic acid/anhydride with H_2O_2. 56

3-2 Product cascade from successive hydrogen atom abstraction from the parent d^4-methane substrate. 59

3-3 Effect of temperature on methane oxidation in propionic acid/anhydride. 64

3-4 Effect of time on methane oxidation in propionic acid/anhydride. 65

3-5 Lifetime of methane oxidation using **1** in propionic anhydride. 69

4-1 Schematic drawing depicting possible steric hindrance as the substrate approaches the active site of $Ru(dmp)_2(H_2O)_2^{2+}$. 71

4-2 Product distribution for reactions of **1** with selected alkanes. 81

4-3 Product distribution of reactions of **1** with selected alkanes in the presence of 1 mol equivalent of $CuCl_2$. 85

4-4 Oxidation of propane with *cis*-$[Ru(dmp)_2(H_2O)_2](CF_3SO_3)_2$ using H_2O_2 at varying temperatures. 89

4-5 Oxidation of propane with *cis*-$[Ru(dmp)_2(H_2O)_2](CF_3SO_3)_2$ and 1 mol equivalent of $CuCl_2$ using H_2O_2 at varying temperatures. 91

4-6 Oxidation of propane with *cis*-$[Ru(dmp)_2(H_2O)_2](CF_3SO_3)_2$ at varying equivalents of $CuCl_2$ using H_2O_2. 93

5-1 Basic building unit of calix[n]arenes and a simple model depicting a cavity or bowl. 95

5-2 Structure of the Koebner trimer 96

5-3 Numbering scheme for 2,6-bis(3-t-butyl-5-methyl-2-hydroxy benzyl)-4-methyl phenol (L) 98

5-4 Numbering scheme for 2,6-bis(3,5-di-t-butyl-2-hydroxy benzyl)-4-methyl phenol (L′). 99

5-5 ORTEP diagrams of H_3L and H_3L' showing 30% probability ellipsoids and atom labeling scheme 107

5-6 ORTEP diagram of $Li_3L(THF)_4$ (**1**) showing 30% probability ellipsoids and atom labeling scheme 113

5-7 ORTEP diagram of $Li_6L_2(THF)_2$ (**2**) showing 30% probability ellipsoids and atom labeling scheme 115

5-8 ORTEP diagram of $Li_6L'_2(CH_2Cl_2)_2$ (**3**) showing 30% probability ellipsoids and atom labeling scheme 116

5-9 ORTEP diagram of $Na_6L_2(Me_2CO)_4$ (**4**) showing 30% probability ellipsoids and atom labeling scheme 123

5-10 ORTEP diagram of $[Na_6L'_2(CH_2Cl_2)_3]_x$ (**5**) showing 30% probability ellipsoids and atom labeling scheme 124

6-1 Schematic diagram of a hypothetical metal complex of a calix[4]arene and representative examples [58, 61] 129

6-2 Schematic diagram of 2,6-bis(3,5-di-t-butyl-2-hydroxy benzyl)-4-methyl phenol (L′). 129

6-3 Schematic diagram of (a) $Ta(OC_6H_3Bu^t\text{-}2,6)(=CHSiMe_3)(CH_2SiMe_3)$ and (b) $Ta(OC_6H_3Ph_2\text{-}2,6)_3(CH_2SiMe_3)_2$ (c) $Ta(OC_6H_3Me_2\text{-}2,6)(CH_2C_6H_5)_3$. 130

6-4 Schematic diagram of the basic structure of dimethyl and dialkyl complexes. 132

6-5 ORTEP diagram of $L'_2Ta_2Cl_4$ (**1**) showing 30% probability ellipsoids and the atom labelling scheme 138

6-6 ^1H NMR (300 MHz) spectrum of $L'_2Ta_2Cl_4$ (**1**) in $CDCl_3$ 142

6-7 ORTEP diagram of $L'TaCl_2(py)$ (**3**) showing 30% probability ellipsoids and the atom labelling scheme 144

6-8 ^1H NMR (300 MHz) spectrum of $L'TaCl_2(py)$ (**3**) in CD_2Cl_2 146

6-9 ^{1}H NMR (300 MHz) spectrum of $L'_2Ta_2Me_4$ (**4**) in CD_2Cl_2. 148

6-10 ORTEP diagram of $L'Ta(CH_2Ph)_2$ (**6**) showing 30% probability ellipsoids and the atom labelling scheme. 152

Abstract of Dissertation Presented to the Graduate School
of the University of Florida in Partial Fulfillment of the
Requirements for the Degree of Doctor of Philosophy

APPLICATION OF THE HOMOGENEOUS OXIDATION OF ALKANES AND THE SYNTHESIS AND CHARACTERIZATION OF METAL COMPLEXES OF A LINKED ARYLOXIDE

By

Benjamin W. F. Gordon

August 1999

Chairman: Dr. Michael J. Scott
Major Department: Chemistry

Methane is the main component of natural gas, largely left behind due to cost of transportation. There are vast stores of natural gas outweighing the known reserves of liquid petroleum. A chemical process by which methane can be transformed into a usable transportable product is very important. The selective transformation of methane into a transportable product, such as methanol or formaldehyde, would be a large step forward in utilizing a vast resource. Research on transforming methane selectively has been met with several obstacles based on poor conversion and selectivity.

Several methods exist for transforming methane to methanol or formaldehyde through heterogeneous metal catalyzed oxidation. Currently, these metal catalyzed processes are energy intensive and result in low conversion and selectivity. Methanol, the desired product, tends to react preferentially. In many cases, methanol is transformed to another product at a fast rate before recovery. This work describes new techniques for preventing the over oxidation using a homogeneous catalyst system under mild temperature conditions and employing solvents that react with methanol. The solvent effectively removes methanol in a reversible process protecting it from further oxidation. The selective oxidation of higher weight alkanes, such as propane and butane, is also discussed where unusual primary carbon selectivity is observed.

The transition metal atoms, tantalum and niobium, have received attention for the interesting chemical reactions, such as metathesis and living polymerization, that they are known to mediate. Aryloxide complexes of these metals undergo unusual chemical transformations especially in the presence of bulky ligand substituents. This work describes the synthesis and characterization of tantalum and niobium complexes of a linked aryloxide ligand. The metal complexes of this ligand are unusual and this dissertation provides the foundation for important future studies of the complexes of linked aryloxides. This is an important contribution to the knowledge of organometallic chemistry.

CHAPTER 1
INTRODUCING HOMOGENEOUS OXIDATION OF LIGHTWEIGHT ALKANES

This chapter introduces an area of research that can be categorized as the homogeneous oxidation of lightweight alkanes by metal oxo complexes, a subclass of a more general area of chemistry encompassing the reactions of high valent metal complexes. The work in chapters 2, 3, and 4 will narrow the concepts introduced here and treat alkane oxidation chemistry in detail as it relates to homogeneous oxidation, entrapment of oxidative intermediates, and the incorporation of oxidants such as dioxygen and hydrogen peroxide into the catalytic process.

Before becoming entrenched in the minutiae of a complex methodology of chemistry, it is worthwhile to step back to take a diffuse look at oxidation chemistry and discuss some physical aspects of methane and dioxygen. The interaction of these two molecules is the simplest case of an alkane interacting with dioxygen but has given birth to an array of complex chemical reactions, some of which are catalytic. These reactions are important in a modern industrial world where methane, in an oxidized form, is a lucrative commodity. This discussion will in turn show how this relationship between methane and dioxygen has resulted in the unique reactivity of homogeneous oxidation.

The reaction of an alkane with molecular oxygen is synonymous with radicals no matter the reaction pathway that describes the interaction. The interaction can be a formal radical pathway such as hydrogen abstraction or a more concerted pathway such as oxygen atom insertion/transfer. Regardless of the true nature of the bond breaking or forming process for these reactions, somewhere within the reaction pathway there must be an intermediate with radical-like character that participates in the transfer of a hydrogen atom or insertion of an oxygen atom.

Considering the molecular orbital (MO) diagrams for methane and dioxygen, Figure 1-1, it is apparent that we are actually dealing with two stable compounds in their natural state. The simplified MO diagram for dioxygen shows a molecule that has a HOMO with two unpaired electrons in a π^*_g anti-bonding molecular orbital. A Lewis

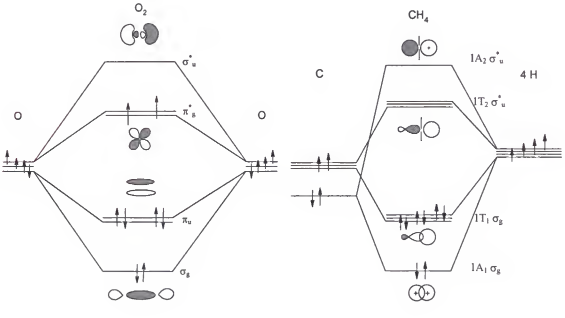

Figure 1-1. Simplified molecular orbital diagrams for dioxygen and methane with graphical orbital representations. Mixing of sp orbitals for dioxygen is considered negligible and has been omitted.

dot structure of dioxygen would reveal a compound that satisfies the octet rule for each atom. The same is true of methane with four σ bonds that are sp^3 hybridized. The molecular orbital coefficients for methane describe a system that consists of a $1t_2$ triply degenerate HOMO, where all electrons are paired, and a lower lying $1a_1$ orbital [1]. This scheme desribes a molecule that is very stable toward spin pairing interactions and has a bond dissociation energy (BDE) of 104 kcal mol^{-1} [2]. Because of the high bond strength, methane is considered to be the most stable alkane and conversely the least reactive for reactions where hydrogen or hydride abstraction takes place. For reference, Table 1-1 shows the BDEs of some related molecules including dihydrogen.

Table 1-1. Selected Bond Dissociation Energies

A:B → $A^{\cdot} + B^{\cdot}$	ΔH = BDE Kcal/mol
H-H	104
CH_3-H	104
C_2H_5-H	98
n-C_3H_7-H	98
i-C_3H_7-H	95
t-C_4H_9-H	91
H_2C=CH-H	104
C_6H_5-H	112
$C_6H_5CH_2$-H	85

It is interesting to note that methane and dihydrogen have the same bond strength, but dihydrogen is much more reactive. This can be directly attributed to the directionality of the σ bond in each molecule. The non-directional bonding in dihydrogen formed by the overlap of 1s orbitals provides easy access to the electrons for reactivity to commence. Conversely, the unidirectional sp^3 hybridized σ bond of methane protects the bond from reaction pathways that non-directional dihydrogen prefer. For example, a quick look through some prominent compilations of transition metal reactions clearly shows that dihyrogen undergoes oxidative addition to transition metals [3]. A simple reaction is the addition of dihydrogen to Vaska's complexes, the most well known of which is *bis*-$(PPhMe_2)_2(CO)IrCl$. This addition is *cis* as determined by NMR and IR spectroscopy. The non-directional character of the hydrogen bond allows dihydrogen to form a relatively strong partial bond in the transition state, assisting the oxidative addition to the transition metal. As pointed out previously, the bonding orbital of methane is unidirectional and usually does not form strong partial bonds in the transition state, leading to decreased reactivity. This also implies that C-C bonds are even less reactive and require an unusual catalytic process for selective cleavage of the C-C bond to take place.

Direct Oxidation of Methane

While methane is reactive, it takes special or harsh conditions for the reactivity to become appreciable. The harsh conditions are fairly obvious, such as the combustion of methane, which with O_2 takes place by lighting a match. Yet methane is quite stable up to 800 °C where it begins to decompose [4]. Processes based on the heightened reactivity of methane at elevated temperatures are numerous. Some representative examples of note are electric arc heating to generate acetylene and aromatics, steam reactions that generate acetylene, ethylene and ethane, and pyrolysis reactions with air or oxygen to produce a methanol intermediate that is fast over oxidized [5]. These processes are interesting in an academic setting but are energy intensive and lack practical application. There is one process, however, that has seen development and involves the direct conversion of methane to a mixture of dihydrogen and carbon monoxide commonly known as syngas, shown in equation 1-1. Using steam, the methane is reformed to syngas. The syngas is then fed into a zeolite catalyst to generate methanol or Fischer-Tropsch parrafins for use as gasoline [6]. The oxidation of methane to syngas is a very energy intensive process but has found use in countries where petroleum resources are scarce, such as South Africa, New Zealand, and Malaysia. Probably the most notable system in use is the Mobil (MTG) process where methanol is introduced into H-ZSM5 producing DME. The DME then dehydrates to olefins which then form C_2-C_{10} hydrocarbons [7]. This process is quite important in developing countries and clearly demonstrates the importance of eliminating the initial step of syngas formation and finding an efficient direct pathway to forming methanol from methane. Other commercial variations of the syngas/Fischer-Tropsch processes deployed around the world are: Mossgas; the Solvay process; Shell (SMDS) and Exxon AGC-21 [8]. Of course the cost to earnings ratio for these processes is fairly poor.

$$CH_{4\,(g)} + H_2O_{(g)} \longrightarrow CO_{(g)} + 3H_{2(g)} \qquad 1\text{-}$$

Autoxidation

How then is selectivity to products such as methanol from methane achieved from a direct route. It is clear that once an oxidation is underway it is usually hard to control propagation and the reaction preferentially oxidizes intermediates until a thermodynamic product is reached. The first semi-selective and mild oxidation was observed with natural oils that deteriorate over time to a mixture of alcohols, ketones, aldehydes, and acids, and was linked to the adsorption of dioxygen [9]. It was also noted that light tends to accelerate the decomposition. This process of decomposition has been studied extensively and is known as autoxidation. The autoxidation is based on a free radical mechanism where some agent (i.e. hv, trace metals) generates an alkyl radical. The free radical reacts with the dioxygen dissolved in the bulk hydrocarbon to form peroxo compounds that propagate the radical chain process outlined in Figure 1-2.

Initiation

$$In_2 \longrightarrow 2\,In\bullet$$

$$In + RH \longrightarrow InH + R\bullet$$

Propogation

$$R\bullet + O_2 \longrightarrow RO_2^\bullet$$

$$RO_2^\bullet + RH \longrightarrow RO_2H + R\bullet$$

Termination

$$R\bullet + RO_2^\bullet \longrightarrow RO_2R$$

Figure 1-2. A general scheme describing the initiation, propagation, and termination steps of a simplified autoxidation of a hydrocarbon.

A characteristic feature of an uncatalyzed autoxidation process is the presence of an induction period. The induction period directly identifies the necessity of having radicals in sufficient concentrations for oxygen to be incorporated into the reaction scheme. The initiation by the direct reaction of a hydrocarbon with dioxygen, Equation 1-2, has been reported but is an unfavorable interaction [10]. However, in the presence of a sufficient amount of free radicals in the system, the addition of oxygen is rapid, almost to the point of being diffusion controlled. The most common mode used to initiate the free radical chain is the addition of peroxides. Due to fascile decomposition at elevated temperatures, peroxides readily generate free radicals and are the most popular additive. Most peroxides decompose readily between 40 and 150 °C, which is considered to be mild and the most common consist of azo compounds, peroxyesters, and alkyl peroxides, Table 1-2.

Table 1-2. Selected initiators for autoxidation.

Compound	Structure	Activation energy (kcal mol^{-1})
Hydrogen peroxide	HOOH	48
t-Butyl hydroperoxide	*t*-BuOOH	42
t-Butyl peroxide	*t*-BuOO*t*-Bu	37
Benzoyl peroxide	PhC(O)OO(O)CPh	30
Acetyl peroxide	$CH_3C(O)OO(O)CCH_3$	31

Another important observation is that the addition of metals significantly shortens or eliminates the induction period. This indicates that metals promote the formation of radicals that are responsible for the reaction with dioxygen to propagate the chain. The most common method in which metals bring about the initiation is through the catalysis of the decomposition of peroxides formed *in situ* or deliberately added to the system. Although peroxides generally decompose at low temperatures, it is desirable to find a catalytic system that can achieve the same results using the same peroxide additive but at substantially reduced temperatures. Only by reducing the temperature is it possible in many systems to prevent the over oxidation of the desired product [11]. This is the mode by which peroxides, stable at lower temperatures, can be homolytically decomposed to generate the reactive peroxide radicals needed to incorporate dioxygen. This mode of initiation is the primary way metals function as autoxidation catalysts.

A relevant example is the oxidation of *p*-xylene to terepthalic acid (TPA) known as the Amoco Mid-Century/TPA process [12]. As shown in Figure 1-3, the metal is indirectly participating in the initial transfer of an electron. The one equivalent change in the oxidation state initiates the free radical process that propagates and branches into traditional autoxidation steps. Bromine plays an important role in the Mid-Century process. The use of an additive such as bromine means the difference between solvent promoted electron transfer and additive promoted ligand transfer.

The addition of bromine to the system, although not needed for the Mid-Centruy process, greatly enhances the production of TPA because of the competition established between electron transfer and ligand transfer as shown in Equations 1-2 and 1-3 [13].

$$R + M^{n+} \longrightarrow R\bullet + M^{(n-1)+} \tag{1-2}$$

$$R + M^{n+}X \longrightarrow RX + M^{(n-1)+} \tag{1-3}$$

The hard and soft acid-base classification has been used to describe the difference between choosing one path over the other. Bromine, being a soft ligand, tends to favor ligand transfer whereas a hard ligand such as acetate tends to favor electron transfer [9]. Referring back to Figure 1-3, cobalt(II) is stable relative to cobalt(III), except when bromine ions are used as an additive. The resultant cobalt(III) species is reduced in a ligand transfer oxidation greatly enhancing the rate of reaction.

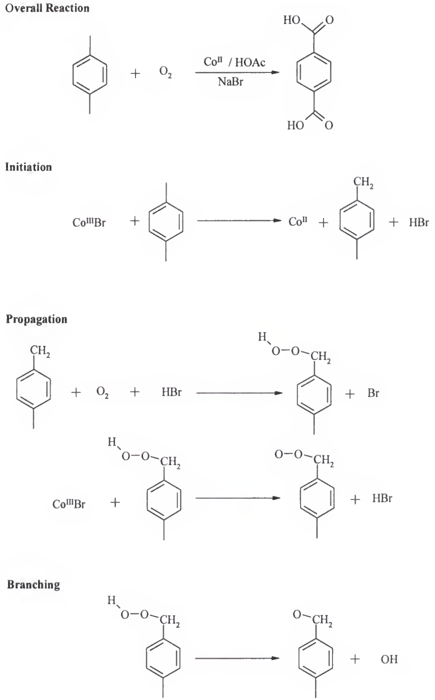

Figure 1-3. Selected steps from the proposed mechanism of the Amoco Mid-Century process. The steps are based on $Co^{(II)}(OAc)_2$ catalyst but are also valid for $Mn^{(II)}$ and $Zn^{(II)}$ analogs. Additives such as MEK and mixed metal systems are treated separately but are known to participate in electron transfer pathways.

The importance of additives in the catalytic process has been demonstrated in this laboratory. In an attempt to refine the TPA process and eliminate the caustic presence of hydrogen bromide, sodium formate was used as a replacement additive. The formate anion readily generates performate, which is a highly unstable peroxy acid that readily decomposes. The decomposition product of performate assumes the role of bromine in this system but is not expected to participate in a ligand transfer reaction. Instead, it participates in an electron transfer reaction thereby initiating the decomposition of the peroxy acid. It is assumed that performate is a victim of decomposition via the cobalt(III)/(II) redox couple inducing the homolysis of the O-O bond. After a 2 hour induction period (the TPA process has an induction period upwards of 12 hours) deactivated cobalt formate along with terephthalic acid in 15% yield precipitates from solution. The exchange of the acetate ligand for formate generates the insoluble cobalt(II) formate, terminating the catalytic cycle. Another interesting apect of this system is the production of 15% terepthalic acid based on starting *p*-xylene. A thousand fold excess of terephthalic acid based on moles of catalyst readily demonstrates the effectiveness of autoxidation and the secondary role the metal catalyst plays in the overall reaction cycle.

Homogeneous Metal Oxo Reactions

Several papers by Russel Drago describe homogeneous metal oxo reactions and have been divided into five general classes [14]. The classification scheme was developed as defined by the role the metal plays in the activation of O_2 and the metal complexes formed.

The first class is O_2 bound to a metal center, Equation 1-4. Metals known to undergo such an interaction characteristically have two oxidation states close in energy and the spin pairing of an electron has a low transitional barrier, implying that the binding O_2 is a reversible process. This is seen with several cobalt(II) salts that exhibit the reversible binding of O_2 [15]. The formation of the O_2 adduct increases the **basicity** and **radical character** of O_2, which then can react with hydrocarbon substrates. This is a very important observation because it defines how the catalytic precursor $Ru(dmp)_2(H_2O)_2^{2+}$ activates O_2 in aqueous media.

$$Co^{II} \quad + \quad O_2 \rightleftharpoons Co^{III}O_2 \qquad (1\text{-}4)$$

The classification of II and III type metal oxo is described by the formation of a high valent metal oxo species that is generated through μ-peroxo formation and peroxide decomposition. Figure 1-4 illustrates the general formation of metal oxo complexes through distinct routes that depend largely on the conditions of the reaction system. The first three classes can first be described as a class I interaction where the initial step is the formation of a superoxide. The superoxide can act as a nucleophile reacting with another metal to form μ-peroxo complexes that homolytically cleave to form two metal oxo complexes, this is class II. The Class II complex is formed directly from dioxygen and is a dioxygenase since both oxidative equivalents are used.

A class III metal oxo forms from peroxides liberating water. The reaction with peroxides can either occur from the direct reaction with O_2 in the presence of a sacrificial reductant, or by the direct addition of peroxides to the system. Class III metal oxo formation is a mono oxygenase where one oxidative equivalent is used in the oxidative

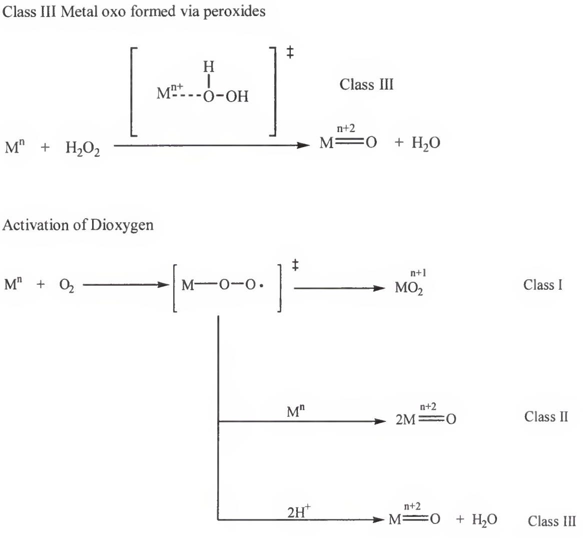

Class III Metal oxo formed via peroxides

Activation of Dioxygen

Figure 1-4. Modes of dioxygen activation and metal oxo formation with the corresponding class designation.

process. Ruthenium and iron TMP complexes have been described by this class, along with some unselective Fenton reactions, where the metal helps generate unselective hydroxyl radicals [16].

The classification IV metal oxo, is generally comprised of Fenton type reactions where metals and peroxides form reactive intermediates. Class IV metal peroxo systems are known to react by producing radicals from peroxide decomposition, which is also considered to be metal catalyzed autoxidation where the most notable reactions include Haber-Weiss and Fenton chemistry [17].

The classification V comprises metal centered oxidizing agents where the metal is the sole oxidant. The role of O_2 is to regenerate the high valent metal species. It plays no active role in the oxidation of the substrate. The Wacker process is the most cited reaction that conforms to class V [18].

Trapping Reactive Intermediates

All of the classes discussed above have one thing in common. When applied to a catalytic process, the selectivity to turnover ratio becomes very important. Even if a catalyst is quite active (oxidizing 90% of a substrate), if the selectivity is poor, the complex is essentially useless. Once an active catalyst has been identified, efforts then focus on the improvement of selectivity without sacrificing conversion. One innovative technique that has developed is the trapping of the intermediates. This technique is a kinetic effect and is influenced by the lifetime of the intermediate. As shown in Figure 1-5, once methane is activated, it cascades rapidly to the thermodynamic minimum CO_2.

In heterogeneous systems, attempts to prevent cascades involve short reaction zones and temperature control. For the oxidation of methane, reactive zones are very

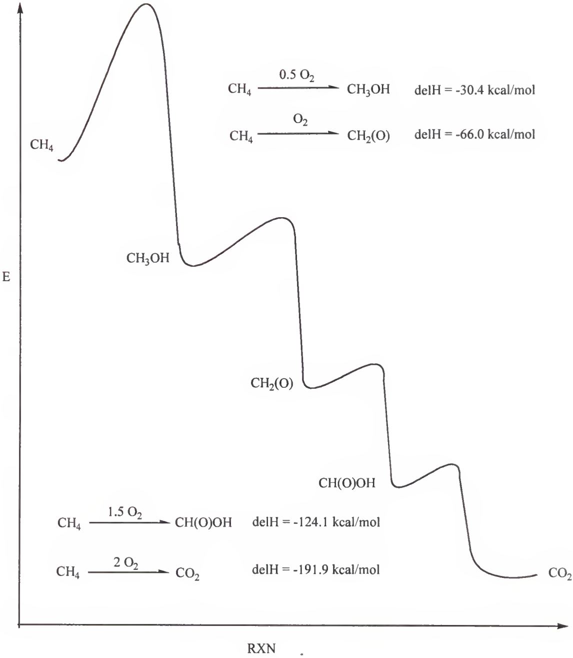

$CH_4 \xrightarrow{0.5\,O_2} CH_3OH$ delH = -30.4 kcal/mol

$CH_4 \xrightarrow{O_2} CH_2(O)$ delH = -66.0 kcal/mol

$CH_4 \xrightarrow{1.5\,O_2} CH(O)OH$ delH = -124.1 kcal/mol

$CH_4 \xrightarrow{2\,O_2} CO_2$ delH = -191.9 kcal/mol

Figure 1-5. Reaction diagram for the product cascade of methane. The molecule CO has been omitted. The reaction curve is exaggerated for dramatic presentation and is not an accurate representation of the barriers of activation and associated energies.

small. The catalyst bed must be supported on gauze, allowing methane and oxygen to flow through the beds only millimeters or less thick. This guaze is heated locally to high temperatures (>700 °C). The methane flows at a fast rate from a cold source through the reactive zone and rapidly cools upon exit [19]. At best the conversion is low (10%), and selectivity amounts to 30% for methanol, a 3% yield. This system is extremely energy intensive and requires expensive equipment to separate methanol and recycle the gas back through the reactor. Because of the low conversion, the time the reaction must remain on stream is too long to make the process profitable.

In homogeneous systems, the rapid removal or cooling of the product stream is not possible. The substrate, whether it is a gas or a liquid, is dissolved into the reactive zone, making separation of products in real-time quite difficult. Attempts have been made to react on phase boundaries between two immiscible liquids with limited success [20]. It becomes clear that innovative and simple techniques must be employed to remove or protect a short-lived kinetic product from within the reactive zone.

Comparing the dielectric constants of methane and methanol, we find that on a relative scale methanol is quite polar. Adjusting solvent polarity in a dilute environment may make catalyst contact time short, extending the life of the kinetic intermediate. Extending the lifetime of imtermediates is important, because on a large scale the dilution of the kinetic product is concentration dependent and will build to a steady state concentration where the product cascade will recommence. The formation of esters from the condensation of alcohols with carboxylic acids or anhydrides is a fast stoichiometric reaction that has been used in recent years as a trap for methanol [21]. Two recent systems, the Catalytica and Sen processes, employ a solvent that, in the presence of methanol, will react to form esters. The resulting ester is stable toward further oxidation due to simple changes in electronegativity of the ester substituent that forms from the solvent.

The Catalytica process developed by Periana and Taube uses soft metal salts such as Hg(II) in 102% H_2SO_4 resulting in 90% methane conversion to methyl bisulfate in 2.5 hours [21f]. The methyl bisulfate can be hydrated with the addition of water to release methanol and regenerate H_2SO_4. This system is a real breakthrough in achieving high selectivity for the difficult reaction of methane oxidation. The drawback to Catalytica and similar systems is the highly corrosive nature and toxicity of an industrial scale reaction. The toxic metal salts have recently been replaced with recoverable platinum salts. The use of concentrated sulfuric acid at high temperatures remains a large drawback [21e].

Green Catalytic Cystems

Current processes for converting methane selectively to methanol are toxic and corrosive and it would be desirable to develop systems that reduce the impact of the these processes on the environment. Regulations have been implemented to protect against excessive pollution in industrial processes, and this legislation has spurred a growing interest in green alternatives to current technologies. Green systems use catalytic materials that can be recovered and reused, and use additives and oxidants that pose little or no harm to the environment. The most abundant and inexpensive green oxidants are hydrogen peroxide and dioxygen. These oxidants produce water as a byproduct of reaction with little or no environmental impact on the large-scale deployment in industry. Currently, the use of hydrogen peroxide is limited (Einchem Corporation TS-1) due to the cost constraints deployed on a large-scale [22]. Dioxygen has been used in many large-scale processes, the Mid-Century being the most notable, and given it's low cost, it is the most desirable oxidant.

Summary

Attempts to develop green systems that use solvents such as water, acetonitrile, carboxylic acids and carboxylic anhydrides have resulted in several interesting catalytic systems that have diverged into several crucial areas of current research on the selective oxidation of alkanes. The catalyst used for all systems is $Ru(dmp)_2(H_2O)_2^{2+}$ where dmp is 2,9-dimethy-l,10-phenanthroline, Figure 1-6. The counter ions, $CF_3SO_3^-$ and PF_6^-, are used exclusively and are considered to be non-coordinating, which helps increase solubility of the complex in aqueous media and provides access to open coordination sites

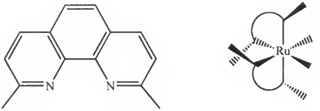

Figure 1-6. Schematic diagram of 2,9-dimethyl-1,10-phenanthroline and $Ru(dmp)_2(H_2O)_2^{2+}$. The diagram is simplified for clarity.

CHAPTER 2
MILD ALKANE OXIDATION WITH DIOXYGEN ACTIVATION IN AQUEOUS ACIDIC MEDIA USING A STERICALLY HINDERED RUTHENIUM COMPLEX

Introduction

Work from this laboratory has focused on the evaluation of metal complexes that activate O_2 for use in facilitating oxidative transformations [23]. Current interests lie in the synthesis of metal oxo precursors capable of a multiple electron transfer reaction and able to function as oxygen atom transfer catalysts. Polypyridyl ruthenium complexes have been studied thoroughly and possess multiple, reversible oxidation states and form stable, isolatable mono and dioxo species [24]. Both *Cis* and *trans* complexes of ruthenium bound by diimine type ligands are known and they have been shown to be versatile oxidants for a variety of oxidative transformations, ranging from benzyl alcohol oxidation to olefin epoxidation [25]. Che *et al.* determined, through studying outer sphere electron transfer reactions between the *cis* and *trans* isomers of dioxo polypyridyl ruthenium complexes, that the *cis* form in most cases is a stronger oxidant [25f]. The relative strength of the two isomers is important considering slight changes in oxidative potential dramatically affect substrate activation. Unfortunately, the trans isomer is more stable, and when exposed to elevated temperatures or changes in oxidation state the *cis* dioxo of bis bipyridyl complexes often isomerises resulting in complex catalytic activity [25]. The thermodynamic stability of the *trans* isomer was confirmed through an INDO/1 molecular orbital investigation of *cis* and *trans* ruthenium-(VI) dioxo ML_4 model complexes and the energy was calculated to be a difference of 35 kcal mol^{-1} [26]. In order to prevent isomerisation, Collin and Sauvage synthesized ruthenium(II) complexes using 6,6'-dimethyl-2,2'-bipyridine (dmbp) and 2,9-dimethyl-1,10-phenanthroline (dmp) as ligands, both forcing the retention of the desired *cis* geometry. The *cis* geometry maintained through steric hindrance of the methyl groups positioned in an alpha geometry to the binding nitrogen atoms [27].

To take advantage of the constrained geometry offered by dmp, this laboratory has synthesized bis aquo complexes of ruthenium, with this ligand, which allows the study of the oxidative properties of a sterically hindered complex. The goal is to generate a ruthenium cation complex that is activated by environmentally benign oxidants, e.g., H_2O_2 or O_2, while retaining the desired *cis* geometry. Set forth in a previous paper, the sterically hindered complex *cis*-$[Ru(dmp)_2(H_2O)_2](PF_6)_2$ (**1**) (as a catalytic precursor) can epoxidize norbornene in the presence of H_2O_2 [28]. Attempts were made to oxidize more difficult substrates, such as methane, but were hindered due degradation and eventual dissociation of the ligand. This type of decomposition is not uncommon in the presence of a high concentration of a strong oxidant and is known to generate inactive Ru^{III} μ-oxo dimers after ligand dissociation has transpired [24b].

This study details the results of using O_2 as the oxidant participating in the oxidation of selected alkanes. Dioxygen is considered to be a mild oxidant and in low concentrations does not participate in ligand decomposition. O_2 is an inexpensive, environmentally friendly oxidant and is an attractive choice for carrying out oxidations where the expected by-product is water.

It is of interest to determine whether a ruthenium cation complex, with accessible coordination sites, can activate O_2 in order to hydroxylate alkanes under mild temperature conditions. To our knowledge, this type of behavior for ruthenium diimmine complexes to activate O_2 and hydroxylate alkanes under relatively mild conditions has not been reported. The current study provides new insight into the mechanism by which O_2 generates a high valent Ruthenium complex, which has been implicated as the active catalyst [29].

Methods

Materials

$RuCl_3 \bullet x\ H_2O$, neocuproine monohydrate, LiCl, $NaCF_3SO_3$, HCF_3SO_3, and ortho-dichlorobenzene were all used as received from Aldrich. Hydrogen peroxide (35%) was used as received from Fischer Scientific (ACS grade). Methane (99.99%) was purchased from Matheson Gas Co. and used as received.

Physical Measurements for Catalyst Characterization

UV-Vis measurements were obtained using a Hewlett-Packard 8543 diode array spectrophotometer using a temperature controlled cell holder with a built in magnetic stirrer. Electrochemical experiments were measured with a glassy carbon working electrode, saturated Calomel (SCE) reference and a platinum wire. The cyclic voltamograms were recorded with an EG&G potentiostat at a 10 mV scan rate. University of Florida Analytical Services performed elemental analysis.

Synthesis of Compounds

Cis-Ruthenium(II) bis(chloride)bis(2,9-dimethyl-1,10-phenanthroline) monohydrate, $\{Ru(dmp)_2Cl_2 \bullet H_2O\}$ was synthesized as reported [27,28]. Analysis:

Calculated for $C_{28}H_{26}N_4CL_2O_2Ru$; C, 55.45; H, 4.29; N, 9.24. Found: C, 55.65; H, 4.35; N, 9.29.

Cis-Ruthenium(II) bis(aquo)bis(2,9-dimehtyl-1,10-phenanthroline) bis(hexaflourophosphate), $[Ru(dmp)_2(H_2O)_2](PF_6)_2$ (**1**) was synthesized as previously reported [28].

Cis-Ruthenium(II) bis(aquo)bis(2,9-dimethyl-1,10-phenanthroline) bis(triflouromethanesulfonate), *cis*-$[Ru(dmp)_2(H_2O)_2](CF_3SO_3)_2$ (**2**). A 1.0g (1.7 millimoles) portion of $Ru(dmp)_2Cl_2 \bullet H_2O$ was added to 5 ml of deionized H_2O. To the heterogeneous solution 100 μL of concentrated HCL is added followed by the addition of 3.6 mmol $AgCF_3SO_3$ adjusted to compensate for all chloride present in solution. Upon addition, the solution became homogeneous and a red to pink precipitate soon formed. This solution is stirred for 4 hours after which time the silver chloride is filtered from the solution. The resulting dark red solution is then stripped under vacuum to remove water, leaving a black/red crystalline precipitate. Analyses calculated for $C_{30}H_{34}N_4F_6O_8RuS_2$; C, 42.25; H, 3.31; N, 6.57. Found: C, 41.40; H, 3.26; N, 6.39.

Oxidation Procedure

The pressurized oxidation of all alkanes was carried out in a 300 ml titanium Parr autoclave with glass liners. A standard reaction time and temperature of 48 hours and 75 ±5 °C respectively were employed in all reactions.

The solution phase products of the reaction were quantified by GC analyses (two Hewlett-Packard 5890 Gas Chromatographs equipped with FID detectors utilizing a 6-ft Chromosorb 15% DEGS column and a 30 m Alltech RSL 160 column (5 μm thickness). Methane, propane, carbon dioxide, and carbon monoxide were quantified using a Varian

3700 Gas Chromatograph equipped with a TCD detector utilizing a 15 ft Carboxen Column. Multiple injections for each sample were performed using injection volumes of 0.1 ml for gas and 0.1 μl for liquid samples.

Safety Precautions

The combination of any oxidant with organic compounds and solvents at elevated temperatures is potentially hazardous. Extreme caution should be taken during the charging and disassembly of the experimental apparatus. Disassembly of reactors should be performed at low temperature and away from potential ignition sources.

Results and Discussion

To achieve good conversion and selectivity in the presence of O_2 (under mild temperatures), investigations into the reactivity of $[Ru(dmp)_2(H_2O)_2](PF_6)_2$ have been limited to work on the mild oxidations of alcohols and olefins, e.g., benzyl alcohol and norbornene. In order to increase the activity of the *cis*-$[Ru(dmp)_2(H_2O)_2]^{2+}$ cation, the PF_6^- (**1**) complex has been exchanged for another poorly coordinating anion $CF_3SO_3^-$ (**2**), which shoul dufrther solvate the ion pair. This separation will enhance the ability to form a reactive high valent metal oxo species implicated as the active species for this catalyst precursor [29]. To determine the importance of ion pairing and the extent of increased access to open coordination sites in solution for **1** and **2**, a comparative study using both anions was carried out. The difficult transformation of selected alkanes has been chosen as the model reaction for this study.

Hydroxylation of Alkanes in Aqueous Solution

Questions regarding the potential of the counter ion to interfer with catalytic activity have been addressed. Through the use of non-coordinating anions such as PF_6^-

and $CF_3SO_3^-$, these anions only weakly coordinate to the metal center and are desirable because of their potential for being incorporated in a homogeneous fashion into aqueous solutions. In previous work, problems were encountered when the complexes were placed in solution due to the formation of close ion pairs, which can interfere with access to coordination sites required for catalysis.

Norbornene was used for initial tests of catalytic activity with complex **1,** and this reaction served as a benchmark for all subsequent work. Several counter ions were considered and based on several test reactions, the anion $CF_3SO_3^-$ was chosen for this study. The reaction of **2** with norbornene displayed a ten-fold increase in reactivity when compared to **1** under identical conditions. Subsequent work has found the perchlorate anion derivative to be active [24,25]. Although in aqueous solution, the perchlorate complex of $Ru^{II}(dmp)_2^{2+}$ is a poor catalyst producing little or no activity. Due to the poor catalytic activity, the perchlorate complex was not used in this study.

The room temperature solubility of both **1** and **2** in water is limited, but by either lowering the pH or heating the solution, the complexes dissolve readily. The reaction has been carried out at temperatures ranging from 70-80 °C and 3 atm of pressure combining the substrate (if gaseous) with a 1:1 He/ox mixture in a sealed autoclave. The use of a high speed stirrer facilitates the mixing of the gas and liquid phases. If the mixture is not stirred at a high rate, reactivity decreases dramatically.

Under these conditions the oxidations of methane, propane, and cyclohexane (Table 2-1 and 2-2, concomitant with complexes **1** and **2**) show a marked difference in reactivity. The catalyst was quite dilute, 2.5×10^{-3} M, which complicates sample analysis. The scale up reactions (SUR), 2.5×10^{-2} M, were carried out only on a screening basis due to the cost of the catalysts and time constraints, but show appreciable results (>15%, Table 2-3). It was more important to define a system consistent with catalyst concentrations of other systems studied, see Chapters 3, 4. As seen in Figure 2-1, when directly comparing the reactivity of both precursors, the oxidation of methane does not clearly reflect the difference in activity of the two complexes because the conversion of methane for both complexes is too low to accurately reflect trends in selectivity toward the desired production of alcohol. The SUR reactions, although inaccurate, can be said to show a marked difference in reactivity even considering modest error. Since the SUR reactions indicate that an aqueous system using either catalytic precursor have the potential to partially oxidize methane to methanol, our attention focused upon these reactions and the use of propane and cyclohexane to clearly define how O_2 is incorporated into the catalytic reaction. As demonstrated in the oxidation of propane and cyclohexane under identical conditions used in Table 2-1 and 2-2, complex **2** was the more active catalyst based on high concentrations of over oxidized products, in this case acetone and cyclohexanone. In aqueous media, the only fundamental difference between complex **1** and **2** is the counter ion. With no fundamental change in the actual Ru^{II} aqua ion, the tendency to form close ion pairs vs solvent separated ion pairs becomes evident.

Several interesting aspects of the reactions were identified from the data. Referring back to Tables 2-1 and 2-2, the pH dependence of the reaction was demonstrated by changes in induction period under different pH conditions. The change in induction period has a direct bearing on how O_2 is incorporated into the reaction. The pH directly affects the oxidation potential of an oxidant. Since the potential of the oxidant

Table 2-1. Alkane oxidations using O_2 and $Ru(dmp)_2(H_2O)_2[CF_3SO_3]_2$ in aqueous acidic media.

Substrate[a]	pH	Alcohol (mmol)	Aldehyde/ Ketone (mmol)	Other (mmol)	Induction Period (hr)
		CH_3OH	CH_2O	CO_2	
Methane	7	0.3	0.3	0.11	10
	1	0.8	0.2	0.64	0.5
	1[b]	0.6	0.3	0.31	4
		$(CH_3)_2CH(OH)$	$(CH_3)_2CO$	$CH_3CH_2CH_2OH$	
Propane	7	--	1.2	--	9
	1	0.7	8.2	0.2	0.6
		$C_6H_{11}OH$	$C_6H_{10}O$		
Cyclohexane	7	0.7	7.1		9
	1	1.8	12.9		1

(a)Reaction Conditions: 5 x 10^{-5} mol catalyst precursor; 1 mole equivalent of H_2O_2 was used to initiate reaction; 250 psi (480 mmol) CH_4; 500 psi 1:1 He/O_2; 20 ml H_2O; 70 °C; 48 hours. The pH was adjusted by addtion of CF_3SO_3H. (b)No initiator was used.

Table 2-2. Alkane oxidations using O_2 and $Ru(dmp)_2(H_2O)_2[PF_6]_2$ in aqueous acidic media.

Substrate[a]	pH	Alcohol (mmol)	Aldehyde/ Ketone (mmol)	Other (mmol)	Induction Period (hr)
		CH_3OH	CH_2O	CO_2	
Methane	7	0.2	--	0.01	12
	1	0.7	0.5	0.33	0.7
	1[b]	0.6	0.4	0.21	5
		$(CH_3)_2CH(OH)$	$(CH_3)_2CO$	$CH_3CH_2CH_2OH$	
Propane	7	0.2	2.0	--	13
	1	1.0	3.7	--	0.8
		$C_6H_{11}OH$	$C_6H_{10}O$		
Cyclohexane	7	0.5	4.2		11
	1	1.3	7.8		1

(a) Reaction Conditions: 5 x 10^{-5} mol catalyst precursor; 1 mole equivalent of H_2O_2 was used to initiate the reaction; 250 psi (480 mmol) CH_4; 500 psi 1:1 He/O_2; 20 ml H_2O; 70 °C; 48 hours. The pH was adjusted by addtion of CF_3SO_3H. (b)No initiator was used.

Table 2-3. SUR screen reactions for methane oxidation using O_2.

Complex	Temperature (°C)	pH	Alcohol (mmol)	Aldehyde (mmol)	CO_2 (mmol)	Conversion (%)
1	75	7	2.3	0.9	32.6	7.5
	75	1	2.1	1.2	46.7	13.0
	100	1	1.3	0.2	55.4	11.9
2	75	7	2.8	1.5	45.6	13.8
	75	1	4.2	1.2	62.4	14.1
	100	1	2.4	0.5	75.1	16.25

Reaction Conditions: Reactions are free of initiator. 5 x 10^{-2} catalyst precursor; 250 psi (480 mmol) CH_4; 500 psi 1:1 He/O_2;50 ml H_2O; The pH was adjusted by addition of HCl. Product conversion is based on total products.

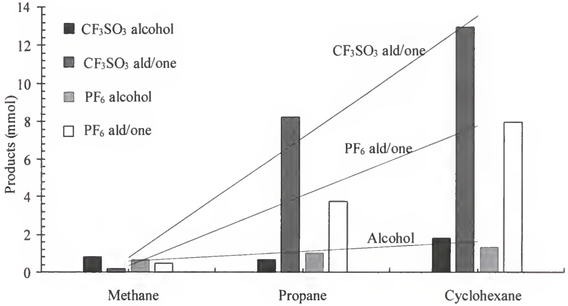

Figure 2-1. Trends in the effect of counter ion on the distribution of primary and secondary oxidation products of methane, propane, and cyclohexane at pH 1 for complexes **1** and **2**.

increases as the acidity of the media increases, *vida infra*. Also, long induction periods exist for catalysts that are not initiated with hydrogen peroxide. Because of previous studies with complex **1,** long induction periods observed are not surprising, and by adding 1 mol equivalent (2 oxidative equivalents) of hydrogen peroxide, it is possible to generate a Ru^{IV} species *in situ* circumventing the need to wait for the slow (greater than 12 hours) adduct formation via O_2. Using initiators such as hydrogen peroxide are common place for reactions that exhibit extended induction periods [25]. By circumventing the process of building steady state concentrations, additives that accelerate reactivity reduce cost of operation usually with no adverse effects on catalyst lifetime or extended reactivity of the system. Because of our desire to design green systems with minimal impact on the environment, hydrogen peroxide was chosen as the exclusive initiator.

The change in induction period has a profound influence on the degree of conversion. Reacting **2** in acidic aqueous solution with methane results in a turnover frequency (tof) of 6.8 hr^{-1} as compared to reactions in neutral pH (under identical conditions) that display a 2 fold (tof 2.8 hr^{-1}) decrease in conversion [30]. Figure 2-2 and 2-3 illustrate the distribution of products and the change in induction period for methane and propane at pH 1 over a 48 hour time period. Upon inspection of Figure 2-2, an induction period is observed followed by the rapid build up of steady state concentrations of methanol and formaldehyde. Once a steady state concentration is established there is a rapid over oxidation to CO_2. An analogous experiment using propane as the substrate cofirms this observation, Figure 2-3. The oxidation of propane defines the induction period and the build up of a steady state concentration of 2-propanol after 40 hours coincides with the rapid over oxidation of 2-propanol to acetone. The turnover frequency per hour was 37 at pH 1 and 5 at pH 7. The analogous trend can also be seen with cyclohexane (tof 62 hr^{-1} pH1 and tof 32 hr^{-1}). Figure 2-4 describes the turnovers per mol of catalyst for methane seen over 48 hours of reaction time. By removing the initiator (lower curve) the induction period increases but does not affect the activity of the catalyst. The turnover frequency of the two reactions at pH 1 are comparable and directly reflects the amount of over oxidation occurring after steady state concentrations are established. When subsequent reactions are performed without initiator by recharging the vessel with substrate and oxidant, the activity of the complex is consistent with no major changes in reactivity.

Incubating the catalyst in a pH 1 solution with excess O_2 and no initiator at 70 °C for 4 hours results in a change in color from a red (Ru^{II}) to a yellow (presumed to be Ru^{IV}) solution. Adding substrate to the incubated solution results in almost instantaneous reactivity. For comparison, one mole equivalent of H_2O_2 was added to a slurry of **2** in water at 70 °C. The slurry changes from a deep red to yellow upon addition and was isolated by stripping the solvent producing a yellow solid. Using the yellow solid in place of **2** leads to little or no induction period (<10 min) and a tof of 4.5 hr^{-1}. The time needed to incorporate the gaseous substrate and oxidant into the liquid phase may account for the lack of reactivity in the first ten minutes of reaction time. Elemental analysis of the yellow solid was identified with the formulation of $[Ru^{IV}(dmp)_2(H_2O)(O)](CF_3SO_3)_2$.

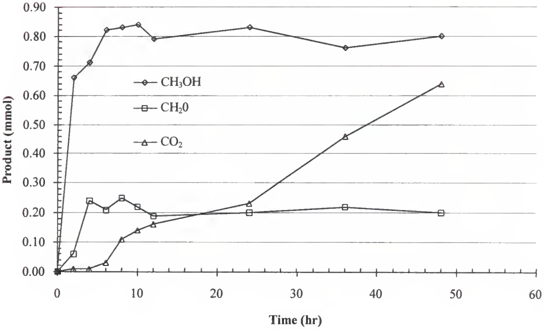

Figure 2-2. Product distribution for the oxidation of methane using 5 x 10^{-5} mol $[Ru(dmp)_2(H_2O)_2](CF_3SO_3)_2$ at pH 1 in the presence of 1 mol equivalent H_2O_2 at 70 °C.

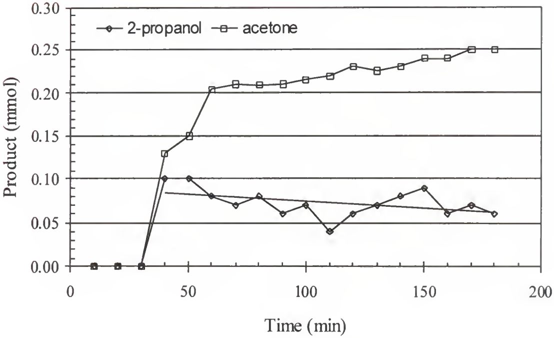

Figure 2-3. Product distribution for the oxidation of propane using 5 x 10^{-5} mol $[Ru(dmp)_2(H_2O)_2](CF_3SO_3)_2$ at pH 1 in the presence of 1 mol equivalent H_2O_2 at 70 °C.

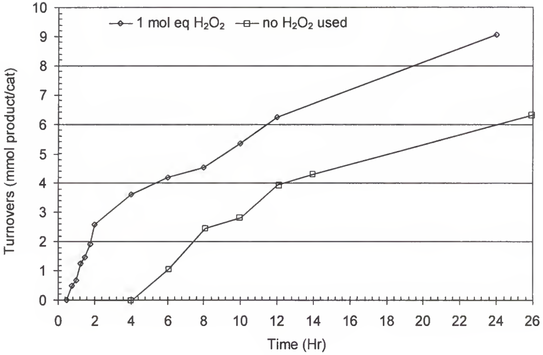

Figure 2-4. Oxidation of methane in water pH = 1 using 5 x 10 $^{-5}$ mol $[Ru(dmp)_2(H_2O)_2](CF_3SO_3)_2$ at 70 °C; typical catalyst turnovers over 24 hours.

This product can be made by using either H_2O_2 or O_2. This suggests that oxidative addition of O_2 to form the metal oxo takes place, Equation 2-1. Illustrated in Figure 2-5

$$\mathrm{Ru^{II}(dmp)_2(H_2O)_2^{2+} + O_2 \xrightarrow[+2\,H^+]{-e^-} Ru^{IV}(dmp)_2(H_2O)(O)^{2+} + H_2O} \quad (2\text{-}1)$$

is the cyclic voltamogram of **2** in water and shows one reversible oxidation couple (ΔE_p= 143 mV, $i_{pc}/i_{pa} = 0.96$) and one irreversible couple. The first reversible anodic wave occurs at 0.72 V vs SCE and is assigned as the two electron Ru^{II}/Ru^{IV} couple, Equation 2-2; the second irreversible anodic wave occurs at 0.95 V vs. SCE and is assigned as the Ru^{IV}/Ru^{VI} oxidative couple. The reversible wave is a two electron process vs $K_3Fe(CN)_6$

$$\mathrm{Ru^{II}(dmp)_2(H_2O)_2^{2+} \xrightleftharpoons{-\,2\,e^-} Ru^{IV}(dmp)_2(H_2O)(O)^{2+} + H_2} \quad (2\text{-}2)$$

and by holding the current constant at 0.75 V $[Ru^{IV}(dmp)_2(H_2O)(O)]^{2+}$ the spectrum corresponds to the one taken for the addition of two oxidative equivalents of H_2O_2 or Ce^{4+}. This *in situ* species should be the direct precursor and using this solution in place of **2** produces analogous results seen in the incubation experiment. This corresponds well to previous studies of the NMR spectra taken of **1** before, during and after the addition of hydrogen peroxide. The spectra reflects the stepwise formation of a paramagnetic Ru^{III} and a diamagnetic Ru^{IV} species [28].

The viability of O_2 as a practical oxidant with complexes that have two possible electron reduction potentials is dependent upon the oxidative potential of the complex in question. The activation of O_2 generally results in weak selective oxidants due to the low

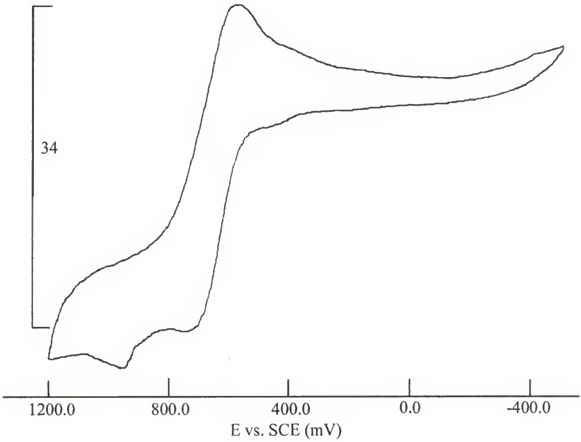

Figure 2-5. Cyclic voltamogram of 2.4 x 10^{-3} M $[Ru^{II}(dmp)_2(H_2O)_2](CF_3SO_3)_2$ in 0.1 M $LiClO_4$ at pH 7.

oxidation potential of O_2 (pH 0, 0.69 V) in water, Figure 2-6. The Porbait plot describes the potentials at which strong, intermediate, and mild oxidants function depending upon pH. At pH 7, O_2 has an oxidative potential of approximately 0.32 V. Comparing that to 1.0 V (adjusted for SCE) for **2** it is difficult to imagine how O_2 is incorporated into the reaction without introducing the idea of a sacrificial reductant. The potential of **2** resides in the central region of intermediate oxidants, a range that spans 0.4 V to 1.5 V. Oxidants in this region are difficult to characterize due to their ability to either be oxidized by, or to oxidize hydrogen peroxide (1.2 V at pH 7). The irreducible anodic wave for complex **2** is 1.23 V at pH 7, essentially the same potential as that of hydrogen peroxide. We have observed the decomposition of H_2O_2 (pH 0, 1.776 V) in the presence of **2** (after spectral changes to the proposed Ru^{IV} have occurred), providing evidence that the Ru^{IV-VI} reduction potential is greater than that of H_2O_2 and can function as a stoichiometric oxidant. The stoichiometric reactivity of the high oxidation state above IV would suggest that the ruthenium species above IV will not be present in large concentrations preferring to react with the nearest available substrate. A redox couple of this nature has an oxidation potential too high for O_2 to form an active species. If the formation of the metal oxo does not proceed through adduct formation with O_2, in the presence of hydronium (in this case a sacrificial reducing agent), a metal peroxide can be formed *in situ* leading to metal oxo formation. Reactivity has been identified in heme systems that initially form a metal peroxide through a proton coupled electron transfer followed by homolytic cleavage of the weak O-O bond forming an active Fe^{n+}=O species [14,31].

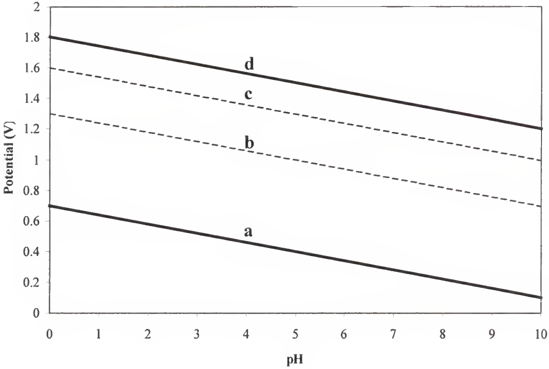

Figure 2-6. Porbait plot [29]of the potentials for: (a) O_2; (b) $Ru^{II}(dmp)_2^{2+}$; (c) $Ru^{IV}(dmp)_2^{2+}$; (d) H_2O_2.

Spectral Changes

To determine the dependence of O_2 adduct formation upon the hydronium ion concentration, the spectral changes of the reaction of **2** with O_2 were studied. By first initating the reaction with 1 mol equivalent of H_2O_2, three isosbestic points are established through time as defined by characteristic metal to ligand charge tranfer (MLCT) bands, as defined previously for **1**. The MLCT bands are proposed as the Ru^{II}/Ru^{III} and Ru^{III}/Ru^{IV} [29]. The initial isosbestic at 429 nm can clearly be seen at pH 7 and 25 °C using excess equivalents of H_2O_2, Figure 2-7. The extinction coefficient for $[Ru^{II}(dmp)_2]^{2+}$ at 500 nm is 11713 L cm^{-1} mol^{-1}, assuming a step wise formation of each successive oxidation state, the rate of oxidation from Ru^{II} to Ru^{III} by H_2O_2 at 25 °C is pseudo first order in Ru^{II} with a $k= 4.0 \times 10^{-4} s^{-1}$. By either raising the temperature or lowering the pH, this isosbestic is lost.

The spectra in Figure 2-8 are the changes observed in **2** at pH 1 at 70 °C in the presence of 1 mol equivalent of H_2O_2 and the addition of O_2 after equilibrium has been established. The expected initial formation of an active high valent species before catalytic activity is observed was approximated by choosing analysis times (30 min, pH 1) corresponding to the induction period (methane, pH 1, initiated, Table 1). The spectra of pH 1 and 7 establish analogous isosbestic points in region A during the first minute after the addition of initiator. Region A is thought to be the change from Ru^{II} to Ru^{III}. The spectra in acidic solution display significant differences in the latter 15 minutes of observation. The first 10 minutes establishes region B (Ru^{IV}) and is essentially identical to that found for the neutral spectra. The change in the spectra at pH 7 is slow after the Ru^{III} (region A) has been established and changes slowly over 10 hours as region B is established. Region

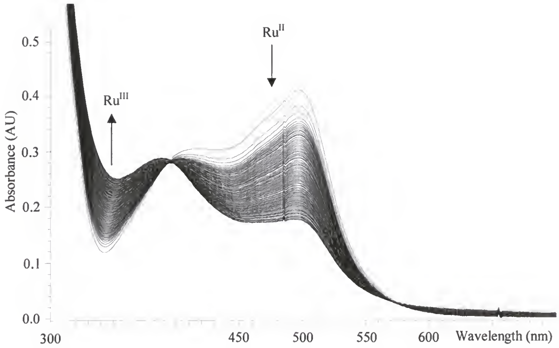

Figure 2.7. UV-VIS spectra of 4.7 x 10^{-5} M $[Ru^{II}(dmp)_2(H_2O)_2](CF_3SO_3)_2$ in H_2O at 25 °C and pH 7. Addition of excess equivalents of H_2O_2 over 30 minutes, one spectra taken every 10 seconds.

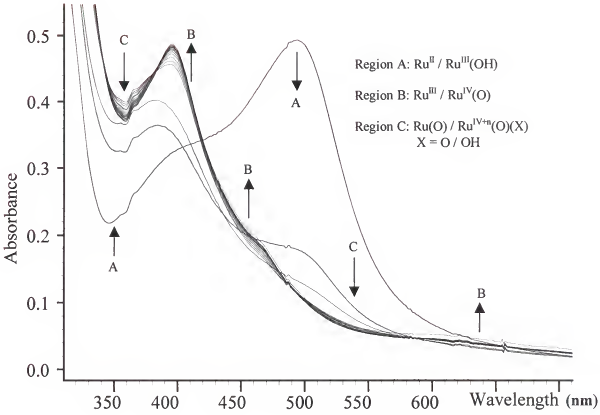

Figure 2-8. UV-VIS spectra of 4.7 x 10^{-5} M [Ru^{II}(dmp)$_2$(H_2O)$_2$](CF_3SO_3)$_2$ in H_2O at 70 °C and pH 1. Addition of 1 mol equivalent of H_2O_2 over 30 minutes, one spectra taken every 10 seconds.

B is believed to be the formation of $[Ru^{IV}(dmp)_2(H_2O)(O)]^{2+}$ and corresponds with the spectra of $[Ru^{IV}(dmp)_2(H_2O)(O)]\ (CF_3SO_3)_2$ ($\epsilon=1.1x10^5$ L cm^{-1} mol^{-1} at 380 nm and k=$4.0x10^{-6}$ s^{-1}) generated from peroxide addition or electrolysis of **2**. After equilibrium in region B has been established (the latter 15 minutes, in acidic solution), the spectrum shows a very slow change developing three new isosbestic points (575 nm, 484 nm, 392 nm) defined as region C. Region C can be one of two proposed species, $[Ru^V(dmp)_2(O)(OH)]^{2+}$ or $[Ru^{IV}(dmp)_2(O)_2]^{2+}$.

A molecular orbital investigation of C_2 symmetric *cis* and *trans* ruthenium dioxo complexes disputes the possibility of producing a stable Ru^V species, Figure 2-9 [26,14,32]. The degenerate d_{xy} and d_{xz} orbitals are a stable filled HOMO that must change symmetry or experience a significant donation (red shift) of electron density from the dmp ligand to the metal center represented by ligand to metal charge transfer (LMCT) bands. The expected LMCT bands are not observed under the experimental conditions for this study. With the retention of C_2 symmetry, the d^3 paramagnetic complex (with 1 unpaired electron) represents a highly unstable species that can be considered an intermediate product to forming the lower energy diamagnetic d^2 species.

The proposed formation of the Ru^{VI} dioxo in the presence of O_2 can only take place in the presence of a sacrificial reducing agent, Equation 2-2, in order to produce an active species *in situ* that continues the catalytic oxidation cycle. The pH dependence of the reaction and observed spectral changes rule out the formation of an O_2 adduct without the presence of a reducing agent. Based on the instability of a Ru^V species, the metal

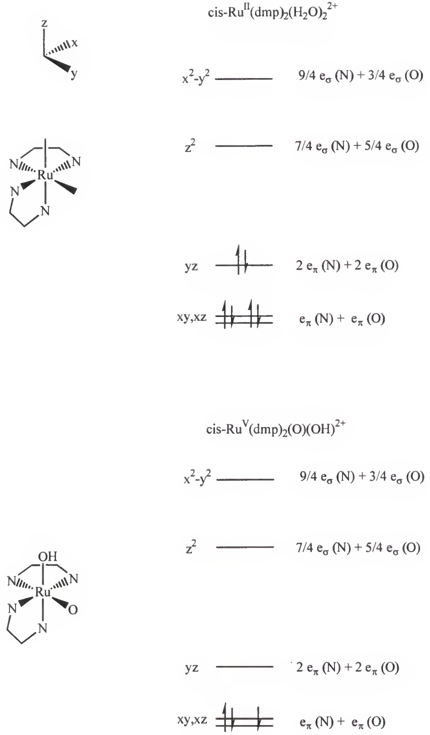

Figure 2-9. Frontier orbital splitting diagrams with the aid of the angular overlap model (AOM) for *cis*-Ru(dmp)$_2$(H$_2$O)$_2^{2+}$ and *cis*-Ru(dmp)$_2$(O)(OH)$^{2+}$ [26].

peroxo intermediate must decompose to a dioxo complex that reacts with any available nucleophilic substrate present.

A graphical representation of the proposed catalytic cycle for this system is shown in Figure 2-10. A mechanism proposed by Robbins and Drago for alkane oxidations using $Ru^{II}(dmp)_2$ clearly states that the use of O_2 as an oxidant will result in long induction periods as the intermediate Ru^{III} analog is produced [29]. This corresponds to the long induction periods we have observed. It is unclear what species of Ru^{III} analogue is produced. From what is known of autoxidation chemistry and metal oxo formation it is safe to suggest that the initial species must be the formation of an O_2 adduct. If initiator is used, Fenton like reactions can generate a metal hydroxo that can also be formed from disproportionation reactions between Ru^{II} and Ru^{IV}, but these reactioins are considered to be a minor product.

The production of Ru^{IV} is also slow using O_2, but in the presence of a sacrificial reductant the adduct generates a metal peroxo. This metal peroxo is equivalent whether it is generated by way of hydrogen peroxide or O_2. This is crucial in systems where an initiator must be used to bypass long induction periods but must not alter the catalytic system. Since a sacrificial reductant is used to form a metal peroxo species, which can also be obtained from peroxide, this system can safely be initiated without degradation of catalytic behavior.

It is debatable which species carries out the oxidation. The formation of a high valent metal species greater than Ru^{IV}, based on established oxidation potentials, is a strong oxidant, but nucleophilic attack on the substrate by Ru^{IV} may also occur. In fact, it

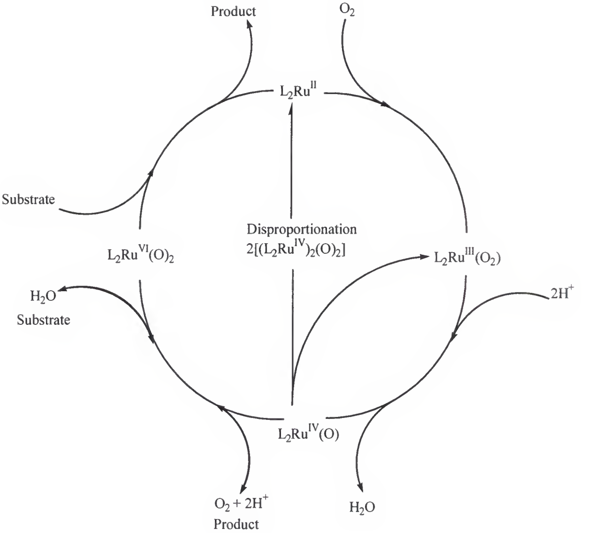

Figure 2-10. Proposed catalytic cycle for the O_2 oxidation of alkanes by $Ru(dmp)_2^{2+}$ in aqueous media.

most certainly happens to some extent, especially in the presence of oxidized products such as methanol and formaldehyde. The initial oxidation of the substrate requires a strong oxidant that can either start electron transfer initiating autoxidation, or hydrogen abstracts to cycle back to Ru^{IV} or Ru^{II}. Recent work with $^{18}O_2$ labeling may help establish how the oxidant is brought into the system, and how by-products are generated from oxidation. If complex **1** forms a metal oxo via a μ-peroxo that cleaves to generate 2 $Ru^{IV}(O)$, labeled water would not be produced as a by product in the system. As shown in Figure 2-10, the steps to form $Ru^{IV}(O)$ in the catalytic cycle would form one equivalent of water. In a system where type II metal oxo formation takes place, the dioxygenase uses both oxidative equivalents. No labeled oxygen would be present in the form of water. Type III, being a monoxygenase, would certainly generate labeled water, providing insight into the initial mechanistic formation of higher valent species.

Conclusions

This system has proven to be unique in the ability to incorporate O_2 and catalyze the oxidation of alkanes. The selective oxidation of light weight alkanes is a difficult reaction that requires a catalyst that is robust enough to activate the strong C-H bond of the alkane without oxidizing the resultant products. The system studied shows that oxidation of alkanes and the activation of O_2 by using a ruthenium bipyridyl complex is possible, even in aqueous solution. The current study complements previous work with complex **1** in acetonitrile and shows that a high valent species higher than Ru^{IV} must be present for catalysis to take place.

Although our system is a slow process, due to limited solubility of the substrate in water and slow production of the active species, it is a desirable system from the standpoint of developing green oxidation systems that utilize oxidants and media that are inexpensive and nontoxic. From an industrial standpoint, the system is little more than a curiosity, providing important information toward discovering systems that overcome the shortcomings of the system presented.

CHAPTER 3

PEROXY ACID MEDIA AS AN EFFECTIVE TRAP OF TRANSITIONAL PRODUCTS FROM THE MILD OXIDATION OF METHANE

Introduction

Work with ruthenium dmp complexes has produced oxidation catalysts that readily oxidize alkanes in the presence of hydrogen peroxide and dioxygen [23,28,29]. In previous systems, the propensity the products resulting from mild alkane oxidations, (e.g. methane) to preferentially oxidize has been a serious drawback. The problem of over oxidation must be addressed in order to develop a catalytic system that has a rational application as an industrial process. One method of product removal is the media trapping of products, which involves the removal or transformation of the desired product/intermediate before deleterious reactions take place.

Methane is quite stable, but once activated, it will cascade to the thermodynamic product CO_2 (refer back to Figure 1-5). Strong homogenous oxidants, such as high valent metal cation complexes (e.g. $Ru(dmp)_2^{2+}$) tend to oxidize products such as methanol and formaldehyde preferentially, and represents a difficult balance between selectivity and conversion. Selectivity and conversion depend heavily on reaction conditions, but as a general rule, high conversion coincides with low selectivity and vice versa. Steady state concentrations play an important role and are directly related to selectivity and conversion. The use of a reactive media to take direct advantage of steady state concentrations has been employed in related systems in order to prevent the further oxidation of methanol while keeping methane conversions high [21]. The development of a technique for trapping methanol improves the rationality for using systems that otherwise show a propensity for oxidizing methane yet over oxidize the functionalized intermediates.

The need for a trapping scheme for $[Ru(dmp)_2(H_2O)_2](CF_3SO_3)_2$ (**1**) has previously been demonstrated in a series of screening reactions [33]. Oxidations in acetonitrile show good conversions of methane (>40% methane conversion) but fail due to poor selectivity resulting from the deep oxidation of desired intermediates such as methanol and formaldehyde (80% yield CO_2) [34-37]. In this chapter attempts have been made to exploit the hydroxyl functionality of the methanol intermediate by developing a catalytic system that utilizes carboxylic acids and anhydrides as co-solvents in order to inhibit the over oxidation of methanol by forming the corresponding methyl ester, Equations 3-1 and 3-2.

$$\mathrm{RC(O)OH} + \mathrm{CH_3OH} \rightleftharpoons \mathrm{RC(O)OCH_3} + \mathrm{H_2O} \tag{3-1}$$

$$\mathrm{RC(O)O(O)CR} + \mathrm{CH_3OH} \rightleftharpoons \mathrm{RC(O)OCH_3} + \mathrm{RC(O)OH} \tag{3-2}$$

Acetic and propionic acids and anhydrides were chosen for this study due to the fast rate of formation of the methyl ester. The reaction of the acid or anhydride with methanol forms the methyl ester *in situ*, effectively removing methanol from the substrate pool [21]. This method is a simple and inexpensive way of preventing over oxidation. Although the methyl esters of both acetic and propionic acid are quite stable toward further oxidation, they can liberate methanol in the presence of water [38-40]. The initial idea was to use only acid as a trapping solvent. The corresponding anhydride can be used as a co-solvent to remove water generated during the reaction, shifting the equilibrium toward production of the methyl ester, and keeping the reaction media anhydrous (Equation 3-3).

$$RC(O)O(O)CR + H_2O \rightleftharpoons 2\,RC(O)OH \qquad (3\text{-}3)$$

The solvent system described above in conjunction with hydrogen peroxide as the oxidant has produced interesting side effects associated with the *in situ* generation of peroxy acids as the true oxidant. The initial oxidant, H_2O_2, reacts readily with either the acid or anhydride. Hydrogen peroxide will preferentially react with the anhydride, as will all water in the system, effectively leaving the system anhydrous with a ready source of free radicals. The reaction of hydrogen peroxide with an anhydride is an exothermic process that coincides with the production of one equivalent of acid that can then function as a trapping media. A note of caution: the addition of a peroxide to an anhydride is potentially explosive (extremely unstable in the presence of activated 4 A sieves) and care must be taken to observe slow addition under cool temperatures.

Initially, the generation of peroxy acids was not intended but has led to homolytic catalysis by **1.** This reaction produces a large concentration of free radicals that can then react with methane or terminate as methanol [38]. The free radical process is accelerated by elevated temperatures and metals and is a classic example of autoxidation. Although the use of peroxy acids is acceptable, it leads to decomposition of the peroxy acid to CO_2 and alcohols. This decomposition is difficult to control and the alternate source of alcohol (methanol in the case of acetic acid/anhydride) from solvent decomposition can prevent the accurate determination of the methyl ester originating from the direct conversion of methane.

Peroxy acids are unstable at elevated temperatures (>50 °C), and in the presence of trace metals the degradation is accelerated [37]. The systems studied herein operate at elevated temperature (≥70 °C) and in the presence of metals, providing an ideal environment for homolysis of the peroxy acid [38]. The initiation through homolytic O-O bond cleavage, Equation 3-4, results in a fast decomposition. The fast decomposition to an alkyl radical propagates the oxidation of methane (Equations 3-5 and 3-6) under mild temperatures. The radical initiation can also terminate, forming alcohols generated from solvent decomposition that consequently react with the co-solvents to produce an equivalent acetate.

$$RCO_3H \longrightarrow RCO_2\bullet + \bullet OH \longrightarrow R\bullet + CO_2 + \bullet OH \qquad (3\text{-}4)$$

$$R'H + R\bullet \longrightarrow R'\bullet + RH \qquad (3\text{-}5)$$

$$R'\bullet + RCO_3H \longrightarrow R'OH + RCO_2\bullet \qquad (3\text{-}6)$$

Two systems have been studied where *in situ* peroxy acids in the presence of **1** are used to oxidize methane. The first system, using acetic acid/anhydride, demonstrates the potential effects on analyses that similar carboxylic acids may manifest in the presence of hydrogen peroxide. To clearly define the acetic co-solvent system. mass balance calculations and blank experiments based on the loss of carbonyl products resulting from decomposition were used.

A second system employing propionic acid/anhydride has been studied resulting in good conversions of methane under identical conditions to the acetic system. The decomposition of perpropionic acid is unlikely to generate methyl acetate from normal modes of decomposition of the peroxy acid. The termination of free radicals result in a product analysis that does not suffer from alternate sources of methyl propionate.

Experimental

Materials and Methods

$RuCl_3 \bullet x H_2O$, neocuproine monohydrate, LiCl, $NaCF_3SO_3$, HCF_3SO_3, propionic acid, propionic anhydride, and *ortho*-dichlorobenzene were all used as received from Aldrich. Ethylene glycol, glacial acetic acid, acetic anhydride, 4-A molecular sieves and hydrogen peroxide (35%) were used as received from Fischer Scientific (ACS grade).

Methane (99.99%) was purchased from Matheson Gas Co. and used as received.

Synthesis of Compounds

Cis-Ruthenium(II) bis(chloride)bis(2,9-dimethyl-1,10-phenanthroline) Monohydrate, $Ru(dmp)_2Cl_2 \bullet H_2O$ was synthesized as reported [27-28].

Cis-Ruthenium(II) bis(aquo)bis(2,9-dimethyl-1,10-phenanthroline) bis(triflouromethanesulfonate), *cis*-$[Ru(dmp)_2(H_2O)_2](CF_3SO_3)_2$ (1) was synthesized as reported [41].

Oxidation Procedure

The pressurized oxidation of methane with hydrogen peroxide was carried out in a Parr hydrogenation apparatus as described previously [28]. The standard reaction mixture employed in most oxidations was comprised of 18 ml of solvent; 3 ml ortho-dichlorobenzene, 5 ml carboxylic acid, 10 ml carboxylic anhydride, $2.4x10^{-2}$ mmol of catalyst, 1 ml 35% H_2O_2 (11 mmol) and 80 psi methane (48 mmol). 1.0g of 4-A sieves were used in selected experiments to help facilitate the removal of water introduced by the initial aqueous peroxide solution. A standard reaction time and temperature of 4 hours and 75 ±5 °C was employed in all reactions. A series of control experiments was performed in the absence or modification of one or more of the above listed components of the standard system and is stated where appropriate.

Reactions using dioxygen were initially carried out under the same conditions as the peroxide but eventually utilized a 300 ml Parr high pressure autoclave equipped with a magnetic stirrer spinning at 1000 rpm.

The solution phase products of the reaction were quantified by GC analyses (two Hewlett-Packard 5890 Gas Chromatographs equipped with FID detectors utilizing a 6-ft Chromosorb 15% DEGS column and a 30 m Alltech RSL 160 column (5 μm thickness). Methane, carbon dioxide and carbon monoxide were quantified using a Varian 3700 Gas Chromatograph equipped with a TCD detector utilizing a 15 ft Carboxen Column. Multiple injections for each sample were performed using injection volumes of 0.1 ml for gas and 0.1 μl for liquid samples.

Ethyl propionate is a product of the decomposition of the in-situ peroxyacid of propionic acid and is not considered an oxidation product. Therefore, ethyl propionate is excluded from the total oxygenated products. The conversion of methane is based on the loss of methane via TCD analyses and may not correspond to total oxygenated products formed due to peroxyacid decomposition.

Safety Precautions

The combination of any oxidant with organic compounds and solvents at elevated temperatures is potentially hazardous. Hydrogen peroxide and neat carboxylic anhydrides is an unpredictable and explosive mixture. Care must be taken to observe slow addition at room temperature. **Extreme caution** should be taken during the charging and disassembly of the experimental apparatus. Disassembly of reactors should be performed at low temperature and away from potential ignition sources.

Results and Discussion

Reactions Using Acetic Acid and Acetic Anhydride

Screening reactions were initially performed to ascertain the feasibility of deploying a catalytic system where standard carboxylic acids are employed, Table 3-1. These very interesting reactions provide insight into the unpredictability of systems where free radical pathways predominate. The screening reactions used to test feasibility were carried out in 250 ml glass hydrogenation reaction vessels with an upper limit of 80 psi for all gaseous substrates. Activated 4-A molecular sieves were used initially to dehydrate the system in order to improve yields of esters. The use of sieves proved to be deleterious to reproducibility, which can be attributed to the adsorption of water and H_2O_2 into the sieves whereby the peroxide is concentrated and fast decomposition ensues liberating reactive free radicals. Introducing 5 ml of H_2O_2 in the presence of sieves proved to be unpredictably explosive.

Regardless of the concerns of reproducibility, screen Experiments 1-3 (Table3-1) show that a maximum conversion of methyl acetate is achieved in less than 4 hours due to the rapid decomposition of the oxidant via molecular sieves. Determining the peroxide efficiency of the system shows direct evidence of decomposition. For Experiment 1-3, the peroxide efficiency is c.a. 20%. Removing molecular sieves improves efficiency and conversion (40%, 62% respectively, Experiment 4) but raised concerns about side

Table 3-1. Screen reactions of **1** with methane in acetic acid/anhydride mixed media.

Experiment	$CH_3C(O)OCH_3$ mmol, (%)	CO_2 mmol, (%)	Total Oxygenates mmol, (%)	CH_4 Consumed (%)
1[a]	5,(44)	5,(44)	7,(62)	30
2[a,b]	4,(40)	3,(30)	7,(69)	26
3[a,c]	5,(57)	1,(11)	7,(80)	19
4[a,d]	10.(49)	9,(44)	10,(49)	62
5[e]	9,(80)	3,(27)	8,(71)	49
6[e,f]	4,(70)	1,(17)	5,(87)	25
7[e,g]	2,(100)	0	2,(100)	--

(a)Reaction conditions: 6.6 x 10^{-5} moles *cis*-$[Ru(dmp)_2(H_2O)_2](CF_3SO_3)_2$, 5 ml 30% H_2O_2, 20 ml CH_3CN, 20 ml $CH_3C(O)OH$, 20 ml $(CH_3C(O))_2O$, 40 psig (23 mmol) CH_4, 3.5 g 4A molecular sieves. Percent products are based on total products seen from all sources. Reaction time 24 hours. (b)Reaction time 12 hours. (c)Reaction time 4 hours. (d)Absence of sieves, reaction time 4 hours.(e)Reaction conditions: 2.4 x 10^{-5} moles **1**, 1 ml 35 % H_2O_2, 3ml *ortho*-dichlorobenzene, 5 ml $CH_3C(O)OH$, 10 ml $(CH_3C(O))_2O$, 40 psi (23 mmol) CH_4. Reaction time 4 hours. (f) Absence of catalyst. (g) Absence of catalyst, methane.

reactions from peroxides in the system. Since total oxidized products based on methane conversion were inconsistent with observed product formation, peroxides formed *in situ* from solvent were suspected to be contributing to the poor efficiency. The generation of a peroxy acid from acetonitrile in the form of $CH_3C(OOH)NH$ is known to be highly unstable leading to elevated dinitrogen levels and CO_2 [42]. Iodometric titrations of solutions containing acetonitrile without catalyst or substrate revealed the presence of peroxides, thus acetonitrile was excluded from future systems. This called for a fundamental change in the system employed where acetonitrile and molecular sieves have been removed, (Table 3-1, Experiments 5-7). Screen reactions with the new system showed good conversion and selectivity toward methyl acetate, yet ratios of conversion and observed products were still inconsistent. By removing the catalyst, the peroxide in solution autoxidizes methane. The removal of catalyst and methane lead to the discovery of a significant pathway of peroxy acid decomposistion. Iodometric titrations of Experiments 6 and 7 for the presence of peroxides support this observation and could account for 30% of observed products in Experiment 5.

A careful set of reactions was carried out to determine the extent of oxidation that is a function of autoxidation by *in situ* generated peroxy acids and the effect sieves and catalyst have upon the methyl acetate production, Table 3-2. As seen in Run 1, typical reaction conditions for the acetic system yield totals of oxidized products inconsistent with the conversion of methane, resulting in 168% yield of total products. As seen in previous screen reactions, the removal of sieves, Run 2, results in a 137% yield of total products based on methane, clearly not accounting for the over production of methyl acetate. The over production can be attributed to the facile decomposition of the peracetic acid generated *in situ*, and should produce a net sum of all carbonyl containing species in the form of carbon dioxide, Equation 3-4.

The discrepancy between total oxidized products observed and methane conversion can be rationalized by following the experimental mass balance of the starting and ending concentration of carbonyl products compared to a theoretical mass balance based on zero decomposition. The difference in the actual and theoretical total is a close approximation to the amount of decomposition occurring during the lifetime of the reaction. For the theoretical mass balance to be feasible, due to the radical nature of the reaction, some assumptions must be made. First, no decomposition of the peroxyacid will occur. Second, the net difference in starting material and final concentration of anhydride

Table 3-2. Oxidation of **1** with methane in acetic acid/anhydride.

Run	MeOAc (mmol)	CO_2 (mmol)	Tot. Prod. (mmol)	Loss Carbonyl[b] (mmol)	Methane Conversion (mmol)
1	6.2	3.4	9.6	3.2	5.7
2[c]	5.4	1.7	7.1	2.2	5.2
3[f]	6.1	1.5	7.6	1.3	4.2
4[d]	1.3	1.7	3.0	2.0	<1
5[c,d]	1.5	1.1	2.6	1.0	<1
6[c,d,e]	1.1	1.6	2.7	--	--
7[e]	3.2	3.7	6.9	3.9	--

(a)Standard reaction conditions: $[Ru(dmp)_2(H_2O)_2](CF_3SO_3)_2$, $2.4x10^{-2}$ mmol; $CH_3C(O)OH$, 5 ml; $(CH_3CO)_2O$, 10 ml; 35% H_2O_2, 1 ml; 4-A sieves, 1.0 g; CH_4, 80 psi; 75 °C; 4 hours. (b) The loss of carbonyl is based on difference in actual and theoretical mass balance of all carbonyl containing compounds. The following are the removed component from each reaction: (c) 4-A sieves; (d) $[Ru(dmp)_2(H_2O)_2](CF_3SO_3)_2$; (e) CH_4; (f) 0.5 ml 35% H_2O_2.

represents the total water generated. The water trapped by the anhydride can be produced from three general sources: initial water introduced with the oxidant; ester formation; and hydrogen peroxide decomposition. Finally, the formation of acetic acid and ester must behave within two limiting cases based on constant starting concentrations of acetic acid and anhydride as 87 and 106 mmol respectively.

The first case assumes methanol does not react with the anhydride. For example, in Run 1, the total loss of anhydride due to water and generation of the corresponding acid during the lifetime of the reaction is 58.9 millimoles and 117.8 millimoles respectively. The theoretical total of acetic acid, including methyl acetate production, corresponds to 198.1 millimoles. The second case assumes all methanol generated reacts with the anhydride. Using Run 1 again as an example, the total loss of anhydride due to water and generation of the corresponding acid prior to ester formation during the lifetime of the reaction is 52.2 and 104.4 millimoles respectively. The reaction of all methanol formed (6.7 millimoles) with anhydride, generates an additional 6.7 millimoles of acid, and 6.7 millimoles of methyl acetate corresponding to a total acetic acid production of 117.8 millimoles. In both cases considered, the *in situ* generation of acetic acid is not dependent upon the pathway of ester formation and the analogous argument can be made for peroxy acid formation via all hydrogen peroxide reacting with acid or anhydride. Therefore, the subsequent formation and decomposition of the peroxyacid will affect the mass balance of acetic acid alone.

The mass balance does not address the more important problem of determining the extent to which the methyl acetate observed is being produced from peroxy acid decomposition, Figure 3-1. If each instance of peracetic acid decomposition produces methyl acetate, one equivalent of CO_2 would be produced. Based on the mass balance of the trapping of methanol and peroxy acetic acid formation and decomposition, it can be concluded that at least 30% of the observed ester formed in Run 1 must result from the oxidation of methane.

Referring again to Table 3-2, Runs 4, 6 and 7 represent the most important experiments where the two main components, methane and catalyst, have been removed from one or more of the reactions (see footnote Table 3-2). With no substrate present, one of two general routes for the generation of methanol is eliminated. If methyl acetate is observed, it can only result from decomposition, providing a viable source of methyl and hydroxyl radicals for the direct formation of methanol. In the absence of methane, Run 7,

$$\begin{array}{l}\left.\begin{array}{l}\left.\begin{array}{l}\left.\begin{array}{rcl}\mathrm{CH_3C(O)OOH} & \longrightarrow & \mathrm{CH_3OH + CO_2}\\ \mathrm{CH_3C(O)OOH + CH_4} & \longrightarrow & \mathrm{CH_3C(O)OH + CH_3OH}\\ \mathrm{H_2O_2 + CH_4} & \longrightarrow & \mathrm{CH_3OH + H_2O}\\ \mathrm{H_2O_2 + CH_3C(O)OH} & \longrightarrow & \mathrm{CH_3C(O)OOH + H_2O}\\ \mathrm{H_2O_2 + CH_3C(O)O(O)CCH_3} & \longrightarrow & \mathrm{CH_3C(O)OOH + CH_3C(O)OH}\end{array}\right]\mathbf{A}\\ \mathrm{CH_3OH + CH_3C(O)OH} \longrightarrow \mathrm{CH_3C(O)OCH_3 + H_2O}\\ \mathrm{CH_3OH + CH_3C(O)O(O)CCH_3} \longrightarrow \mathrm{CH_3C(O)OCH_3 + CH_3C(O)OH}\end{array}\right]\mathbf{B}\\ \mathrm{H_2O + CH_3C(O)O(O)CCH_3} \longrightarrow \mathrm{2\,CH_3C(O)OH}\end{array}\right]\mathbf{C}\\ \hline \mathrm{3\,H_2O_2 + 3\,CH_4 + 41/2\,CH_3C(O)O(O)CCH_3} \longrightarrow \mathrm{3\,CH_3C(O)OCH_3 + 5\,CH_3C(O)OH + CO_2}\end{array}$$

A

$$\begin{array}{rcl}\mathrm{CH_3C(O)OOH} & \longrightarrow & \mathrm{CH_3OH + CO_2}\\ \mathrm{CH_3C(O)OOH + CH_4} & \longrightarrow & \mathrm{CH_3C(O)OH + CH_3OH}\\ \mathrm{H_2O_2 + CH_4} & \longrightarrow & \mathrm{CH_3OH + H_2O}\\ \mathrm{H_2O_2 + CH_3C(O)OH} & \longrightarrow & \mathrm{CH_3C(O)OOH + H_2O}\\ \mathrm{H_2O_2 + CH_3C(O)O(O)CCH_3} & \longrightarrow & \mathrm{CH_3C(O)OOH + CH_3C(O)OH}\\ \hline \mathrm{3\,H_2O_2 + 3\,CH_4 + CH_3C(O)O(O)CH_3} & \longrightarrow & \mathrm{3\,CH_3OH + 2\,H_2O + CH_3C(O)OH + CO_2}\end{array}$$

B

$$\begin{array}{rcl}\mathrm{3\,H_2O_2 + 3\,CH_4 + CH_3C(O)O(O)CH_3} & \longrightarrow & \mathrm{3\,CH_3OH + 2\,H_2O + CH_3C(O)OH + CO_2}\\ \mathrm{CH_3OH + CH_3C(O)OH} & \longrightarrow & \mathrm{CH_3C(O)OCH_3 + H_2O}\\ \mathrm{CH_3OH + CH_3C(O)O(O)CCH_3} & \longrightarrow & \mathrm{CH_3C(O)OCH_3 + CH_3C(O)OH}\\ \hline \mathrm{6\,H_2O_2 + 6\,CH_4 + 5\,CH_3C(O)O(O)CH_3} & \longrightarrow & \mathrm{6\,CH_3C(O)OCH_3 + 10\,CH_3OH + 2\,CO_2}\end{array}$$

C

$$\begin{array}{rcl}\mathrm{6\,H_2O_2 + 6\,CH_4 + 5\,CH_3C(O)O(O)CH_3} & \longrightarrow & \mathrm{6\,CH_3C(O)OCH_3 + 10\,CH_3OH + 2\,CO_2}\\ \mathrm{H_2O + CH_3C(O)O(O)CCH_3} & \longrightarrow & \mathrm{2\,CH_3C(O)OH}\\ \hline \mathrm{3\,H_2O_2 + 3\,CH_4 + 41/2\,CH_3C(O)O(O)CCH_3} & \longrightarrow & \mathrm{3\,CH_3C(O)OCH_3 + 5\,CH_3C(O)OH + CO_2}\end{array}$$

Figure 3-1. Mass balance of methanol trap and peroxyacetic acid formation for acetic acid/anhydride with H_2O_2.

the 3.2 mmol of methyl acetate and 3.2 mmol of CO_2 (3.2 mmol loss of carbonyl) must then come from the decomposition of the peroxy acid. The peracetic acid would be expected to be unstable when exposed to an environment where the lifetime of the carboxyl radical is expected to be short. The above result further demonstrates that a significant proportion of the yields of methyl acetate present under standard reaction conditions can be attributed to the decomposition of the peroxy acid. According to the mass balance, the majority of CO_2 in Run 1 must come from decomposition.

The absence of catalyst in Run 4 decreases the extent of decomposition by a factor of three with little or no oxidation of the methane. The presence of 1.7 mmol of CO_2 and the loss of 2.1 mmol of carbonyl products in the carbonyl mass balance, which correlates well with experimental observations, further demonstrates that metal accelerates the decomposition to an extent that a significant amount of decomposition occurs. The observation that temperature alone is not capable of decomposing peracetic is important and is reflected in the low conversion of methane. Further investigation by excluding both methane and catalyst from Run 6, although redundant in light of the above results, shows little or no change in the amount of decomposition. Once again, the low conversion of methane in the absence of **1** provides evidence that temperature alone is not adequate to initiate the aggressive decomposition of the peroxy acid.

The CO_2 appears to be generated, or more appropriately the carbonyl lost from decomposition, approximates the amount of methyl acetate generated from sources other than the oxidation of methane. By taking the decomposition into consideration, a more reasonable result to the relative amount of methyl acetate produced from the oxidation of methane can be seen. Thus, for Run 1, the methyl acetate generated from methane is approximated to be 3.0 mmol with 0.2 mmol of CO_2 generated from over oxidation. Based on 3.2 mmol of total oxidized products a 94 % selectivity to methyl acetate exists. The excess methyl acetate not accounted for by mass balance provides conclusive evidence that methane is oxidized.

An accurate quantification of methyl acetate being generated from methane by using enriched deuterium and ^{13}C samples to trace product sources proves uninformative in the acetic acid/anhydride co-solvent system [43]. For example, by using CD_4 the alkyl radical derived from the solvent will extract a proton, generating two species that upon further reaction can proceed by a cascade of further abstractions via two distinct pathways, Figure 3-3. Neither pathway is preferential but statistically, (denoted by the 1 or 3) depending on the abundance of either hydrogen or deuterium, one pathway will occur with a higher frequency. In a system with extensive decomposition, the end result is a mixture of labeled species from the solvent and substrate. Similar reactions can be seen if the methyl(s) of the co-solvents have been labeled. The complete mixing of deuterium prevents the determination of the product source of methyl acetate. ^{13}C labeling experiments allow observation of the evolution of an enriched signal as $^{13}CO_2$ from the solvent or methyl acetate from labeled methane is produced. This can provide relative rates of decomposition or oxidation, but it is not quantitative.

Reactions Using Propionic Acid and Propionic Anhydride

Upon substitution of propionic acid/anhydride for acetic acid/anhydride, the decomposition of the peroxy acid and resultant product yields can be observed directly.

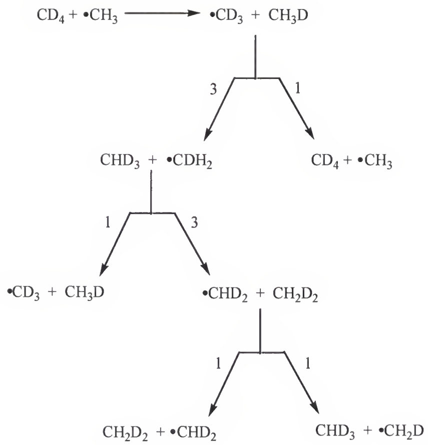
$CD_4 + \bullet CH_3 \rightarrow \bullet CD_3 + CH_3D$
3
1
$CHD_3 + \bullet CDH_2$
$CD_4 + \bullet CH_3$
1
3
$\bullet CD_3 + CH_3D$
$\bullet CHD_2 + CH_2D_2$
1
1
$CH_2D_2 + \bullet CHD_2$
$CHD_3 + \bullet CH_2D$

Figure 3-2. Product cascade from successive hydrogen atom abstraction from the parent d^4-methane substrate. Complete scrambling is represented in a tier down format resulting in the 4 distinct products CD_4, CH_3D, CH_2D_2 and CHD_3.

The stability of perpropionic acid in the presence of metals and elevated temperature is closely related to that of the acetic system. In propionic acid/anhydride, the decomposition of the peroxy acid yields **ethyl not methyl** radicals. The mass balance can now be deconvoluted because all products can be tracked directly without the production of the methyl ester coming from more than one source. With only one source for the production of methanol, an accurate determination of the true amount of CO_2 resulting from the oxidation of methane is provided.

Under standard conditions, Run 8, the propionic co-solvents display reactivity similar to the acetic system producing 5.3 mmol of methyl propionate, 1.2 mmol of ethyl propionate and 1.6 mmol of CO_2. The propionic acid/anhydride solvent results in **higher conversions of methane**, with less decomposition of the peroxy acid. With decomposition products clearly traceable, the propionic system under mild conditions shows the remarkable ability to oxidize methane. For this system, the amount of products does not exceed the theoretical conversion of methane, but this observation can be misleading. To be accurate, CO_2 must be adjusted by subtracting the amount attributed to decomposition. The number of moles of ethyl propionate is used to correction for the decomposition of the peroxy acid. Accounting for decomposition, a total of 0.4 mmol CO_2 and 5.7 mmols of total products are generated exclusively from the oxidation of methane. The respectable selectivity to methyl propionate (76% based on original total products) has improved to 93% based on adjusted total products. The 5.3 mmols of methyl acetate corresponds to 220 total turnovers or 55 turnovers per hour. Because of the relatively high rate of conversion at low-temperature and pressure, this system is competitive with current processes that use either dioxygen or hydrogen peroxide to oxidize methane [5-12,18-21].

Another series of systematic experiments was performed to determine the effects of decomposition by removing components from the propionic system as shown in Table 3-2. The experiments to note are 8, 11 and 12 where the removal of methane and catalyst are compared to standard reaction conditions (see footnote Table 3-2). To be thorough, we have removed the catalyst from Run 11 resulting in a five-fold decrease in methyl propionate. From Run 11, 0.3 mmol of methyl propionate were produced, and the identification of decomposition products suggest that perpropionic acid is decomposing. The decomposition initiates the oxidation of methane by hydrogen atom abstraction via ethyl radicals. This is confirmed by both the production of 0.2 mmol ethane as well as the low concentration of ethyl propionate found. To insure methyl propionate is not produced from a radical side chain such as C-C bond cleavage, Run 12 was performed in the absence of the substrate. The result of Run 12 shows no methyl propionate in the product analysis as expected, with ethyl propionate and CO_2 as the intended products of decomposition.

The metal is a vital component in both systems as seen by the amount of methyl acetate produced in the presence of **1**. Similar reactions using $Ru(dmp)_2Cl_2$, $RuCl_3 \bullet 6H_2O$ and $[Ru(dmp)_2(H_2O)](PF_6)_2$ have demonstrated little or no reactivity. It is surprising that changing from one poorly coordinating anion to another would display such a remarkable change in reactivity. To provide insight into the unique reactivity of **1**, studies of both systems were conducted over variable time and temperature.

Table 3-3. The oxidation of methane in propionic acid/propionic anhydride[a]

Run	Me Propionate (mmol)	Et Propionate (mmol)	CO_2 (mmol)	Tot. Prod. (mmol)	Me Conv. (mmol)
8	5.3	1.2	1.6	6.9	7
9[b]	4.8	0.8	1.4	6.2	7
10[c]	5.1	1.3	1.4	6.5	6
11[d]	0.3	0.4	0.6	0.9	trace
12[e]	--	1.4	0.7	--	--
13[d,e,f]	--	trace	trace	--	--

(a) Standard reaction conditions: $[Ru(dmp)_2(H_2O)_2](CF_3SO_3)_2$, $2.4x10^{-2}$ mmol; $CH_3CH_2C(O)OH$, 5 ml; $(CH_3CH_2CO)_2O$, 10 ml; 35% H_2O_2, 1 ml; 4-A sieves, 1.0 g; Methane, 80 psi; 75 °C; 4 hours. The following are the removed component from each reaction: (b) 0.5 H_2O_2; (c) $1.2x10^{-2}$ $[Ru(dmp)_2(H_2O)_2](Otf)_2$; (d) $[Ru(dmp)_2(H_2O)_2](CF_3SO_3)_2$; (e) CH_4; (f) 4-A sieves.

Table 3-4. The oxidation of methane in the propionic acid/propionic anhydride: system adjusted for decomposition of perpropionic acid.

Experiment	Methyl Propionate (mmol)	CO_2 (mmol)	Total Product (mmol)	Methane Conversion (mmol)
8[a]	5.3	0.4	5.7	7
9[a]	4.8	0.6	5.4	7
10[a]	5.1	0.1	5.2	6
11[a]	0.8	--	0.8	trace

a. The CO_2 content has been adjusted from Table 2 for the amount of ethyl propionate present in each reaction.

In Figure 3-2, the temperature dependence of **1** in propionic acid/anhydride can be seen with no conversion of methane at or below 50 °C. Increasing the temperature above 50 °C, the oxidation of methane can be seen with optimum conversion at 70-80 °C. The temperature dependence of **1** is acceptable considering most current work takes place at or above 75 °C [37-39]. The lifetime of the reaction, Figure 3-3, is generally 4 hours. Recharging the system with anhydride and hydrogen peroxide results in little or no catalytic activity. A distinct change in color and the formation of precipitate after 2 hours suggests that **1** is decomposing in the presence of peroxides. Mass spectral analysis of reacting **1** with peracetic acid in water shows a consistent change of mass units in multiples of 14 (e.g., 14, 28, 42, 55) [44]. This change has been attributed to the methyl in the 2 and 9 position of being oxidized (loss of 2 Hydrogen and gain of Oxygen) in the presence of peroxy acids with the analogous result seen with hydrogen peroxide. The oxidation would increase the steric requirement of the dmp ligand and promote further degradation of the ligand. The degradation leads to the loss of coordination of dmp subjecting the destroyed complex to Fenton reactions, potentially forming insoluble hydroxides and acetyl complexes that eventually precipitate from solution [4,5,14].

Reactions in Carboxylic Media with O_2 as Oxidant

The limitations of the acetic and propionic acid/anhydride system using hydrogen peroxide prompted the change to dioxygen as the oxidant in an attempt to prevent poisoning of the catalyst by aggressive decomposition. The activity of **1** in aqueous media with O_2 as an oxidant has been demonstrated [41]. Initial attempts at oxidation were performed in acetic acid, Table 3-4. The acetic system was used prior to discovering

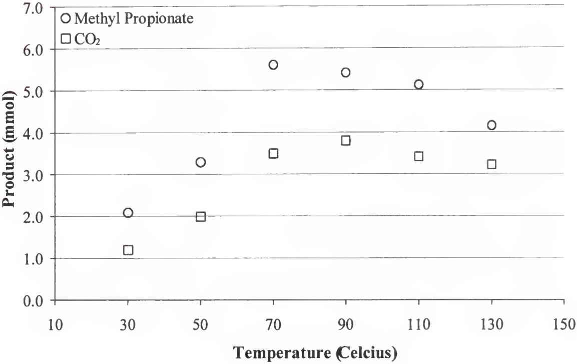

Figure 3-3. Effect of temperature on methane oxidation in propionic acid/anhydride. Reaction conditions: $[Ru(dmp)_2(H_2O)_2](CF_3SO_3)_2$, $2.4x10^{-2}$ mmol; $CH_3C(O)OH$, 5 ml; $(CH_3CO)_2O$, 10 ml; 35 % H_2O_2, 1 ml; 4-A sieves, 1 g; CH_4, 80 psi; 4 hour reaction time.

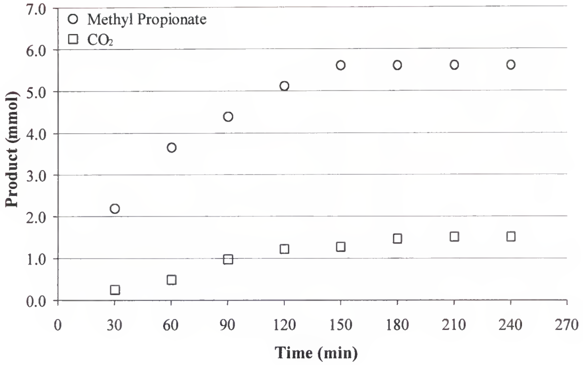

Figure 3-4. Effect of time on methane oxidation in propionic acid/anhydride. Reaction conditions: $[Ru(dmp)_2(H_2O)_2](CF_3SO_3)_2$, 2.4x$10^{-2}$ mmol; $CH_3C(O)OH$, 5 ml; $(CH_3CO)_2O$, 10 ml; 35 % H_2O_2, 1 ml; 4-A sieves, 1 g; CH_4, 80 psi; 75 °C

the propionic acid as a complimentary and superior cataytic system. The acetic system still adds insight into the complex catalytic system being studied.

Screen Run 12, over a time period of 48 hours, resulted in 17% conversion of methane with 19 % selectivity to methyl acetate. The low selectivity to methyl acetate was compensated for by lowering the amount of peroxide added to the system, Run 13. The conversion of methane drops dramatically, but selectivity to methyl acetate improves to 50%. The peroxide efficiency for Runs 12 and 13 is greater than 100%. When the peroxide efficiency is greater than 100%, an alternative oxidant must be involved in the conversion of methane. Dioxygen undoubtedly serves as the additional oxidant and this finding is not surprising considering the autoxidative conditions of the system being studied. To make sure that oxidation does not exclusively come from peroxy acid decompostition, the addition of peroxide was eliminated from Run 14. This established a control experiment where the metal does not participate in the oxidation without assistance of an unstable peroxy acid in solution. By removing only the catalyst from the system, Run 15, the absence of any reactivity intimates that the peroxy acid must be stable in small quantities. After 48 hours, iodometric titrations were performed on Run 15 to confirm the existence of peroxides in solution. Surprisingly, peroxide was found in Run 15. Apparently, it takes higher concentrations for the peroxy acid to undergo autocatalysis generating methyl acetate.

The inconsistent conversion found in Runs 12 and 13 was resolved by using only anhydride as the solvent. When acetic anhydride was used in place of acetic acid, the stability and reproducibility of the catalytic system increased dramatically. The cause of this increased stability, other than the change from glass hydrogenation apparatus to a

Table 3-5. Oxidation of methane in acetic acid and anhydride using O_2.

Run	Selectivity to $CH_3C(O)OCH_3$ mmol	CO_2 Conversion mmol	H_2O_2 Efficiency (%)	CH_4 Conversion (%)
12[a,b]	0.4	0.6	>100	17
13[a,c]	0.2	0.2	>100	6
14[a,d]	0	0	0	0
15[a,e]	0	0	0	0
16[f]	4.5	0.5	>100	2
17[f,g]	3.6	1.5	>100	7

(a) Reaction conditions: 6.6×10^{-5} moles **1**, 20 ml glacial acetic acid, 20 ml acetic anhydride, 20 psi CH_4, 40 psi air, 75 °C, 48 hours. (b) 250 µl 30% H_2O_2. (c) 150 µl 30% H_2O_2. (d)Absence of H_2O_2. (e)Absence of catalyst. (f)Reaction conditions: 5.0×10^{-5} moles **1**, 20 ml acetic anhydride, 3 ml *ortho*-dichlorobenzene, 100 µl 30% H_2O_2, 300 psi methane, 400 psi 1:1 He/O_2, 75 °C, 48 hours. (g)100 psi methane

sealed high-pressure autoclave, was not investigated. Reproducible reactions, Runs 16 and 17, were carried out in a high pressure autoclave in acetic anhydride resulting in low methane conversion (<10%) and methyl acetate selectivity above 70%. The low methane conversion rates were misleading due to the higher concentration present in the reaction vessel. The high rate of stirring and increased pressure of methane means that a higher concentration of methane was dissolved in the solvent leading to the higher conversions when compared to reactions performed in hydrogentation reactors. The increased conversion and stability in the system was promising, but acetic anhydride was abandoned at this time for propionic anhydride.

Propionic anhydride reactions were carried out under identical conditions used for the acetic anhydride system, Table 3-5. Run 18 represents a control experiment, which compares the change in reactivity upon removal of propionic acid. After 48 hours on stream, 7 mmol of methane was converted to 5.3 mmol (77%) methyl propionate. When the catalyst was removed, Run 19, the reactivity dropped dramatically resulting in trace methane converted to 0.3 mmol (33%) methyl propionate. Removing methane, Run 20, resulted in decomposition products and no conversion of methane. Removal of both methane and catalyst, Run 21, resulted in almost no reactivity.

Table 3-6. Oxidation of methane in propionic acid and anhydride using O_2.

Run	Methyl Propionate, mmol	Ethyl Propionate, mmol	CO_2,, mmol	Methane conversion (%)
18[a]	5.3	1.2	1.6,	8
19[a,b]	0.3	0.4	0.6	--
20[a,c]	--	1.4	0.7	--
21[a,b,c]	--	trace	trace	--
22[d]	6.4	trace	trace	7
23[d,b]	trace	trace	--	--
24[d,c]	--	trace	trace	--

(a) Reaction conditions: 5.5 x 10^{-5} mmol **1**, 20 ml propionic acid, 20 ml propionic anhydride, 100 µl 30% H_2O_2, 300 psi CH_4, 250 psi 1:1 He/O_2, 75 °C, 48 hours.(b) Catalyst removed. (c) Methane removed. (d)Reaction conditions: Same as above with propionic acid removed

Using experimetnal conditions identical to previous runs except for the removal of propionic acid, Run 22, conversions of methane were comparable to Run 18 where the acid was present, but only traces of decomposition products were present. This system over 48 hours resulted in 266 turnovers or a turnover frequency of 5.5 turnovers per hour. Systematic removal of catalyst and methane, Runs 23 and 24, lead to no reactivity. This conclusively supports the need for **1** to be present for reactivity to commence and that the system is stable under elevated temperatures with small concentrations of peroxy acid present in solution. Following the lifetime of the anhydride reaction over a 96 hour time period, degradation of perpropionic acid is evident only after 72 hours online, Figure 3-4. The degradation of the catalyst, because of the use of dioxygen as the primary oxidant, has been curtailed.

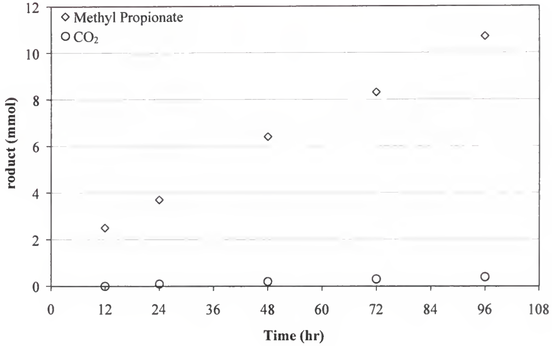

Figure 3-5. Lifetime of methane oxidation using **1** in propionic anhydride.

Conclusions

By limiting the amount of hydrogen peroxide added to the system, we have developed a system that has a long lifetime and an appreciable rate of oxidation. The acetic acid system was a complex system suffering from multiple pathways for generating methanol leading to products exceeding 100% total oxidized products. The observed high conversion was accounted for by comparing the actual and theoretical mass balance. The mass balance showed that the total compound containing the carboxylic functional group must be accounted for. The discrepancy between actual and theoretical carboxylic products directly translates into the amount of CO_2 produced from decomposition. From this study of peroxy acid decomposition, an alternative system was developed where decomposition products can be directly followed. The decomposition of perpropionic acid produced ethanol as a by-product. The only source of methyl propionate was from the oxidation of methane.

The short lifetime of the catalyst in high concentrations of peroxides forced the move to a less aggressive oxidant and lowered peroxide concentrations. By studying the acetic and propionic systems with and without the acid counter part of the solvent system, a stable and long lived catalytic system using propionic anhydride was developed.

CHAPTER 4
HOMOGENEOUS SELECTIVE OXIDATION OF ETHANE, PROPANE, BUTANE, ISO-BUTANE AND PENTANE

Introduction

The study of the oxidation of saturated hydrocarbons of C_2-C_5 chain length by $[Ru(dmp)_2(H_2O)_2](CF_3SO_3)_2$ (**1**) was prompted by the success of oxidizing methane. There is interest in investigating the potential for the unique reactivity of **1** toward larger substrates that typically undergo hydrogen atom abstraction. Due to the steric properties of the 2,9-dimethyl-1,10-phenanthroline (dmp) ligand, complex **1** is locked into a cis geometry. The cis geometry creates a pocket where the substrate can bind and react, Figure 4-1. The approach of the substrate to the active site can experience unusual

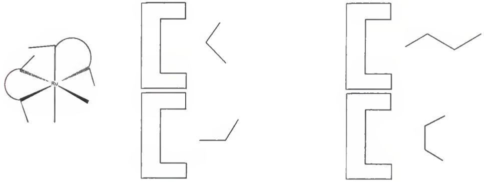

Figure 4-1. Schematic drawing depicting possible steric hindrance as the substrate approaches the active site of $Ru(dmp)_2(H_2O)_2^{2+}$.

interactions that can lead to preferential binding and reactivity. Small molecules such as methane or ethane can approach **1** in a non-discriminate manner but larger molecules, such as propane and butane, may encounter steric effects at the reactive site. The steric effects can lead to the potential for preferring an end-on approach versus side-on. The selective oxidation of hydrocarbons that typically comprise natural gas is a topic of much interest. The partial selective oxidation of saturated lightweight hydrocarbons be a valuable transformation. The intent of this study is to selectively oxidize hydrocarbons at an unfavorable position by taking advantage of the known steric requirements of the dmp ligand.

Lightweight hydrocarbons comprise natural gas, of which methane is the major component [25]. Methane is largely discarded due to the expense of transport and storage. The other components of natural gas, mainly C_2-C_4 alkanes, can be separated by distillation and are normally dehydrogenated to generate reactive alkenes. Ethylene and propylene are used in well known industrial productions of acetaldehyde, acetone, vinyl acetate, acrolein acrylic acid, methacrolein and methacrylic acid [37]. Butane is used is cracked and reformed to generate acetic acid, although the BASF carbonylation of methanol accounts for 95% of acetic acid production in the world [37]. Natural gas hydrocarbons are underutilized mainly due to the unselective oxygenation reactions associated with the general modes of autoxidation they undergo. Our first excursion into investigating selective autoxidation, although a contradiction, has proven to be promising.

Extending earlier work with the $Ru(dmp)_2^{2+}$ precursor, the oxidation of C_2-C_5 alkanes results in unusual reactivity for selected aliphatic hydrocarbons at the primary C-H bond. Two mechanisms, hydrogen atom abstraction and oxygen atom insertion, are proposed for similar systems that also oxidize alkanes [14]. The first mechanism, hydrogen atom abstraction, encompasses a large range of oxidation chemistry, the most notable of which is autoxidation, Equations 4-1 and 4-2. The abstraction of a proton produces alkyl radicals that are normally unselective. The alkyl radical will tend to abstract

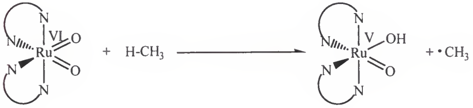

(4-1)

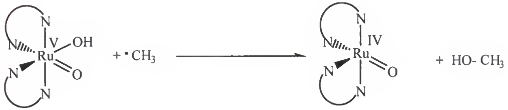

(4-2)

a hydrogen from the carbon with the highest degree of substitution. Terminal carbons have higher bond strengths than C-H bonds in the interior chain. The relative bond strengths of substituted carbons account for much of the observed products seen in similar oxidative systems [45-46]. The relative stability of alkyl radicals favors a more substituted carbon. A substrate, where primary, secondary and/or teritary carbons exist, will isomerize to a carbon radical with higher substitution thereby increasing stability. The isomerization is due in part to the weak C-H bond of the tertiary carbon. [47-49].

Isomerization is a fast process and the resultant alkyl radical reacts immediately with an oxidant. As this lifetime shortens concerted mechanisms or preferential binding of substrate prevails, thus primary products can become more predominant. In the hydrogen abstraction mechanism, the *cis*-$\{Ru^{VI}(O)_2\}^{2+}$ moiety can abstract a hydrogen atom to produce an alkyl radical. The radical can react with the hydroxo ligand "rebounding " to generate a hydroxylated product.

Oxygen atom insertion, a concerted mechanism Equations 4-3 and 4-4, involves a five coordinate carbon similar to CH_5^+. The three-center intermediate undergoes scission of the C-H bond forming a coordinated alcohol, which is displaced from the ruthenium complex. The oxygen atom insertion mechanism is proposed for the epoxidation of alkenes by ruthenium-oxo complexes by way of a non-radical mechanism [50-52].

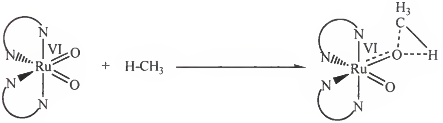

(4-3)

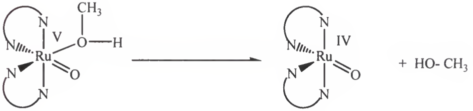

(4-4)

In an earlier report from this laboratory, the activation of alkanes by ruthenium complexes of derivatized phenanthroline ligands were reported to catalyze reactions that proceed by a combination of hydrogen abstraction and electron transfer. These catalysts appear to undergo reactivity mechanistically similar to oxygen atom insertion. The Hammet correlation of these catalysts, however does not correlate well to oxygen atom insertion and are known as proton coupled electron transfer [51]. Several other ruthenium polypyridyl complexes, chiefly work by Che and coworkers, have been suggested to proceed through a proton coupled electron transfer mechanism [24,51].

Earlier work has demonstrated the activation of methane under mild conditions using a ruthenium-oxo complex [33]. This report involves the oxidation of C_2-C_5 alkanes with *cis*-$[Ru(dmp)_2(H_2O)_2][CF_3SO_3]_2$ and hydrogen peroxide. The metal catalyst has shown surprising selectivity for the oxidation of the primary C-H bond in propane and butane. Propane has been used as a probe substrate to investigate the catalyst selectivity for primary and secondary C-H bonds.

Experimental

Reagents

cis-$[Ru(dmp)_2(H_2O)_2][CF_3SO_3]_2$ was synthesized as previously reported [42]. Acetonitrile, 99% ethanol, ortho-dichloromethane, pentane, 35 % H_2O_2, and Analytical standards for propane, butane and pentane were purchased from Aldrich and used as received. All gases were used as received from Matheson Gas Company. All oxidations were carried out in 250 ml glass hydrogenation batch reactors as previously described [28]. A series of nitrogen gas purges were used (approximately 40 psi) to remove air from the reactor. The purge was followed by a series of substrate purges to provide minimal out source contamination.

Analyses

Analysis and quantification of liquid phase products were carried out using a Hewlett-Packard 5890 Series II Gas Chromatograph equipped with an FID detector and outfitted with a 30 m HP 50+ (50% Ph Me Silicone Gum; 1 μm thickness). Gas bound products were analyzed using a Varian 3700 Gas Chromatograph outfitted with a TCD detector carrying a 15 ft Carboxen Column, 1 μm thickness. Concentrations of the substrate and products were quantified by employing ortho-dichloromethane as the liquid based internal standard.

Oxidation Procedure

A typical reaction mixture consisted of 60 ml of acetonitrile, 40 psig total pressure for gaseous reactants, 1.6×10^{-4} moles of catalyst and 5 ml (5.0×10^{-2} moles) of 35% hydrogen peroxide. Experiments in the absence of oxidant, catalyst, substrate, or combination of the previous were performed as blanks. All reactions were cooled for 30 minutes in ice before disassembly of the apparatus and subsequent analysis.

Selectivity to any product is the moles of a given product divided by the total moles of all products formed expressed as a percent. The percent peroxide efficiency is the moles of H_2O_2 needed to account for all the oxidized products divided by the moles of H_2O_2 consumed. The percent conversion of alkane is the moles carbon in the oxidized products divided by the moles of alkane added to the reactor.

Safety Precautions

The heating of a hydrocarbon in the presence of a large concentration of oxidant (i.e. H_2O_2) can lead to free radical induced detonation. Care must be taken to use dilute conditions to prevent deleterious reactions from occurring. Extreme caution should be taken during the charging and disassembly of the experimental apparatus. Proximity to electrical devices should be avoided, and thorough cooling of the apparatus is recommended before disassembly.

Results and Discussion

$[Ru(dmp)_2(H_2O)_2](CF_3SO_3)_2$ Catalyzed Reactions of Selected Alkanes with H_2O_2

The oxidation of higher alkanes was carried out in glass hydrogenation reactors for 4 hours. Ovenight runs (>15 hours) were tested, but it was later determined that beyond 4 hours the activity of the catalyst decreases with all catalytic activity ceasing after 6 hours. The results of the oxidation of alkanes, ethane, propane, n-butane, iso-butane and pentane in acetonitrile are summarized in Table 4-1. Hydrogen peroxide and acetonitrile were used exclusively as the oxidant and medium for this study. A previous study of the oxidation of methane in acetonitrile was successful and was used as the basis for this study [28]. Propane, iso-butane and pentane were used as substrates to provide information about regioselectivity of **1** as chain length and carbon substitution are changed.

The oxidation of ethane results in an 18% conversion with selectivity: 2% to ethanol; 70% to acetaldehyde; 28% to acetic acid, corresponding to 22.3 turnover numbers with a turn over frequency (tof) of 5.6 hr^{-1}. The oxidation of ethane exhibits extensive over oxidation similar to the oxidation of methane in acetonitrile using H_2O_2 [28]. The experiments involving the oxidation of ethane were performed for completeness, and have no bearing on the regioselectivity of the catalyst. The result from ethane is similar to methane oxidations with considerable over oxidation present. It is interesting that acetaldehyde, a fairly reactive substrate, is the bulk product found in solution. The thermodynamic product for this reaction is acetic acid. It is unclear why the acetaldehyde, a kinetic product, is stable toward further attack by **1**. Several homogeneous

Table 4-1. Oxidation of C_2-C_5 alkanes using **1** with H_2O_2.

Substrate	Primary Alcohol (mmol)	Secondary Alcohol (mmol)	Tertiary Alcohol (mmol)	Aldehyde (mmol)	Ketone (mmol)	Acid (mmol)	Conversion (%)
Ethane	0.08	--	--	2.5	--	1.0	18
Propane	0.05	0.07	--	2.1	1.2	--	18
Butane	0.08	0.94	--	0.10	0.31	1.2	13
Iso-butane	0.04	--	3.9	--	--	--	21
Pentane	0.58	1.2/1.2[a]	--	2.2	1.9/2.6[a]	--	50

(a) The secondary alcohol for pentane is a mixture of alcohol in the 2 and 3 position as is the ketone mixture.

gas phase methane oxidation systems use ethane and propane as additives [52]. The use of additives accelerates the oxidation of methane by the C-C cleavage products of ethane and propane. There is very little C-C bond cleavage seen for this system, although CO_2 and methane were detected in trace amounts.

The oxidation of propane result in 18% conversion with selectivity: 2% 1-propanol; 2% 2-propanol; 61% propionaldehyde; 35% acetone, corresponding to 21.4 turnover numbers and a tof of 5.3 hr^{-1}. The bulk material found in solution was propionaldehyde, formed from the over oxidation of 1-propanol. This result is somewhat surprising since oxidations of propane generally result in acetone with only trace products resulting from oxidation at the primary position. Work with a similar ruthenium polypyridyl complex has found acetone to be the main product, and this pathway is the normal mode of oxidation of propane through hydrogen atom abstraction [9]. For the system studied here, primary products account for 63% of all products detected in solution, demonstrating an interesting shift toward primary products that is unprecedented and contrary to expected reactivity.

The oxidation of butane has a 1:1 product distribution of primary to secondary products and results in selectivity: 3% to 1-butanol; 36% to 2-butanol; 4% to butyraldehyde; 12% to butanone; 45% to butyric acid. The overall reactivity of the system results in a tof of 4.1 hr^{-1}. Butyric acid the main bulk product in solution whose pervading smell was evident during product analysis. The overall conversion of this system is low compared to other substrates, but follows a similar trend as the propane oxidation previously discussed. In this system, again primary carbon oxidation takes place with increased frequency compared to the more reactive secondary position.

Functionalization of propane (iso-butane), through substitution of a methyl group in the secondary position, changes reactivity. The oxidation of iso-butane generates the tertiary product expected. The conversion of iso-butane (21%) is similar to that of ethane and propane but generates predominantly one product, *t*-butanol with a tof of 6.1 hr^{-1}. The tertiary alcohol is very stable toward further oxidation, and has been used as a solvent in highly reactive oxidative systems [53]. A small amount of 2-methyl propanol present in the reaction mixture, but this species comprises less than 1% of the total products in solution.

Pentane is the only liquid hydrocarbon included in this study. The conversion is quite high (50%) and directly reflects the increased solubility in the oxidation medium. The resultant products are secondary alcohols and ketones combine for a total of 75% of products present with alcohols accounting for 62% of all secondary products. The remaining 25% of total products is primarily the aldehyde (58%).

The overall reactivity of the oxidations of ethane, propane, butane, iso-butane and pentane are depicted in Figure 4-2. The hydrocarbons with chain length >2 were initially expected to react preferentially at the secondary or tertiary position, but this system showed a surprising selectivity toward primary products for propane and butane. With iso-butane and pentane, the predicted products were found with the weaker C-H bond preferentially oxidized. Oxidation of higher alkanes by way of a hydrogen atom abstraction mechanism is expected to produce oxygenates at the weakest C-H bond. The change in selectivity for propane and butane was investigated further by adding a co-reductant ($CuCl_2$) to slow over oxidation and potentially shift the product distribution

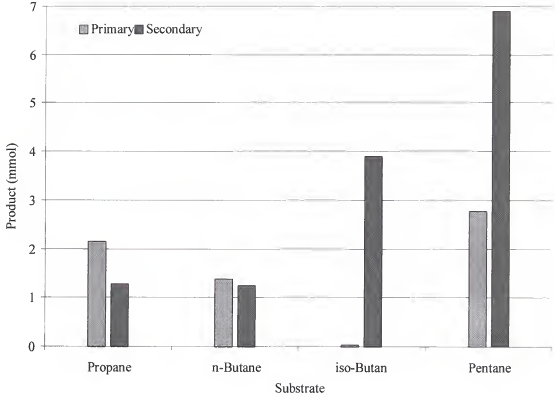

Figure 4-2. Product distribution for reactions of **1** with selected alkanes. Ethane has been omitted due to lack of secondary functionality.

away from over oxidized primary and secondary products. By shifting the product distribution, steady state concentrations become more accessible and the aftereffect of over oxidation can be directly compared as steady depletion is curtailed.

$[Ru(dmp)_2(H_2O)_2](CF_3SO_3)_2$ Catalyzed Reactions of Selected Alkanes with $CuCl_2$ and H_2O_2

When $CuCl_2$ is present in solution as a co-reductant, the increased rate of decomposition inhibits the over oxidation and conversely maintains a high concentration of alcohol. This accelerated decomposition provides information concerning the selectivity of **1** for the resultant alcohol with a parallel decrease in selectivity for the aldehyde and ketone, Table 4-2.

With the addition of $CuCl_2$, the catalyst in the oxidation of ethane induces a 22% conversion with selectivity: 4% to ethanol; 74% to acetaldehyde; 22% to acetic acid. The oxidation of ethane (tof 6.5 hr^{-1}) still generates extensive over oxidation products similar to the oxidation of methane. The resultant product distribution contains more alcohol as compared to the reaction without co-reductant, yet has increased concentrations of acetaldehyde. The increased concentration of acetaldehyde is anamolous with no conventional explanation. Interactions of intermediate products with the co-reductant can be proposed, but are beyond the scope of this study. This increase in conversion with $CuCl_2$ added is not expected for the peroxide decomposition proposal. The presence of CO_2 can make the actual conversion misleading if the source of CO_2 is from ethane.

The oxidation of propane results in an 18% conversion with selectivity: 6% to 1-propanol; 19% to 2-propanol; 61% to propionaldehyde; 14% to acetone. This corresponds to 21 turnover numbers and a tof of 5.42 hr^{-1}. The bulk material found in

Table 4-2. Oxidation of C_2-C_5 alkanes using **1** with H_2O_2 in the presence of $CuCl_2$.

Substrate	Primary Alcohol (mmol)	Secondary Alcohol/Ketone (mmol)	Tertiary Alcohol (mmol)	Aldehyde (mmol)	Ketone (mmol)	Acid (mmol)	Conversion (%)
Ethane	0.18	--	--	3.1	--	0.90	22
Propane	0.21	0.64	--	2.1	0.49	--	18
Butane	0.26	0.15	--	0.11	0.46	1.1	11
Iso-butane	0.01	--	3.5	--	--	--	18
Pentane	0.94	1.6/2.7[a]	--	1.3	1.3/1.3[a]	--	48

(a) The secondary alcohol for pentane is a mixture of alcohol in the 2 and 3 position as is the ketone mixture.

solution is again propionaldehyde, with little difference in overall conversion. The addition of $CuCl_2$ to the propane oxidation had produced a significant shift in the primary and secondary product distribution. A dramatic increase witnessed in concentrations of 1-propanol and 2-propanol and the corresponding decrease in acetone confirms that the co-reductant is retarding over oxidation and thereby increasing steady state concentrations.

The oxidation of butane in the presence of co-reductant results in an overall decrease in reactivity, but a dramatic change in product distribution toward primary oxidation products. The oxidation of butane results in selectivities: 13% 1-butanol; 7% 2-butanol; 5% butyraldehyde; 22% butanone; 53% butyric acid. In the presence of 1 equivalent of CuCl2, a three fold increase in the amount of primary and six fold increase in the amount of secondary alcohol is observed with a decrease in overall butane conversion to 11 %. The amount of aldehyde, ketone and acid products generated are relatively unchanged but 65% of all oxidized products were a result of an oxidation of a primary carbon in the substrate. The low conversion rate (13%) of butane is indicative of a special instance where reactivity and product distribution are not well defined and raise questions concerning branched versus linear alkanes and unusual distribution of expected products. The low conversion of butane, is a result of a change in the mechanistic and steric requirements of the system. This change results in a different reaction coordinate than say propane, producing a relatively large amount of acid compared to ketone. The overall conversion is again low compared to other substrates, but now follows the trend of propane closely where the majority of products formed are a result of the oxidation of the primary carbon. The shift in product distribution is even more pronounced than that

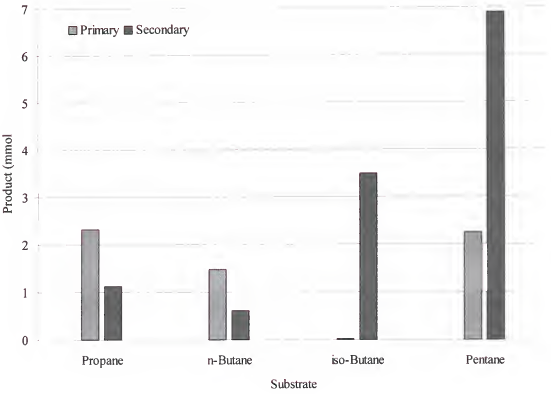

Figure 4-3. Product distribution of reactions of **1** with selected alkanes in the presence of 1 mol equivalent of $CuCl_2$.

seen for propane accounting for 71% of all products being generated in the primary position. Of the alkanes discussed, the most likely to produce the corresponding carboxylic acid, under the condition that sterics plays an important role, is pentane.

The conversion of iso-butane (18%) was similar to that of ethane and propane with *t*-butanol formed as the main product with a corresponding tof of 5.5 hr^{-1}. The concentration of observed 2-methyl propanol has decreased, which suggests that primary products are generated in the latter stages of the oxidation. The co-reductant limits the availability of oxidant. The lack of oxidant prevents the generation of primary products seen in reactions where $CuCl_2$ is not present.

The oxidation of pentane with co-reductant results in another high conversion (48%) with a tof of 14.3 hr^{-1}. The products are again mainly secondary alcohols and ketones accounting for 75% of total products with alcohols accounting for 62% of all secondary products. The remaining 25% of total products is comprised largely of aldehyde (58%).

The use of a co-reductant has proven to be useful in curtailing extensive over oxidation, which is seen in the shift in product distribution for both propane and butane. The addition of $CuCl_2$ provides high initial concentrations of oxidant needed for catalytic activity to commence while catalyzing the decomposition of H_2O_2 in latter stages of the reaction. The question regarding whether $CuCl_2$ is acting as a Fenton reagent is immaterial, for at this point, $Ru(dmp)_2^{2+}$ acts as a Fenton reagent to a some extent. Fenton side reactions are unavoidable in systems where autoxidation via hydrogen abstraction takes place. To rule out a competing mechanistic pathway via $CuCl_2$ catalyzed oxidation, a blank oxidation of propane was run in absence of **1** with $CuCl_2$. No oxidation of propane was observed.

$[Ru(dmp)_2(H_2O)_2](CF_3SO_3)_2$ Catalyzed Oxidation of Propane

The interesting change in selectivity seen in the oxidations of propane and butane in the presence of a co-reductant prompted the further investigation of propane in order to probe the selectivity of **1** at the primary and secondary C-H bonds. A typical distribution of products in the oxidation of propane with **1** was given in Table 4-1. After 4 hours at 75 °C, a 18 % conversion of propane was observed which corresponds to 3.4 millimoles of oxidized products. The selectivity for this reaction is surprising since 63% of the total oxidized products result from the activation of the primary C-H bond. The product analysis also was unable to detect the presence of carboxylic acid. The absence of propionic acid prompted a test for residual acidity in the reaction mixture. Using 0.0989N sodium hydroxide solution as the titrant, only trace acid was found (<0.1 millimoles). Thus the total moles of product formed, excluding the trace acid, would require 6.8 millimoles of H_2O_2, is a peroxide efficiency of 11%. The low peroxide efficiency and the high aldehyde content suggest that extensive over oxidation of 1-propanol is occurring. The over oxidation of the 1-propanol can occur by either direct oxidation by **1**, or oxidation of the free alcohol in solution by the large excess of H_2O_2 present.

To eliminate the possibility that the oxidation of propane can occur by H_2O_2 alone, a blank experiment was performed in the absence of **1**. Traces of aldehyde and alcohol (< 0.1 millimole) were present and were not accurately quantified. These observations strongly suggest that the metal catalyzed pathway is preferred. After four hours, the reaction rate slows markedly the H_2O_2 oxidizes the catalyst and fouls the reactivity of the system. Subsequent reduction of the initial amount of oxidant proved to be detrimental for producing high concentrations of products and accurate product analyses.

To help reduce the amount of over oxidation while keeping initial oxidant concentrations high, one mole equivalent of $CuCl_2$ was added to the propane oxidation reaction with all other conditions held constant producing the results shown in Table 4-2. The 1:1 $CuCl_2$ addition led to the same conversion of propane (18%) and a slight increase in selectivity for primary carbon products to 67%. In the initial stages of the reaction the only available substrate, propane, is converted to alcohol. The majority of the H_2O_2 is used for this purpose. During the latter stages of the reaction catalyzed by **1**, most of the peroxide is used to convert alcohol to aldehyde or ketone with a small amount used to oxidize propane. Decomposition, in the presence of $CuCl_2$, occurs concurrent with propane oxidation at a comparable or slower rate and, in the latter stages of the reaction, the oxidant is consumed before the last few percent of propane is converted and alcohol is oxidized.

The large peroxide concentrations at the start of the reaction, when alcohol concentrations are low, accounts for the high conversion of propane. As the alcohol concentration increases, the amount of available peroxide decreases rapidly due to decomposition induced by $CuCl_2$. The change in rate of decomposition accounts for the decrease in total conversion and increase in alcohol selectivity. Blank runs performed in the absence of **1** show that $CuCl_2$ does not catalyze the oxidation of propane.

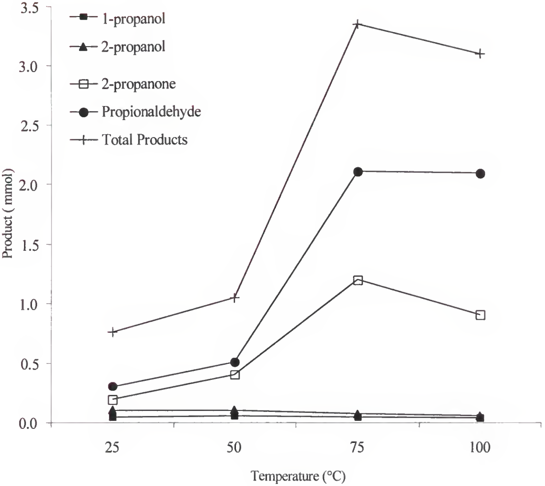

Figure 4-4. Oxidation of propane with *cis*-[Ru(dmp)$_2$(H$_2$O)$_2$](CF$_3$SO$_3$)$_2$ using H$_2$O$_2$ at varying temperatures.

Temperature Effects on the Oxidation of Propane

To further facilitate the decomposition of peroxide, the oxidation of propane was observed at different isothermal temperatures, Figure 4-4. The increased conversion with temperature is accompanied by an increase in the production of aldehyde and ketone. From 50 to 75 °C there is a distinct change in the ratio of promary to secondary products. At or below 50 °C the ratio of primary to secondary products is approximately 1:1. As the temperature increases to 75 °C the ratio of primary to secondary products is 2:1 respectively. The ratio of aldehyde to ketone follows this same pattern, being 1:1 below 50 °C and 2:1 at or above 75 °C. The primary to secondary alcohol ratio is always 1:1, and as the temperature increases, the concentration of each alcohol drops, corresponding to an increase in over oxidized products. The steady state concentrations should decrease as the system becomes more reactive.

The relative amounts of aldehyde to ketone are important in describing the relative reactivity of the primary and secondary C-H bond. The large quantity of aldehyde produced above 50 °C in the reaction suggests that **1** is preferentially oxygenating the primary carbon. The decrease in conversion at 100 °C is attributed to the fast decomposition of H_2O_2.

Adding $CuCl_2$ to the temperature study displays, a remakable change in the region from 25 to 100 °C, Figure 4-5. Only a small difference in product distribution is seen at 25 °C. The distribution of products begins to change, with a marked increase in the amounts of primary and secondary alcohol in solution, as temperature is increased above 50 °C. The ratio of primary to secondary alcohol changes from 1:1 at low temperature to

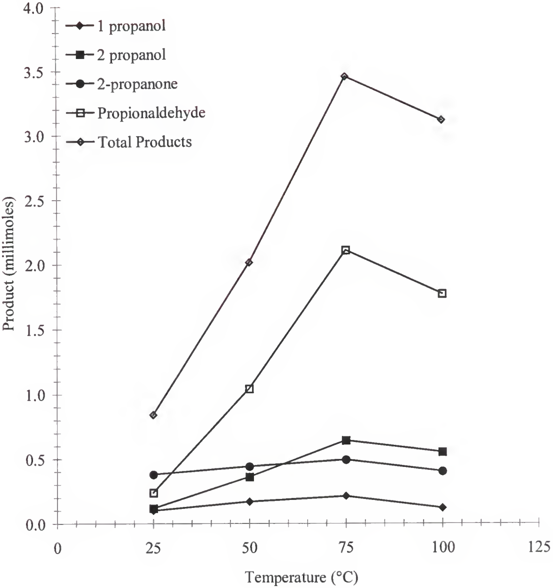

Figure 4-5. Oxidation of propane with *cis*-$[Ru(dmp)_2(H_2O)_2](CF_3SO_3)_2$ and 1 mol equivalent of $CuCl_2$ using H_2O_2 at varying temperatures.

1:4 at higher temperatures. At 75 °C, the amount of primary alcohol represents a 4 fold increase over previous reactions where $CuCl_2$ is not present. A more pronounced change in product distribution is the 9 fold increase in the secondary alcohol. The change in the ratio of secondary alcohol is so significant that the actual ratio of secondary alcohol to ketone switches from 1:1 at low temperature to 1.5:1 at high temperature respectively.

In the previous system, where $CuCl_2$ is not present, the steady state concentration of the most reactive species (the alcohol) decreases with heightened temperature. With the addition of a co-reductant, the concentration of alcohol actually increases, and in the case of secondary products, it becomes the dominant product. The detrimental amount of over oxidation is reduced due to the heightened decomposition of peroxide.

If the primary carbon is more reactive than the secondary carbon, this would lend some credence to the observed distribution of products. As the rate of decomposition of peroxide increases, the over oxidation of the alcohol decreases. This decrease in over oxidation results in higher concentrations of the alcohol. If $CuCl_2$ is not involved in the oxidation, and decomposition of peroxide is its sole function in the system, and an increase the number of equivalents at a constant temperature should produce the same result as temperature variation with 1 equivalent.

To test this theory, a systematic set of experiments were completed where varying equivalents of $CuCl_2$ were added in order to develop a profile of product distribution as a function of $CuCl_2$, Figure 4-6. The addition of 2 equivalents of $CuCl_2$ at 75 °C decreases the conversion of propane to 7% while shifting the distribution of products away from the over oxidation of the alcohol. At two equivalents, the alcohol ratio switches from a

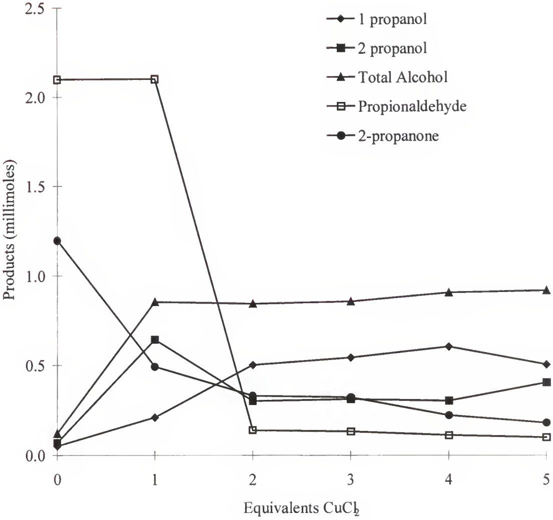

Figure 4-6. Oxidation of propane with *cis*-$[Ru(dmp)_2(H_2O)_2](CF_3SO_3)_2$ at varying equivalents of $CuCl_2$ using H_2O_2.

primary to secondary ratio of 1:2 at 1 equivalent to 2:1 at 2-4 equivalents. With no co-reductant present, the aldehyde represents 61% of all products formed. At two equivalents of $CuCl_2$, the alcohol represents c.a. 64% of all products formed. At copper chloride concentrations above a 2:1 ratio, small changes in conversion occur with the alcohol approaching 80% of all products formed. This small change in conversion is due to decomposition of the hydrogen peroxide, at this point, being a rate limiting step in the reaction.

Conclusions

The selective oxidation of propane by **1** proved to be an interesting system where selectivity to the primary C-H bond results in a 61% selectivity to propionaldehyde and a 35% selectivity to acetone. With a co-reductant present, the selectivity toward propionaldehyde is unchanged, but the selectivity to acetone drops dramatically to 14%. These products are formed due to the over oxidation reaction induced, not by the catalyst, but by the primary oxidant. Since the selectivity to propioinaldehyde is not affected by the co-reductant, the primary alcohol, being the direct precursor to the aldehyde, is the preferentially oxidized product. The observation that acetone is affected greatly by the co-reductant supports this supposition since the secondary carbon is much less reactive. The steric geometry of **1** could induce the preferential oxidation of alkanes at the primary C-H bond. It is unclear at this time whether the preferential oxidation at the primary carbon is due to sterics induced by the ligand, or is a function of the mechanism by which the substrate is being oxidized.

CHAPTER 5
LINKED ARYLOXIDES LIGANDS: SYNTHESIS AND CHARACTERIZATION OF ALKALI METAL CLUSTERS OF A PARTIAL CALIX[N]ARENE

Introduction

Comparable to glucose based cyclodextrins, calix[n]arenes accommodate a bowl like structure where oxygen donor atoms converge about the rim of a cavity created by the macrocyclic structure. Both structures are known for their ability to incorporate substrates inside the cavity created by the bowl, Figure 5-1 [54-59]. The cavity created in calix[n]arenes by linked aryloxides has reactive hydroxyl groups that, through intramolecular hydrogen bonding, predispose these ligands to bind metal complexes upon the rim of the cavity. Recent interest has focused on the preparation of metal complexes with calix[n]arenes where the metal center is left unprotected on the rim above the macrocyclic ring, in particular group 4-6 metals have been used to prepare several highly electrophilic complexes [58-60]. Floriani and co-workers have prepared tantalum complexes where it is beneficial to alkylate one of the oxygen donor atoms on the

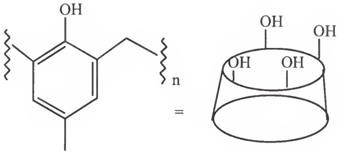

Calix[n]arene Calix[4]arene

Figure 5-1. Basic building unit of calix[n]arenes and a simple model depicting a cavity or bowl.

calixa[4]arene to reduce the anionic charge of the ligand [58,61,62]. The resultant ether linkage is susceptible to attack by the high valent metal center reducing the reactivity of the complex [62].

The large number of oxygen donors proves to be problematic when preparing complexes of group 5 metals. Koebner prepared a linear trimer of aryl oxides from the acid catalyzed reaction of *p*-cresol with a *bis*-hydroxy derivative, Figure 5-2 [63]. An interesting aspect of this trimer is its similarity to an incomplete calix[4]arene macrocycle. The lack of the fourth aryloxide group negates the need to methylate to reduce the build up of charge. It is worthwhile to note that the intra-molecular hydrogen bonding in a linear arrangement should make the ligand rigid enough to react with metal centers. A simple synthetic method can be devised where changing the *ortho* and *para* substituents on the aromatic ring can lead to ligand modification that confers varied steric and electronic properties on the metal center.

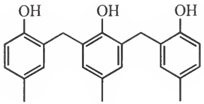

Koebner Trimer

Figure 5-2. Structure of the Koebner trimer.

Due to the missing fourth aryl oxide seen in calix[4]arenes, the Koebner trimer has the potential for adopting a u-shape, which is akin to the bowl desribed for calixarenes. The u-shape is a steric conformation and can impart interesting properties on a metal center. The metal centers bound in the protective u-shaped pocket of the trimer is quite different when compared to the unprotected metal normally seen for calix[n]arenes [4]. The similarity of calix[n]arenes and the Koebner trimer diverges beyond similar building blocks. As stated previously, the change in the environment of a metal center incorporated, in essence, into the wall of a bowl can possibly influence the reactive properties of the complex. Because of this possibility of the metal center having unique reactivity an examination of the Koebner trimer and the related properties of the metal complexes of early transition metals was begun [64].

Group 1 metals are known to form bridged structures with the anionic donors of aryloxide ligands, and a large and diverse collection of these cluster complexes are known [68-69]. Only a few examples of calix[n]arene clusters of group 1 metals are known [65-67]. This report describes the lithium and sodium salts of Koebner trimer type ligands that form unusual structures and have the potential as precursors for the preparation of reactive transition metal complexes [64].

Experimental

General Procedure

All reactions except the synthesis of L and L' were carried out in a N_2-filled Vacuum Atmospheres Nexus One drybox. Solvents were dried and distilled by standard methods. ^{1}H NMR spectra were obtained using a VXR 300 spectrometer using Varian VNMR software. HMQC and HMBC spectra were obtained using a Mercury 300 spectrometer also using Varian VNMR software. IR spectra were recorded on a Bruker Vector 22 spectrometer using OPUS software for data collection.

Synthesis of Linked Aryloxide Ligands

2,6-bis(3-t-butyl-5-methyl-2-hydroxy benzyl)-4-methyl phenol (L)

Following a modification of a literature procedure, [63,70-72] 6.25 g (37.16 mmol) of 2,6-bis(hydroxymethyl)-*p*-cresol and 30 ml heptane were combined in a 250mL three-neck flask. A seven-fold excess of 2-*t*-butyl-4-methyl phenol (c.a. 45 g) was added and the mixture was heated until homogeneous. Slow addition of 2 mL of concentrated hydrochloric acid initiated the reaction and the mixture was heated at refluxed for 1 hour

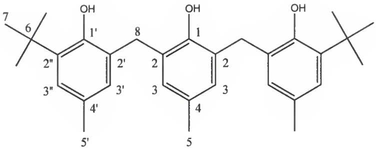

Figure 5-3. Numbering scheme for 2,6-bis(3-t-butyl-5-methyl-2-hydroxy benzyl)-4-methyl phenol (L).

using a Dean Stark trap to remove water (c.a. 3 ml). Heptane and excess phenol were then removed by vacuum distillation. The dark brown residue was refluxed in 40 ml of heptane for 1 hour. Upon cooling to room temperature, the resulting precipitate was collected by filtration, washed with cold heptane, and dried to afford 10.62 g (62%) of 2,6-bis(3-*t*-butyl-5-methyl-2-hydroxy benzyl)-4-methyl phenol as an off-white powder. Slow diffusion of pentane into a saturated solution of methylene chloride produced crystals suitable for X-ray analysis. ^{1}H NMR 300 MHz ($CDCl_3$) δ: 1.38 (s, 18H, 7), 2.23 (s, 9H, 5,5'), 3.82 (s, 4H, 8), 6.52 (s, 2H, 1':OH), 6.91 (s, 2H, 3), 6.96 (s, 4H, 3',3''), 7.86 (s, 1H, 1:OH). ^{13}C ($CDCl_3$): 20.6 (5), 20.9 (6), 30.2 (7), 31.5 (8), 34.3 (5'), 126.0 (3"), 127.0 (2), 127.5 (2'), 128.9 (3'), 129.5 (4'), 129.7 (3), 130.7 (4), 135.9 (2"), 147.6 (1), 149.2 (1'). IR KBr (cm^{-1}): ν(O-H): 3593, 3380, 3299. *Anal.* Calc. for $C_{31}H_{40}O_3$: C, 80.83; H, 8.75. Found: C, 80.60; H, 8.82%. Melting Point: 163-164 °C

2,6-bis(3,5-di-t-butyl-2-hydroxy benzyl)-4-methyl phenol (L′)

Following the procedure described above, the product was isolated in 68% yield as a white solid. Single crystals were obtained by diffusing pentane into a saturated diethyl ether solution. ^{1}H NMR (C_6D_6): 1.20 (s, 18H, 7), 1.40 (s, 18H, 9), 1.96 (s, 3H, 5), 3.78 (s, 4H, 8), 6.32 (s, 2H, 1':OH), 6.83 (s, 2H, 3), 7.20 (d, 2H, $^4J_{HH}$ 2.44 Hz, 3'), 7.33 (d, 2H, $^4J_{HH}$ 2.44 Hz, 3"), 7.59 (s, 1H, 1:OH). ^{13}C NMR (C_6D_6) 20.7 (5), 30.4 (7), 32.0 (9,), 32.3 (8), 34.6 (5'), 35.0 (6), 122.6 (2 & 3"), 125.7 (3'), 127.6 (2'), 129.8 (3), 131.1

(4), 136.0 (2”), 143.2 (4’), 148.2 (1), 150.1 (1’). IR KBr (cm^{-1}) ν(O-H): 3610, 3441, 3357. *Anal.* Calc. for $C_{37}H_{52}O_3$: C, 81.57; H, 9.62. Found C, 81.00; H, 9.62%. Melting Point: 150-151 °C

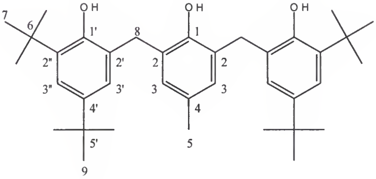

Figure 5-4. Numbering scheme for 2,6-bis(3,5-di-t-butyl-2-hydroxy benzyl)-4-methyl phenol (L′).

Synthesis of Lithium Salts of L and L′

Lithium 2,6-bis(3-t-butyl-5-methyl-2-hydroxy benzyl)-4-methyl phenolate (**1,2**)

A solution of *n*-butyl lithium (474 μl, 2.5 M in hexane, 1.184 mmol) was added to a rapidly stirred solution of 182 mg of L (0.395 mmol) in 10 ml of THF. After stirring for 4 hours, the solvent was removed under vacuum and the resultant pale yellow solid was washed with 5 ml pentane and dried to afford 173 mg (57%) of $Li_3L(THF)_4$ (**1**) as a white precipitate. Slow diffusion of pentane into a saturated THF solution yielded single crystals of **1**. ^{1}H NMR for **1** (CD_2Cl_2): 1.26 (s, 18H, 7), 1.60 (br m, 16H, THF) 2.02 (s, 3H, 5), 2.11 (s, 6H, 5’), 3.16 (d, 2H, $^2J_{HH}$ 15.14 Hz, 8), 3.31 (br m, 16H, THF), 3.80 (d, 2H, $^2J_{HH}$ 15.14 Hz, 8), 6.69 (d, 2H, $^4J_{HH}$ 1.95 Hz, 3), 6.75 (s, 2H, 3”), 6.80 (d, 2H, $^4J_{HH}$ 1.95 Hz, 3’). ^{13}C NMR for **1** (CD_2Cl_2): 19.4 (THF) 20.4 (5), 20.6 (6), 32.1 (7), 34.8 (5’), 35.2 (8), 68.1 (THF), 124.4 (3”), 126.9 (2), 127.6 (2’), 129.8 (3’), 130.2 (4’), 130.4 (3), 132.2 (4), 136.5 (2”), 159.0, (1’), 159.2 (1). *Anal.* Calc. for ($Li_3L(THF)_4$) $C_{47}H_{69}Li_3O_{67}$: C, 73.61; H, 9.07. Found: C, 73.37; H, 8.89%.

Substitution of ether for the reaction solvent utilized for the preparation of **1** afforded $Li_6L_2(Et_2O)_x$ (**2**) in 69% yield. The product contained varying amounts of residual ether and yields for **2** were calculated assuming complete loss of ether. NMR spectra were recorded on material obtained directly from the reaction mixture. ^{1}H NMR for **2** (CD_2Cl_2): 0.94 (m, Et_2O), 1.28 (s, 36H, 7), 1.99 (s, 6H, 5), 2.09 (s, 12H, 5'), 3.14 (d, 4H, $^2J_{HH}$ 15.14 Hz, 8), 3.18 (m, Et_2O), 3.83 (d, 4H, $^2J_{HH}$ 15.14 Hz, 8), 6.74 (d, 4H, $^4J_{HH}$ 1.95 Hz, 3), 6.78 (s, 4H, 3"), 6.83 (d, 4H, $^4J_{HH}$ 1.95 Hz, 3'). ^{13}C NMR for **2** (CD_2Cl_2): 15.0 (Et_2O), 20.4 (5), 20.6 (6), 32.0 (7), 34.8 (5'), 35.1 (8), 65.2 (Et_2O) 124.4 (3"), 126.9 (2), 127.7 (2'), 129.8 (3'), 130.3 (4'), 130.4 (3) , 132.2 (4), 136.6 (2"), 159.3 (1,1'). Single crystals of **2** suitable for crystallographic work were obtained from the slow diffusion of pentane into a saturated THF solution.

Lithium 2,6-bis(3,5-di-t-butyl-2-hydroxy benzyl)-4-methyl phenolate (3)

A solution of *n*-butyllithium (627 µl, 2.5 M, 1.568 mmol) was added to a rapidly stirred solution of 285 mg of L' (0.523 mmol) in 10 ml of ether. After stirring for 4 hours, the solvent was removed and the resulting gummy, orange solid was redissolved in benzene. After stirring for one hour, a white precipitate formed. The precipitate was collected by filtration, washed with pentane and dried resulting in 250 mg (85%) of $Li_6L'_2(Et_2O)_x$ (**3**). As above, the product contained varying amounts of residual ether and yields for **3** were complete loss of ether. Single crystals were obtained from the slow diffusion of pentane into a saturated solution of dichloromethane. ^{1}H NMR for **3** (CD_2Cl_2): 1.17 (s, 36H, 7), 1.29 (s, 36H, 9), 1.99 (s, 6H, 5), 3.20 (d, 4H, $^2J_{HH}$ 14.65 Hz, 8), 3.85 (d, 4H, $^2J_{HH}$ 14.65 Hz, 8), 6.78 (s, 4H, 3), 6.93 (d, 4H, $^4J_{HH}$ 2.93 Hz, 3'), 7.04 (d, 4H, $^4J_{HH}$ 2.93 Hz, 3"). ^{13}C NMR (CD_2Cl_2): 20.5 (5), 32.1 (7), 34.1 (9), 35.1 (8), 35.5 (5' & 6), 124.0 (Ph-*C*), 126.4 (Ph-*C*), 129.8 (Ph-*C*), 130.3 (Ph-*C*), 135.9 (Ph-*C*), 137.9 (Ph-*C*) Single crystals for elemental analysis were obtained from THF solution, and each cluster contained two coordinated THF molecules as well as three lattice solvents, confirmed by NMR analysis. *Anal.* Calc. for ($Li_6L'_2(THF)_2 \cdot 3THF$).$C_{94}H_{138}Li_6O_{11}$: C, 75.99; H, 9.36. Found: C, 75.84; H, 9.13%.

Synthesis of sodium complexes

Sodium 2,6-bis(3-t-butyl-5-methyl-2-hydroxy benzyl)-4-methyl phenolate (**4**)

A solution of 250 mg of L (0.543 mmol) in 10 mL of diethyl ether was treated with 88 mg of sodium methoxide (1.629 mmol). After stirring for 4 hours, the solvent was removed from the pale yellow homogenous solution under vacuum. The pale yellow solid was washed with 2 ml of pentane and dried to yield 269 mg (73%) of $Na_6L_2(Et_2O)_x$. The material contained variable amounts of coordinate ether, and the yield were calculated assuming two residual molecules per cluster. Single crystals of an analogous material, $Na_6L_2(Me_2CO)_4$ (**4**) were obtained from a saturated acetone/pentane solution and used in the crystallographic analysis. Material crystallized from THF, $Na_6L_2(THF)_4$ was utilized for the reported NMR spectra and elemental analysis data. ^1H NMR (CD_2Cl_2): 1.23 (s, 36H, 7), 1.63 (m, 16H, THF), 1.86 (s, 6H, 4), 2.07 (s, 12H, 4'), 3.05 (d, 4H, $^2J_{HH}$ 15.14 Hz, 8), 3.32 (m, 16H, THF) 3.60 (d, 4H, $^2J_{HH}$ 15.14 Hz, 8), 6.61 (s, 4H, 3), 6.73(s, 8H, 3'&3"). ^{13}C NMR (CD_2Cl_2): 20.0 (THF), 20.6 (5), 25.7 (5'), 34.2 (7), 34.6 (8) , 68.08 (THF), 120.7 (3"), 126.4 (2), 127.9 (2'), 129.5 (3'), 131.8 (3), 132.2 (2"), 137.0 (Ph-*C*). *Anal.* Calc. for ($Na_6L_2(THF)_4$) $C_{78}H_{106}Na_6O_{10}$: C, 69.83; H, 7.96. Found: C, 69.96; H, 7.89%.

Sodium 2,6-bis(3,5-di-t-butyl-2-hydroxy benzyl)-4-methyl phenolate (**5**)

Following the procedure described above, the cluster $Na_6L'_2(Et_2O)_x$ was obtained in 86% yield, assuming two residual ether molecules per cluster complex. As stated previously, sodium hydride can be used in place of sodium methoxide. The slow evaporation of pentane into a saturated solution of dichloromethane afforded the material utilized for analysis and characterized by X-ray crystallography, $Na_6L'_2(CH_2Cl_2)_4$ (**5**) ^1H NMR (CD_2Cl_2): 1.18 (s, 36H, 7), 1.26 (s, 36H, 9), 1.91 (s, 6H, 5), 3.14 (d, 4H, $^2J_{HH}$ 15.14 Hz, 8), 3.60 (d, 4H, $^2J_{HH}$ 15.14 Hz, 8), 6.62 (s, 4H, 3), 6.95 (d, 4H, $^4J_{HH}$ 2.44 Hz, 3'), 7.98

(d, 4H, ${}^4J_{HH}$ 2.44 Hz, 3''). ^{13}C NMR (CD_2Cl_2): 20.2 (5), 30.2 (7), 32.0 (9), 34.0 (8), 34.6 (5'), 35.0 (6), 123.1 (2), 128.2 (3''), 129.8 (3'), 131.6 (2'), 134.9 (3), 136.3 (2''), 163.0 (Ph-*C*). The crystal structure indicated that two of the three dichloromethanes were weakly bound to the sodium atoms and the analysis indicates partial loss of dichloromethane upon prolonged heating under vacuum prior to analysis. *Anal.* Calc. for ($Na_6L'_2(CH_2Cl_2)_2$) $C_{76}H_{102}Cl_4Na_6O_6$: C, 65.61; H, 7.39. Found: C, 65.73; H, 7.96%.

Collection and Reduction of X-ray Diffraction Data

Crystallization solvents are reported above. Single crystals were coated with Paratone-N oil, attached to a glass fiber, and transferred to a CCD X-ray diffractometer controlled by a pentium-based PC running the SMART software package.

The structures were solved by direct methods using SHELXS and were refined by full matrix least-squares and Fourier techniques using the SHELXTL-PLUS program package. Space groups for all of the structures were determined from an examination of the systematic absences in the data, and the successful solution and refinement of the structures confirmed these assignments. In general, all non-hydrogen atoms were refined anisotropically. Hydrogen atoms were assigned idealized locations and were given a thermal parameter equivalent to 1.2 times the thermal parameter of the carbon atom to which it was attached. In the cases where the *t*-butyl groups or solvent molecule were severely disordered, the atoms were refined isotropically without including hydrogen atom positions in the least squares refinement.

The asymmetric unit of H_3L contains three independent ligand molecules as well as two dichloromethane solvent molecules, one of which was disordered about an inversion center. The positions for the solvent molecules were both modeled with partial occupancies of 0.5. The hydroxyl hydrogen atoms were located in the difference Fourier map, and their thermal and positional parameters were refined. The structure of H_3L' has one complete molecule in the asymmetric unit as well as a diethyl ether solvate. One of the *t*-butyl groups was disordered over two positions, and the two positions were modeled site occupancy factors of 0.75 and 0.25. One of the terminal methyl groups of ether molecule was highly disordered and the carbon atom was refined isotropically on three positions with site occupancies of 0.5, 0.25 and 0.25. As with L, the hydroxyl hydrogen atoms were refined. Complex **1** crystallizes with 2 THF solvate molecules, one of which was disordered and modeled at half occupancy. All four of the hexanuclear clusters, **2**, **3**, **4**, and **5**, crystallized on an inversion symmetry operation. In structure **2**, one *t*-butyl group was disordered over two positions with site occupancy factors of 0.7 and 0.3. The thermal parameter of the carbons on the higher occupancy site was refined anisotropically while the lower occupancy site was refined isotropically. Along with **2**, a disordered pentane crystallized on an inversion center and it was assigned site occupancy of 0.5. with the central carbon atom was refined isotropically. In addition to the cluster, the structure of **3** contains a disordered dichloromethane molecule. The molecule was refined with two orientations for the chlorine atoms with site occupancy factors of 0.7 and 0.3. Structure **5** contained a highly disordered dichloromethane solvate molecule in the lattice. In the ligand backbone, one of the *t*-butyl groups resides over multiple positions with varied site occupancy factors, and one carbon atom was refined isotropically. The carbon atom of the methylene chloride bound to Na(1) is disordered over two positions about the inversion center, while the dichloromethane in close proximity to Na(3) resides in two distinct arrangements with site occupancies factors of 0.8 and 0.2 with the site closest to the metal having the highest density.

Results and Discussion

Synthesis of 2,6-Bis(3-t-Butyl-5-Methyl-2-Hydroxybenzyl)-4-Methyl Phenol and 2,6 Bis(3,5-di-t-Butyl-2-Hydroxybenzyl)-4-Methyl Phenol

Two different trimers were synthesized with either methyl or *t*-butyl groups in the *para* position on the ancillary aryloxide rings. The procedure was similar to the preparation by Koebner, where the ligands, 2,6-bis(3-t-butyl-5-methyl-2-hydroxybenzyl)-

4-methyl phenol (L) and 2,6-bis(3,5-di-t-butyl-2-hydroxybenzyl)-4-methyl phenol (L′), were isolated using a condensation method [72]. Starting materials are freely soluble in hydrocarbon solvents whereas the products, L or L′ exhibit slight solubility. Distillation of the excess phenol and recrystallization of the crude product readily isolates the trimer resulting in high yields of an analytically pure material. The reaction can be adapted by modifying the substituents in the 2 and 4 positions to produce trimers with a broad range of properties. Trimer ligands can be functionalized to produce ligands that posses a desired electronics and/or steric structure. This substitution allows the ligand and metal centers steric and electronic properties to be finely tuned with minimal effort. This is a simple methodology for designing ligands with desired traits for application in synthesizing reactive metal complexes.

Structure of H_3L and H_3L'

The solid state structures of H_3L and H_3L' adopt an s-shaped formation with the outer aryl groups located above and below the central phenoxide, Figure 5-5. Metric information for H_3L and H_3L' can be found in Table 5-1. The peripheral aryl groups contort in order to minimize the distance between oxygen atoms. The oxygen atoms form a linear arrangement with distances 2.748(2) and 2.654(4) Å in order to maximize hydrogen bonding contacts shown in Table 5-2. The immediacy of the oxygen atoms encourages intramolecular hydrogen bonding, similar to that seen in calix[n]arenes [54-55]. Two intra molecular interactions can take place at any one time in the trimer, leading to reduced strength of hydrogen bonding when compared to calix[4]arene. The infrared spectra of calix[4]arene is described by one stretching frequency at 3150 cm^{-1} [54].

Table 5-1. Crystallographic and Selected Parameters for 2,6-bis(3-*t*-butyl-5-methyl-2-hydroxy benzyl)-4-methyl phenol (H_3**L**) and 2,6-bis(3,5-di-*t*-butyl-2-hydroxy benzyl)-4-methyl phenol (H_3**L′**).

Compound	H_3**L** •0.29 CH_2Cl_2	H_3**L′**•Et_2O
Crystal data		
Formula	$C_{31.29}H_{40.58}Cl_{0.58}O_3$	$C_{41}H_{52}O_4$
Formula weight	482.86	618.91
Crystal system	Monoclinic	Monoclinic
Space group	$P2_1/c$	$P2_1/c$
a (Å)	11.8503(6)	16.9797(8)
b (Å)	42.540(2)	9.6532(5)
c (Å)	16.8835(8)	24.576(1)
ß (°)	95.028(1)	108.31(1)
V	8478.5(7)	3824.1(3)
Z	12	4
T (K)	173	173
R (%)[a]	7.83	6.80
wR^2 *(%)*[b]	20.38	20.25
Bond distances (Å) *and angles* (°)		
O(1)-C(1)	1.376(4)	1.402(3)
O(2)-C(7)	1.391(4)	1.385(3)
O(3)-C(13)	1.398(4)	1.374(3)
O(1)-C(1)-C(6)	120.7(3)	117.5(2)
O(1)-C(1)-C(2)	117.6(3)	120.2(2)
O(2)-C(7)-C(8)	116.1(3)	122.4(2)
O(2)-C(7)-C(12)	121.8(3)	116.2(2)
O(3)-C(13)-C(18)	122.6(3)	118.0(2)
O(3)-C(13)-C(14)	114.6(3)	120.9(2)

Table 5-1. continued

Compound	H_3**L** •1/3 CH_2Cl_2	H_3**L′**•Et_2O
O(1)-C(1)-C(6)-C(19)	2.9(2)	2.1(2)
C(1)-C(6)-C(19)-C(8)	-93.6(2)	-88.5(2)
C(6)-C(19)-C(8)-C(7)	95.9(2)	97.6(2)
C(19)-C(8)-C(7)-O(2)	2.0(2)	-1.1(2)

[a] $R = \Sigma| |F_o| - |F_c| | / \Sigma |F_o|$.

[b] $wR^2 = \{ \Sigma [w(F_o^2 - F_c^2)^2] / \Sigma [w(F_o^2)^2] \}^{1/2}$.

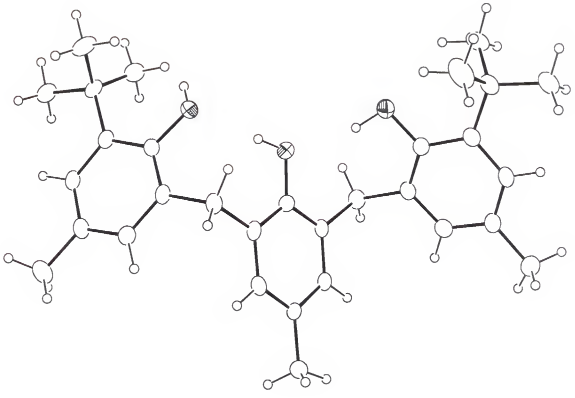

H$_3$**L**

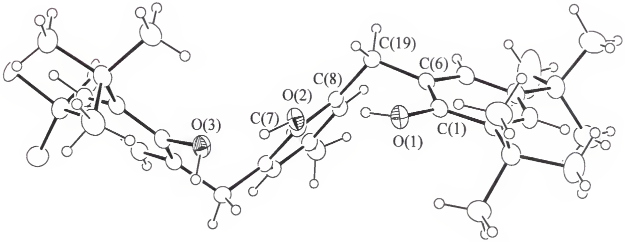

H$_3$**L′**

Figure 5-5. ORTEP diagrams of H$_3$L and H$_3$L′ showing 30% probability ellipsoids and atom labeling scheme. Selected distances, angles and hydrogen bonding are contained in Table 5-1,5-2.

Table 5-2. Selected Hydrogen Bonding for 2,6-bis(3-*t*-butyl-5-methyl-2-hydroxy benzyl)-4-methyl phenol (H_3**L**) and 2,6-bis(3,5-di-*t*-butyl-2-hydroxy benzyl)-4-methyl phenol (H_3**L′**).

	Donor-H	H...Acceptor	Donor...Acceptor	<(DHA)
Complex H_3L				
O1-H1A...O2	0.95(6)	1.82(6)	2.774(4)	174(5)
O2-H1B...O3	0.89(4)	1.87(4)	2.754(4)	176(4)
Complex H_3L'				
O3-H3...O2	0.91(5)	1.85(5)	2.748(4)	166.9(5)
O2-H2...O1	0.91(4)	1.77(4)	2.654(4)	164.0(4)
O1-H1...O10	0.90(4)	1.82(4)	2.684(3)	159.1(4)

Contrary to the single absorbance observed in the spectra for the calix[4]arene, the tris-aryloxide infrared spectra indicate three absorbances, one sharp stretch at 3593 cm^{-1} and two broad absorbances at 3380 cm^{-1} and 3299 cm^{-1}. This is consistent with the solid state structure shown in Figure 5-5, where three distinct interactions are depicted.

Synthesis and Structure of the Lithium Salts of L and L′

The addition of alkyl lithium reagents to solutions of H_3L and H_3L' initiates a reaction that is rapid and several different lithium products can be isolated. The product isolated is dependent upon the reaction conditions employed and the work-up strategy used. Tetrahydrofuran is an excellent ligand for the lithium atom and highly crystalline lithium salt clusters of H_3L and H_3L' can be isolated from the reaction mixture. The ^1H NMR of the isolated clusters show two sets of resonances for the linking methyl groups in the trimer structure. Unlike the free ligand, the two distinct resonances indicate that a rigid structure is maintained in solution. Diffusing pentane into a saturated solution of the lithium salt of H_3L in THF yields large, single crystals of $Li_3L(THF)_4$ (**1**) depicted in Figure 5-6. Crystallographic and geometric parameters for **1** are presented in Tables 5-3 and 5-4.

The ligand structure of **1** is similar to that seen for calix[4]arene with the exception that the fourth aryloxide required to complete the bowl is missing. The lithium atom located in the middle of the cavity links the outermost oxygen atoms forcing H_3L to adopt a bowl or u-shape geometry. The two remaining lithium atoms are situated above the rim of the ligand structure. They are joined together by the oxygen atom of a THF molecule and each forms a bridge between a central and outer oxygen atom of the trimer. Solvate molecules of THF complete the tetrahedral coordination sphere for each lithiium

Table 5-3. Crystallographic and selected parameters for $Li_3L(THF)_4$ (**1**), $Li_6L_2(THF)_2$ (**2**), $Li_6L'_2(CH_2Cl_2)_2$ (**3**).

Compound	**1**•1½ THF	**2**•½ C_5H_{12}	**3**•2 CH_2Cl_2
Crystal data			
Formula	C_{53} H_{80} Li_3 $O_{8.50}$	$C_{72.50}$ H_{90} Li_6 O_8	C_{78} H_{106} Cl_8 Li_6 O_6
Formula weight	873.99	1131.09	1464.87
Crystal system	Orthorhombic	Monoclinic	Triclinic
Space group	*Aba2*	*C2 / c*	$P\bar{1}$
a (Å)	31.591(2)	23.4714(14)	10.0696(7)
b (Å)	23.6549(12)	18.3750(12)	13.1879(9)
c (Å)	15.0567(8)	18.6545(11)	15.8852(11)
α (°)			84.656(1)
β (°)		121.5630(10)	78.035(1)
γ (°)			77.705(1)
$V(Å^3)$	11251.7(10)	6855.2(7)	2013.7(2)
Z	8	4	1
T (K)	173(2)	173(2)	173(2)
R (%)^a	7.48	8.63	7.72
wR^2 (%)^b	19.86	28.50	19.63

^{a} $R = \Sigma \mid |F_o| - |F_c| \mid / \Sigma |F_o|$.

^{b} $wR^2 = \{ \Sigma [w(F_o^2 - F_c^2)^2] / \Sigma [w(F_o^2)^2] \}^{½}$.

Table 5-4. Selected Bond Distances (Å) and Angles (°) for $Li_3L(THF)_4$ (**1**), $Li_6L_2(THF)_2$ (**2**), $Li_6L'_2(CH_2Cl_2)_2$ (**3**).

Compound	**1**•1½ THF	**2**•½ C_5H_{12}	**3**•2 CH_2Cl_2
Li(1)-O(1)	1.933(7)	1.989(9)	1.916(9)
Li(1)-O(3)	1.952(7)	1.981(9)	1.921(9)
Li(1)...Li(2)	2.773(9)	3.211(11)	3.102(12)
Li(1)...Li(3)	2.820(9)	2.476(12)	2.453(12)
Li(1)...C(7)	2.495(7)	2.319(10)	2.264(10)
Li(1)...C(8)		2.581(10)	2.524(10)
Li(1)...C(12)		2.624(10)	2.554(10)
Li(1)-O(10)	1.989(7)	1.910(9)	
Li(1)-Cl(1)			2.576(9)
Li(2)-O(1')		2.027(8)	2.008(8)
Li(2)-O(2)	1.899(7)	1.963(8)	1.985(9)
Li(2)-O(2')		1.970(8)	1.962(9)
Li(2)-O(3)	1.871(6)	2.024(8)	2.034(9)
Li(2)-O(20)	1.952(6)		
Li(2)-O(40)	2.086(7)		
Li(2)...Li(3)	2.619(8)	2.595(11)	2.617(11)
Li(3)-O(1)	1.876(7)	1.897(9)	1.913(9)
Li(3)-O(2)	1.889(7)		
Li(3)-O(2')		1.853(9)	1.826(9)
Li(3)-O(3)		1.914(9)	1.924(9)
Li(3)-O(30)	1.965(7)		
Li(3)-O(40)	2.080(7)		
O(1)-Li(3)-O(3)		101.0(4)	98.3(4)
O(1)-Li(1)-C(7)	93.1(3)	93.1(4)	95.3(4)
O(2)-Li(2)-O(2')		101.2(4)	101.7(4)

Table 5-4 continued

Compound	**1**•1½ THF	**2**•½ C_5H_{12}	**3**•2 CH_2Cl_2
(2)-Li(2)-O(3)	103.2(3)	95.6(3)	96.6(4)
O(3)-Li(2)-O(1')		167.4(5)	168.3(5)
O(2)-Li(3)-O(3)	102.5(3)		
O(3)-Li(1)-O(1)	126.4(3)	95.6(4)	98.3(4)
O(10)-Li(1)-O(1)	114.1(3)	120.4(4)	
O(10)-Li(1)-O(3)	114.4(3)	119.3(4)	
O(1)-Li(1)-Cl(1)			106.1(4)
O(3)-Li(1)-Cl(1)			119.1(4)
C(1)-O(1)-Li(1)	121.0(3)	151.3(4)	150.6 (4)
C(1)-O(1)-Li(3)	124.4(3)	113.2(3)	148.9(4)
C(7)-O(2)-Li(2)	123.1(3)	122.6(4)	120.1(4)
O(1)-Li(2)-O(20)	120.5(3)		
O(2)-Li(2)-O(20)	122.4(3)		
O(1)-Li(2)-O(40)	112.3(3)		
O(2)-Li(2)-O(40)	94.8(3)		
C(13)-O(3)-Li(3)		151.3(4)	150.6(4)
C(13)-O(3)-Li(1)	118.0(3)	111.6(4)	119.0(4)
O(2)-Li(3)-O(30)	124.8(4)		
O(3)-Li(3)-O(30)	120.8(3)		
O(2)-Li(3)-O(40)	95.3(3)		
O(3)-Li(3)-O(40)	109.1(3)		

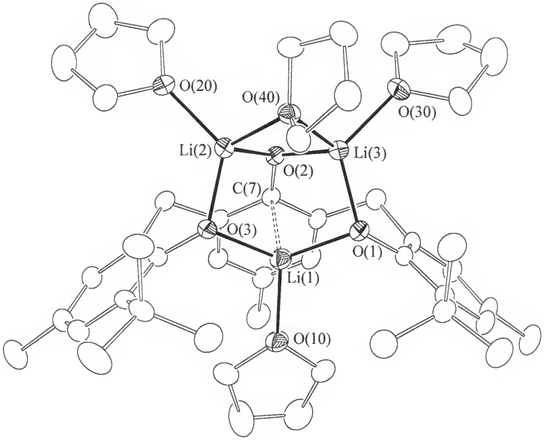

1

Figure 5-6. ORTEP diagram of $Li_3L(THF)_4$ (**1**) showing 30% probability ellipsoids and atom labeling scheme. Selected distances and angles are represented in Table 6-3,6-4.

atom. The central lithium adopts a pseudo tetrahedral geometry by interacting with the ipso carbon of the central phenoxide ring. The ipso interaction is quite long, 2.495(7) Å indicating that the lithium atom is between a trigonal and pseudo-tetrahedral geometry, but this interaction contributes to the stable bowl shape structure.

The lithium atoms form an isosceles triangle with a small separation of 2.619(9) Å and two metal-metal distances of 2.773(9)Å and 2.820(9)Å that are almost equivalent. The shorter distance is found between the two lithium atoms that share two bridging oxygen atoms. These two metal atoms vary in their distance to the aryloxide oxygen atoms from 1.876(7)Å to 1.899(7)Å. These distances are shorter than those found for the central lithium atoms with distances of 1.933(7)Å and 1.952(7)Å. The distances found in this cluster are all typical of lithium-aryloxide clusters where bond distances range from 1.775(7)Å to 2.020(2) Å [67]. By linking the aryloxides together, an asymmetric structure develops for L and L′. This is quite different when compared to the C_3 arrangement usually found for lithium-aryloxide complexes [68].

By using diethyl ether instead of THF, an expanded cluster of two ligands can be formed. This extended structure is produced with either L or L′ and its formation can directly attributed to changes in stability due to the weaker ether lithium interactions. The ether can readily be displaced by polar solvents used in recrystallization. Crystallization of the cluster of H_3L prepared from THF yields $Li_6L_2(THF)_2$ (**2**) as shown in Figure 5-7. A similar species can be isolated from methylene chloride with the formula $Li_6L'_2(CH_2Cl_2)_2$ (**3**) as shown in Figure 5-8. Crystallographic information for both **3** and **4** are can be found in Tables 5-3 and 5-4.

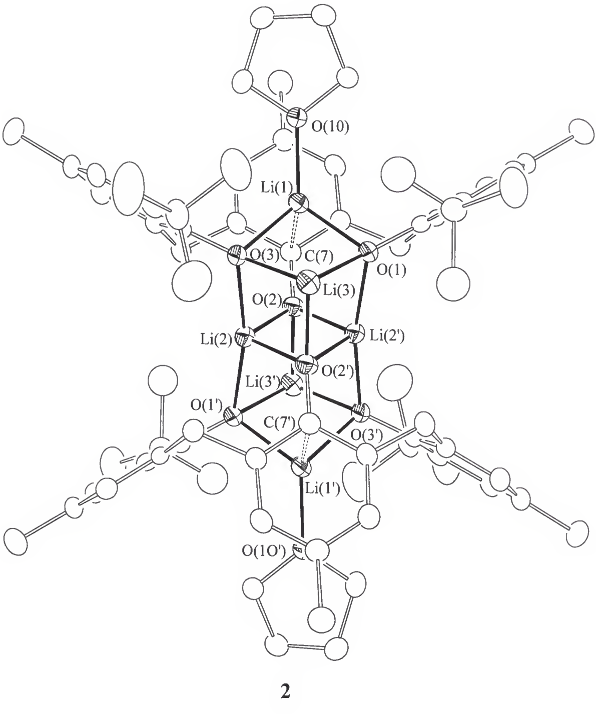

2

Figure 5-7. ORTEP diagram of $Li_6L_2(THF)_2$ (**2**) showing 30% probability ellipsoids and atom labeling scheme. Primed and unprimed atoms are related by an inversion center. For clarity, Only one orientation of the disordered *t*-butyl group is shown. Selected distances and angles are represented in Table 5-3,5-4.

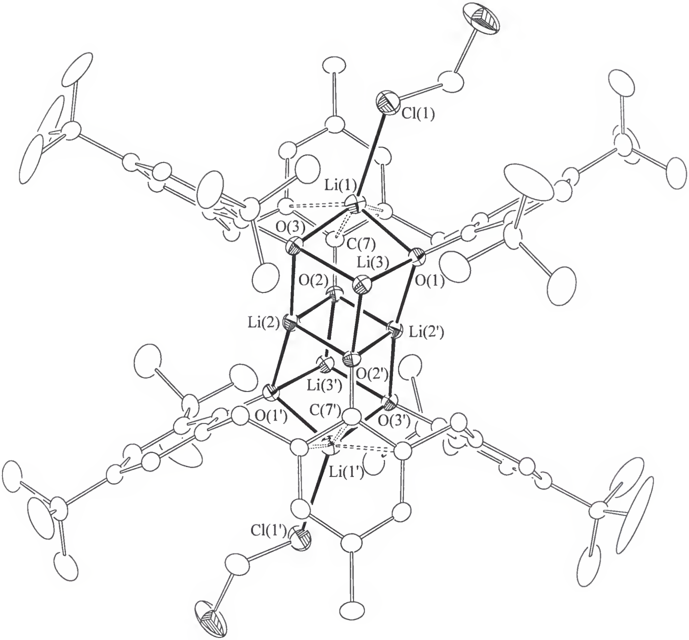

3

Figure 5-8. ORTEP diagram of $Li_6L'_2(CH_2Cl_2)_2$ (**3**) showing 30% probability ellipsoids and atom labeling scheme. Primed and unprimed atoms are related by an inversion center. Selected distances and angles are represented in Table 5-3,5-4.

The extended clusters of L and L′ form in the absence of THF (a good donor solvent) by increasing coordination number to compensate for the missing donor interaction. This increase in coordination number for the metals in **2** and **3** is accomplished by forming additional bonding interactions. These bonding interactions, or bridges, form between the metal atoms and the oxygen donor atoms of the aryl oxide trimer. These bridges include several that form between two ligand units in the same cluster.

The lithium atoms of **2** and **3** are found in three distinct coordination environments. The lithium atoms bridging between the central aryloxide oxygen atoms from the two ligands form a Li_2O_2 unit with an angle of 101.2(4)° in **2**. These same lithium atoms also interact with the outer aryloxide oxygen atoms of both ligands with and angle of 167.4(5)° in **2**. This angle is quite large when compared to *p*-t-butyl calix[4]arene, which has an angle of 151(1)° [66]. Two other lithium atoms occupy a distorted trigonal pyramidal environment located between the two outer aryl oxide oxygen atoms of one ligand and the central oxygen atom of the inversion related ligand. There is a long Li(3)-C(212) distance of 2.523(11) Å in **3**, which suggest that a weak interaction exists between the hydrogen atoms of the ligand *t*-butyl groups. The metal-aryloxide donors distances are asymmetric with bonds of 1.913(9), 1.924(9), and 1.826(9)Å. The first two bond distances are from the lithium atom to the outer aryloxide oxygen atoms of the same ligand. The last, short distance is between the lithium atom and the central oxygen atom of the symmetry related ligand. The final lithium environment is similar to that seen for the lone three coordinate lithium atom in **1**. In the cavity created by L or L′, the lithium binds to the two outer aryloxide oxygen atoms and the ipso carbon of the central phenoxide ring. The lithium also interacts with the donor atom of a solvent molecule.

The solvent interacting with the lithium atom in the cavity position imparts a strong influence over the bonding properties of that metal atom. By replacing a good donor such as THF with a weaker donor, the interactions of the metal atom with the ipso carbon and aryloxide oxygen atoms strengthen. When THF is included in the coordination sphere of **2**, the distances of the metal center to the ipso carbon and aryloxide oxygen atoms are 2.319(10), 1.989(9), and 1.981(9)Å respectively. Replacing the good donor with methylene chloride (considered a poor donor), the interaction in **3** is weak and the remaining interactions between the lithium atom and the ipso carbon and aryloxide oxygen strengthen. This change is distinct since the lithium-oxygen atom distances in **3** decrease by more than 0.06Å and the metal moves closer to the ipso carbon to a distance of 2.264(10)Å.

Synthesis and Structure of the Sodium Salts of L and L′

Using sodium hydride sodium methoxide in ether deprotonates the phenol groups of L and L′, producing clusters similar to those found for the lithium salts **2** and **3**. Attempts to prepare sodium clusters analogous to **1** were unsuccessful, possibly due to the inability of THF to stabilize the trimetallic cluster due to the increased size of the metal atom. When sodium clusters are isolated from ether, the ligands are quite labile with total loss of ether when the clusters are subjected to a vacuum atmosphere. Polar molecules can be incorporated onto the clusters after isolated from ether and by addition of the isolated cluster into the appropriate solvent. The clusters $Na_6L_2((CH_3)_2CO)_4$ (**4**) and $[Na_6L'_2(CH_2Cl_2)_3]_x$ (**5**) can be obtained from solutions of acetone and methylene chloride respectively. The clusters of **4** and **5** are illustrated in Figures 5-9 and 5-10. Crystallographic information can be found in Tables 5-5 and 5-6.

With the increase in size of metal atom, the solvent is allowed greater access to the metal centers. The smaller volume of the lithium cluster cores of **2** and **3** prevents solvent from binding to metal atoms other than those found in the center of the u-shaped bowl. The increased volume of the sodium clusters **4** and **5** allow solvent to interact with the sodium atoms linking the central aryloxide oxygen atom to the outer aryloxide oxygen atoms of the other ligand.

As was seen in the lithium clusters, the solvent modifies the geometry of the cluster. In cluster **4**, acetone interacts with the sodium atom situated in the u-shaped cavity. The interaction of acetone with the apical sodium atom in the ligand bowl results in ipso carbon atom and aryloxide oxygen atom distances of 2.739(3), 2.363(2), and 2.396(2)Å respectively. For a similar sodium crystal structure of $(NaOPh)_6$, the sodium atom to aryloxide oxygen atom distances average 2.31(1)Å with a short ipso interaction of 2.79(1)Å [69]. The shortest sodium metal-ipso interaction in *p*-t-butylcalix[4]arene is longer than that seen in **4**.

The same effect noted in **3** can be seen in **5** by substituting methylene chloride onto the cluster. The ipso carbon and aryloxide oxygen atom distances are 2.619(3), 2.280(3), and 2.338(3)Å respectively. The ipso carbon interaction has decreased significantly due in part to the poor donor qualities of methylene chloride. The sodium atom compensates for the decrease in electron density by increasing the interaction with the π-cloud of the central phenoxide ring approaching that of a Na-C single bond [73-74].

Table 5-5. Crystallographic and selected parameters for $Na_6L_2(Me_2CO)_4$ (**4**), $[Na_6L'_2(CH_2Cl_2)_3]_x$ (**5**).

Compound	**4**	**5**•$2CH_2Cl_2$
Crystal data		
Formula	$C_{74}H_{98}Na_6O_{10}$	$C_{79}H_{90}Cl_{10}Na_6O_6$
Formula weight	1285.46	1627.95
Crystal system	Monoclinic	Triclinic
Space group	$P2_1/n$	$P\bar{1}$
a (Å)	13.1739(8)	11.7956(9)
b (Å)	19.2332(12)	13.8242(10)
c (Å)	14.0181(9)	14.7874(11)
α (°)		107.537(1)
β (°)	97.184(1)	92.230(1)
γ (°)		109.474(1)
V (Å^3)	3524.0(4)	2141.5(3)
Z	2	1
T (K)	173(2)	173(2)
R (%)[a]	5.59	7.00
wR^2 (%)[b]	10.94	19.11

[a] $R = \Sigma \mid |F_o| - |F_c| \mid / \Sigma |F_o|$.

[b] $wR^2 = \{ \Sigma [w(F_o^2 - F_c^2)^2] / \Sigma [w(F_o^2)^2] \}^{1/2}$.

Table 5-6. Selected Bond distances (Å) and Angles (°) for $Na_6L_2(Me_2CO)_4$ (**4**), $[Na_6L'_2(CH_2Cl_2)_3]_x$ (**5**).

Compound	**4**	**5**•$2CH_2Cl_2$
Na(1)-O(1)	2.363(2)	2.280(3)
Na(1)-O(3)	2.396(2)	2.338(3)
Na(1)-O(10)	2.309(3)	
Na(1)…C(7)	2.739(3)	2.619(3)
Na(1)…C(8)	2.751(3)	2.750(3)
Na(1)…C(12)	2.796(3)	2.659(3)
Na(1)…Na(2)		3.842(2)
Na(1)…Na(3)	3.177(2)	3.146(2)
Na(1)-Cl(1)		2.858(2)
Na(2)-O(1')	2.290(2)	2.301(2)
Na(2)-O(3)	2.302(2)	2.304(2)
Na(2)-O(2)	2.320(2)	2.269(2)
Na(2)-O(2')	2.318(2)	2.317(2)
Na(2)…Na(3)	3.101(2)	3.125(2)
Na(3)-O(1)	2.404(2)	2.328(2)
Na(3)-O(2')	2.226(2)	2.190(2)
Na(3)-O(3)	2.376(2)	2.315(2)
Na(3)-O(20)	2.337(3)	
Na(3)-Cl(2)		3.255(2)
O(3)-Na(1)-O(1)	89.34(8)	89.77(8)
C(1)-O(1)-Na(1)	109.1(2)	150.4(2)
C(13)-O(3)-Na(1)	112.0(2)	152.2(2)
O(10)-Na(1)-O(1)	119.67(9)	
O(10)-Na(1)-O(3)	124.14(9)	
O(1)-Na(1)-Cl(1)		134.49(8)
O(3)-Na(1)-Cl(1)		103.55(7)

Table 5-6.continued

Compound	**4**	**5**•2CH_2Cl_2
C(7)-O(2)-Na(2)	117.4(2)	120.4(2)
O(3)-Na(2)-O(1')	170.24(9)	173.12(10)
O(3)-Na(2)-O(2)	92.19(8)	93.31(9)
O(2)-Na(2)-O(2')	100.81(8)	98.42(8)
O(1)-Na(3)-O(3)	88.87(8)	89.15(9)
C(1)-O(1)-Na(3)	151.5(2)	150.4(2)
C(13)-O(3)-Na(3)	151.0(2)	152.2(2)
O(20)-Na(3)-O(1)	129.38(9)	
O(20)-Na(3)-O(3)	132.10(9)	
O(1)-Na(3)-Cl(2)		146.42(8)
O(3)-Na(3)-Cl(2)		124.40(8)

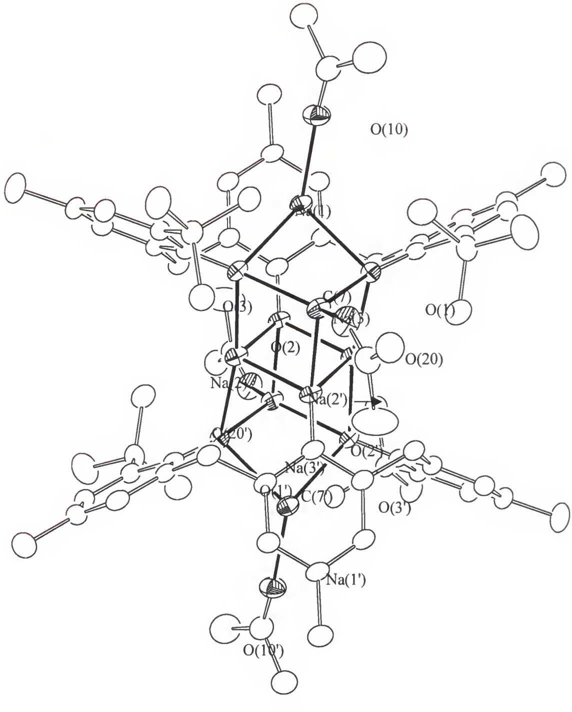

4

Figure 5-9. ORTEP diagram of $Na_6L_2(Me_2CO)_4$ (**4**) showing 30% probability ellipsoids and atom labeling scheme. Primed and unprimed atoms are related by an inversion center. Selected distances and angles are represented in Tables 5-5,5-6.

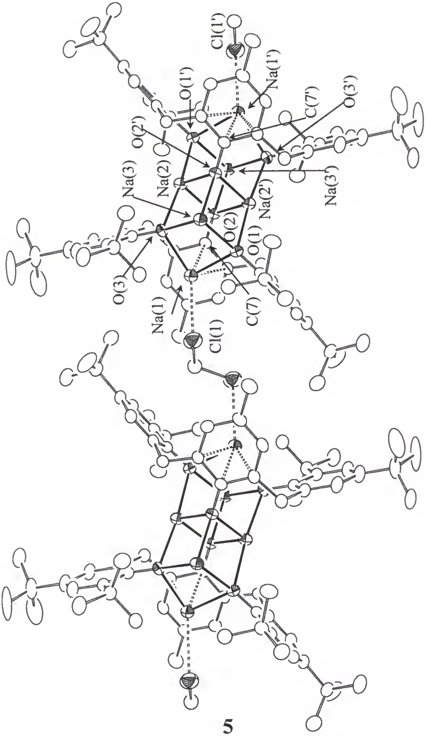

5

Figure 5-10. ORTEP diagram of $[Na_6L'_2(CH_2Cl_2)_3]_x$ (**5**) showing 30% probability ellipsoids and atom labeling scheme. Primed and unprimed atoms are related by an inversion center. For clarity, the disordered dichloromethane molecule interacting with Na(3) and Na(3') have been excluded. Only one orientation of the disordered *t*-butyl group is shown. Selected distances and angles are represented in Table 5-5,5-6.

Even with this contraction, the O(1)-Na(1)-O(3) angle is nearly identical in **4** and **5** with angles of 89.34(8) and 89.77(8)° respectively.

The interaction between chlorine and sodium is short, 2.858(2)Å, forms a bridge to neighboring clusters in the solid state, forming an infinite polymer. The sodium atom linking the outer aryloxide rings does not interact well with methylene chloride. Disorder of methylene chloride in the solid state structure reveals that methylene chlodride only partially occupies the position 3.255(2)Å away from the sodium atom. Substituting a better donor such as acetone into this position instigates the expansion of the metal core cluster seen in **4**. The distances of the sodium atoms to the outer aryloxide oxygen atoms in **4** are 2.404(2) and 2.376(2)Å while in **5**, these bonds are 2.328(2) and 2.315(2)Å. As seen with lithium cluster **2** and **3**, the metal-aryloxide bonds are asymmetric with a much shorter interaction to the central aryloxide oxygen atom.

Conclusions

The Koebner trimer, resembling a calix[4]arene, offers many advantages for the preparation of unusual alkali clusters and transition metal complexes. The strong intramolecular hydrogen-bonding interactions result in a constrained geometry that under the right conditions produces complexes with unique steric and electronic properties.

The synthesis of trimetallic clusters has produced some unique compounds that depend upon experimental conditions. The trimetallic clusters of lithium can be isolated from THF where the good donor property and small metal size, favor this type of cluster formation. In poor donor solvents such as diethyl ether, asymmetric hexanuclear clusters can be isolated with the metals occupying three distinct environments. As poor donor solvents are substituted onto the metal cluster, the cluster core changes favoring increased electron density donation through ipso-carbon interactions.

The free ligand has strong intra-molecular hydrogen bonds that prefer an s-shape of the outer aryloxide rings in the solid state. By incorporating metals such as lithium and sodium, a different u-shaped geometry of the ligand has been identified. The u-shape is consistent for all cluster complexes isolated where ipso carbon interactions and bridging of the outer aryloxides play an important role in stability this geometry. Due to the close proximity of the oxygen atoms in either the s or u shape, meridinal binding of L and L′ should be possible. It will be interesting to see if the ligand, complexed to metal atoms, preferentially chooses one geometry over the other, and may be dependent on the nature of the metal atom used.

CHAPTER 6
SYNTHESIS AND CHARACTERIZATION OF TANTALUM AND NIOBIUM COMPLEXES OF A TRIMER OF LINKED ARYLOXIDES

Introduction

The synthesis of aryloxide ligated Group 5 metal centers have application in a number of chemical transformations namely C-C bond formation such as olefin metathesis and living polymerizations [75]. The ligation of high valent metals by aryloxide substituents generates complexes considered to be electrophilic which are favorable for binding alkenes, and alkynes both of which are electron rich substrates. By using a sufficiently bulky aryloxide, the steric demand on the metal center can result in undesirable C-H activation. The use of cumbersome aryloxides in conjunction with a high valent metal center, where the electrophilicity has been sufficiently augmented, can lead to intramolecular processes typified by cyclometallation or intermolecular ligand loss [76]. Recently, work with a calix[4]arene, where the calixarene consists of 4 aryloxide units linked by a methylene bridge, has produced group 5 metal complexes of dichlorides and alkyls, Figure 6-1 [58-62]. Intra-molecular hydrogen bonding between the hydroxyl groups of the aryloxides stabilizes the bowl-like structure. Floriani and co-workers have recently made tungsten, niobium and tantalum complexes of calix[4]arenes where the metal is bound to the oxygen atoms and is positioned above the bowl [54]. Methylating one of the oxygen donor atoms compensated for the deleterious build-up of anionic charge on the complexes of tantalum. This ether bond is susceptible to attack by other electrophyllic metal centers producing undesirable reactivity [58]. Rothwell et. al. have provided numerous examples of complexes of group 5 metal centers bound to bulky aryloxides that are highly reactive and will cyclometallate when the ligand is sufficiently bulky [76].

Interest in synthesizing Ta^V complexes of bulky aryl oxides while preventing some of the drawbacks described by other investigators, has prompted the use of ligands that are less prone to cyclometallate. In order to prevent adverse reactivity seen with other systems of bulky aryloxides, a trimer of linked aryl oxides can be used as the ligand for synthesizing electrophilic, high-valent metal complexes that resist cyclometallation and ligand loss. This study makes use of a linked trimer ligand derivatized from the Koebner trimer described in the literature, but has been modified to impart a steric environment about the metal center [63]. The sterics imposed upon the metal center are important for driving the regiospecificity at the metal center. The linked nature of the trimer is akin to a calix[4]arene where the fourth aryloxide unit has been removed and is also related to work by Rothwell and co-workers, except that bulky aryloxides have been linked to prevent unwanted cyclometallation reactions, Figure 6-2.

Aryloxide complexes of Ta^V can support a variety of organometallic reactions, most notably CH bond activation and thermal α-hydrogen abstraction to produce alkylidene functional groups. Rothwell has used 2,6-dialkyphenoxide ligands to isolate alkyl and alkylidene structures, Figure 6-3 [77]. The alkylidene complex $Ta(OC_6H_3Bu^t\text{-}2,6)(=CHSiMe_3)(CH_2SiMe_3)$ readily forms at room temperature, and this ease of formation is attributed to the steric pressure exerted on the metal. An interesting note is that the M=C rotational barrier for $Ta(OC_6H_3Bu^t\text{-}2,6)(=CHSiMe_3)(CH_2SiMe_3)$ is fast.

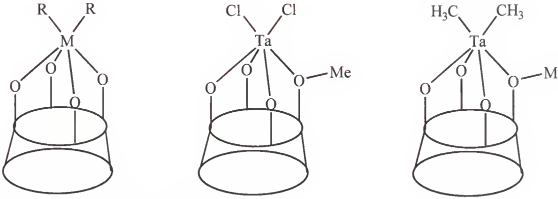

R=Halogen, alkyl M=Ta, Nb

Figure 6-1. Schematic diagram of a hypothetical metal complex of a calix[4]arene and representative examples [58,61].

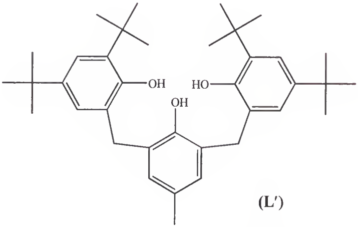

(L′)

Figure 6-2 Schematic diagram of 2,6-bis(3,5-di-t-butyl-2-hydroxy benzyl)-4-methyl phenol (L′).

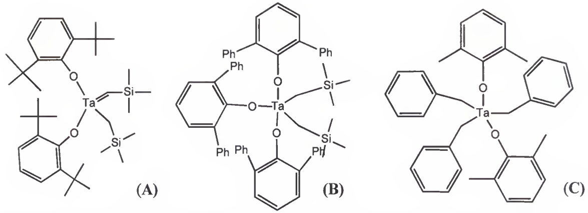

Figure 6-3 [78]. Schematic diagram of (a) $Ta(OC_6H_3Bu^t\text{-}2,6)(=CHSiMe_3)(CH_2SiMe_3)$, (b) $Ta(OC_6H_3Ph_2\text{-}2,6)_3(CH_2SiMe_3)_2$, and (c) $Ta(OC_6H_3Me_2\text{-}2,6)_2(CH_2C_6H_5)_3$.

trigonal bi-pyramidal structure. The increase in size of the 2,6 substituent is does not produce the same steric pressure on the ligand seen for the bulky benzyl ligands.

The double bond appears to be more fascile compared to $Ta(\eta\text{-}C_5H_5)_2$ complexes which is attributed to the less stringent orbital requirements of the $Ta(OAr)_2$ complexes [78-79]. In the case of $Ta(OC_6H_3Me_2\text{-}2,6)_2(CH_2C_6H_5)_3$ the benzyl groups actually exert steric pressure on the aryloxides forcing them to bend away from the a trigonal bi-pyramidal structure [78a]. A solid state structure of $Ta(OC_6H_3Bu^t_2\text{-}2,6)_2(Me)_3$ has more of a true trigonal bi-pyramidal structure.

As described in the preceding chapter, with Koebner type ligands the investigation of group 1 metal clusters formed by bridging oxygen donor atoms and lithium and sodium metals showed the propensity to form unusual cluster complexes that are highly dependent upon experimental conditions [80]. In general, the trimers assume a u-shaped shaped geometry where three unique metal environments exist. The u-shaped geometry positions the oxygen atoms of the aryl oxides in close proximity. This orientation should be desirable for the complexation of electrophillic metal centers, allowing the metal to sit in a steric pocket created by aryl rings.

This report describes preliminary work on the synthesis and characterization of tantalum and niobium complexes of a Koebner trimer ligand. Aspects of the electronic spectra and solid state structure of dichloro and dialkyl complexes are also discussed.

Experimental

General Procedure

All reactions were carried out in a N_2-filled Vacuum Atmospheres Nexus One drybox. Solvents were purchased from Aldrich and Fisher and were dried and distilled by standard methods. ^1H NMR spectra were obtained using a VXR 300 spectrometer using Varian VNMR software. Ta_2Cl_{10} 99.99% purity was purchased from Strem chemical and used as received. Starting materials 2,6-bis(3,5-di-t-butyl-2-hydroxy benzyl)-4-methyl phenol, $TaCl_2Me_3$, $NbCl_2Me_3$, and $TaCl_2(CH_2C_6H_5)_3$ were synthesized according to literature procedure [79-81]. All other materials were purchased from Aldrich or Fisher and used as received. A schematic describing the basic stucture of the dichloride and dialkyl complexes in depicted in Figure 6-4.

Synthesis of Chloride Structures

Synthesis of [[2,6-bis(3,5-di-t-butyl-2-hydroxy benzyl)-4-methyl-phenolato]-tantalum dichloride]$_2$ (**1**)

In a 150 ml round bottom flask, 2.01 g (6.7 mmol) of $TaCl_2Me_3$ was added to 40 ml of methylene chloride. To the pale yellow solution, 3.65 g (6.7 mmol) of 2,6-bis(3,5-di-t-butyl-2-hydroxy benzyl)-4-methyl phenol (L) in 15 ml of methylene chloride was added dropwise evolving methane gas upon addition. The orange solution was stirred for 4 hours producing a bright yellow precipitate. The yellow precipitate was filtered and washed with cold pentane resulting in 3.88 g (72%) of **1**. Single crystals suitable for

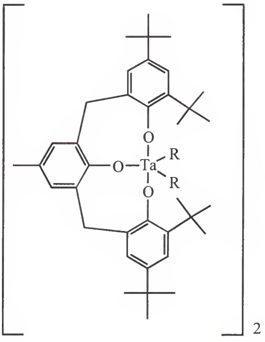

Dichloride complex **1** and **2**:
M = Ta, Nb
R = Cl

Dimethyl complex **4** and **5**:
M = Ta, Nb
R = Me

Figure 6-4. Schematic diagram of the basic structure of dimethyl and dialkyl complexes.

X-ray analysis were obtained by the slow evaporation (-30 °C) of a saturated solution of chloroform. ^{1}H NMR for **1** ($CDCl_3$):δ 1.28 (s, 36H), 1.36 (s, 36H), 2.22 (s, 6H), 3.35 (d, 4H, $^2J_{HH}$ 13.42 Hz), 4.93 (d, 4H, $^2J_{HH}$ 13.42 Hz), 7.03 (s, 4H), 7.26 (s, 4H), 7.35 (s, 4H). ^{13}C NMR ($CDCl_3$):δ 31.3, 31.6, 31.7, 34.1, 34.8, 35.7, 124.4, 126.0, 131.2, 132.5, 136.9, 139.7, 140.9, 141.2, 147.8, 158.0. *Anal.* Calc. for $C_{74}H_{98}Cl_4O_6Ta_2$: C, 56.00; H, 6.22 %. Found: C, 56.75; H, 6.33 %.

Alternative synthesis

In a 100 ml round bottom flask, 0.253 g (0.48 mmol) of $TaCl_2(CH_2C_6H_5)_3$ was added to 20 ml of methylene chloride. To the deep red solution, 0.26 g (0.48 mmol) of L′ in 2 ml of methylene chloride was added. The deep orange solution was stirred for 72 hours producing a yellow precipitate. The precipitate was filtered and washed with cold pentane to afford 0.23 g (61 %) of **1**. NMR spectra taken indicate that the product is identical to that isolated above. The synthesis using $TaCl_2Me_3$ is more efficient and results in higher yields, so the alternate synthetic route was abandoned but is described here for completeness.

Synthesis of [[2,6-bis(3,5-di-t-butyl-2-hydroxy benzyl)-4-methyl phenolato]-niobium dichloride]$_2$ (**2**)

In a procedure analogous to the one used for **1**, a solution of 3.91 (7.2 mmol) of L′ in 10 ml of pentane was added dropwise to a solution of 1.51 g (7.2 mmol) of $NbCl_2Me_3$, generating methane gas upon addition. The red solution was allowed to stir for 4 hours producing an orange precipitate. The orange precipitate was filtered and washed with cold pentane yielding 4.32 g (85 %) of (**2**). Single crystals for X-ray analysis were obtained from the slow evaporation (-30 °C) of a saturated solution of chloroform. ^1H NMR ($CDCl_3$):δ 1.34 (s, 36H), 1.43 (s, 36H), 2.28 (s, 6H), 3.34 (d, 4H, $^2J_{HH}$ 13.35 Hz), 5.05 (d, 4H, $^2J_{HH}$ 13.35 Hz), 7.06 (s, 4H), 7.21 (d, 4H, $^4J_{HH}$ 2.12 Hz), 7.30 (d, 4H, $^4J_{HH}$ 2.12 Hz). ^{13}C NMR ($CDCl_3$):δ 31.2, 31.5, 33.9, 34.1, 34.6, 35.5, 123.1, 125.2, 130.8, 132.4, 137.9, 139.8, 140.1, 140.3, 147.2, 160.6.

Synthesis of pyridine adduct [2,6-bis(3,5-di-t-butyl-2-hydroxy benzyl)-4-methyl phenolato]-tantalum dichloride (**3**)

The dimeric structure of **1** can be cleaved by addition of 2 equivalents pyridine to a methylene chloride solution. After 4 hours, the suspension is homogeneous and the solvent was removed under vacuum to yield a yellow solid. Pentane was added to extract out excess pyridine and the mixture was stirred for 2 hours as a yellow precipitate formed. The yellow solid was filtered to yield **3**. Crystals suitable for crystallography were obtained by evaporation of a saturated solution of methylene chloride. ^1H NMR

(CD_2Cl_2):δ 1.33 (s, 9H), 1.39 (s, 9H), 1.47 (s, 9H), 1.60 (s, 9H) 2.19 (s, 3H), 2.97 (d, 1H, $^2J_{HH}$ 14.16 Hz), 3.46 (d, 1H, $^2J_{HH}$ 14.16 Hz), 3.62 (d, 1H, $^2J_{HH}$ 14.16 Hz), 5.15 (d, 1H, $^2J_{HH}$ 14.16 Hz) 6.66 (s, 1H) 6.97 (m, 2H), 7.32 (d, 1H) 7.39 (m, 2H), 7.51 (m, 2H, py), 7.99 (m, 1H, py), 9.31 (m, 2H, py). ^{13}C NMR (CD_2Cl_2):δ 20.72, 31.53, 31.66, 31.72, 32.11, 34.50, 34.60, 34.76, 35.71, 35.91, 123.1, 123.3, 125.4, 126.1, 127.2, 127.9, 128.1, 128.3, 128.4, 132.9, 133.9, 135.1, 140.4, 140.9, 141.6, 146.5, 147.1, 151.4, 156.7, 156.8, 159.0.

Synthesis of Dimethyl Structures

Synthesis of [[2,6-bis(3,5-di-tbutyl-2-hydroxy benzyl)-4-methyl phenolato]-dimethyl-tantalum]$_2$ (**4**)

In a 150 ml round bottom flask, 1.20 g (0.76 mmol) of **1** was added to 40 ml of toluene. To the yellow solution, 1.52 ml (1.5 mmol) of $ZnMe_2$ (2 M in toluene) was added. The pale yellow solution was allowed to stir for 4 hours, and the $ZnCl_2$ was removed by filtration to give a pale yellow solution. The toluene was removed under vacuum leaving an off white precipitate. The precipitate was suspended in methylene chloride and stirred for 1 hour, cooled to –30 °C, filtered, and dried under vacuum to yield 2.4 g (78%) of (**3**). ^1H NMR ($CDCl_3$):δ -0.42 (s, 6H, Me), 1.09 (s, 6H, Me), 1.34 (s, 36H), 1.40 (s, 36H), 2.18 (s, 6H), 3.21 (d, 4H, $^2J_{HH}$ 13.18 Hz), 4.97 (d, 4H, $^2J_{HH}$ 13.18 Hz), 7.00 (s, 4H), 7.22 (d, 4H, $^4J_{HH}$ 2.44), 7.26 (d, 4H $^4J_{HH}$ 2.44 Hz). ^{13}C NMR ($CDCl_3$):δ 18.2 (Me), 20.0 (Me), 21.3, 30.8, 31.6, 33.4, 34.3, 35.0, 122.4, 125.4, 130.0, 132.1, 136.0, 136.6, 137.1, 138.4, 144.3, 157.2.

Synthesis of [[2,6-bis(3,5-di-tbutyl-2-hydroxy benzyl)-4-methyl phenolato]-dimethyl-niobium]$_2$ (5)

In a 150 ml round bottom flask, 1.50 g (1.06 mmol) of **1** was added to 40 ml of toluene. To the red solution, 2.26 ml (2.12 mmol) of $ZnMe_2$ (2 M in toluene) was added. The yellow solution was allowed to stir for 4 hours and the $ZnCl_2$ was removed by filtration to give a bright yellow solution. The toluene was removed under vacuum leaving a yellow precipitate. The precipitate was suspended in methylene chloride and stirred for 1 hour, cooled to –30 °C, filtered, and dried under vacuum to yield 1.01 g (67 %) (**4**) as a yellow powder. ^{1}H NMR ($CDCl_3$):δ 0.00 (s, 6H, Me), 1.35 (s, 36H), 1.41 (s, 36H), 1.62 (s, 6H, Me), 2.20 (s, 6H), 3.22 (d, 4H, $^2J_{HH}$ 13.19 Hz), 4.76 (d, 4H, $^2J_{HH}$ 13.19 Hz), 7.00 (s, 4H), 7.19 (d, $^4J_{HH}$ 2.35 Hz), 7.24 (d, 4H, $^4J_{HH}$ 2.35 Hz). ^{13}C NMR ($CDCl_3$):δ 19.7(Me) 21.3, 30.8, 31.3 (Me), 31.6, 33.4, 34.4, 35.1, 122.3, 125.7, 130.0, 132.5, 136.5, 137.1, 138.3, 144.4, 158.1.

Synthesis of [2,6-bis(3,5-di-tbutyl-2-hydroxy benzyl)-4-methyl phenolato]-dibenzyl-Tantalum (**6**)

In a 100 ml round bottom flask, 0.252 g (0.16 mmol) of **1** was suspended in 30 ml of methylene chloride. To the yellow suspension, 630 µl (0.64 mmol) of $(C_6H_5CH_2)MgCl$ (1 M in ether) was added. The pale yellow solution was allowed to stir for 4 hours at which time dioxane was added (to facilitate the precipitation of magnesium salts) and allowed to stir for another hour. The solution was filtered and the methylene chloride was removed under vacuum to yield a yellow precipitate. The yellow precipitate was suspended in pentane and stirred for 1 hour, cooled to –30 °C overnight, filtered, and dried under vacuum to yield (62%) of **6** as a yellow solid. ^{1}H NMR for (C_6D_6):δ 1.38 (s,

18H), 1.66 (s, 18H), 1.83 (s, 3H), 2.74 (s, 2H, CH_2Bz), 3.08 (d, 2H, $^2J_{HH}$ 13.18 Hz), 3.74 (s, 2H, CH_2Bz), 4.52 (d, 2H, $^2J_{HH}$ 13.18 Hz), 6.62 (s, 2H), 6.98 (m, 2H), 7.18 (d, 2H, $^4J_{HH}$ 1.47 Hz), 7.35 (m, 2H), 7.50 (d, 4H, $^4J_{HH}$ 1.47 Hz), 7.86 (d, 1H) ^{13}C NMR (C_6D_6):δ 21.5, 31.4, 32.0, 33.4, 34.5 (CH_2Bz), 35.8, 38.2 (CH_2Bz), 122.7, 126.2, 128.6, 128.8, 129.8, 130.6, 132.2, 132.7, 137.7, 138.3, 144.9, 148.2, 157.4, 157.9

Results and discussion

Synthesis of Ta, Nb Chloride Complexes

Several methods for the preparation of the metal chloride complexes were attempted. The direct addition of aryloxides to Ta_2Cl_{10} is a well documented route for ligating the metal, producing HCl as a by product [78b]. Attempts to follow the same procedure by the direct addition of 2,6-bis(3,5-di-tbutyl-2-hydroxy benzyl)-4-methyl phenol (L′) to Ta_2Cl_{10} required heat to initiate reactivity and resulted in complex dimeric products where in some instances the ligand had lost its *t*-butyl group in the *ortho* position of the outer aryloxides. To circumvent the problems encountered, an alternative preparation using tris alkyl complexes of the metal chlorides was used, whereby the alkyl an excellent leaving group is evolved. Initial attempts with $TaCl_2(CH_2C_6H_4CH_3)_3$ produced no discernable reaction at room temperature most likely due to the bulk of the xylyl ligand preventing the favorable approach of L′ to the metal. Elevated temperatures result in a mixture of products. Because of its smaller size, $TaCl_2(CH_2C_6H_5)_3$ was used as a replacement for the bulky xylyl reagent. With this reagent, the room temperature reaction with L′ was a slow process (72 hours) yet the system generated the desired product **1** in good yields.

In order to improve upon the slow reaction of $TaCl_2(CH_2C_6H_5)_3$ with L′, the smaller more reactive complex $TaCl_2Me_3$ was synthesized according to literature procedure affording analytically pure materials when isolated from pentane. The 1:1 addition of L′ to a solution of $TaCl_2Me_3$ in methylene chloride initiates a vigorous, exothermic reaction where (**1**) precipitates. This reaction is quite clean affording high yields of **1** over 4 hours. The complex is readily soluble in chloroform and upon evaporation of a saturated solution produces large sensitive crystals of **1** suitable for X-ray analysis. The solid state structure of **1** is depicted in Figure 6-4. Crystallographic and geometric parameters for **1** are presented in Tables 6-1 and 6-2.

The niobium compound was prepared in the same fashion, except the product does not precipitate from methylene chloride during the course of the reaction but can still be isolated at greatly reduced yields. Repeating the reaction in pentane, (**2**) readily precipitates from solution. Large crystals of **2** can be isolated using the same procedure as used for the isolation of **1**. The solid state structure of **2** is isostructural with the tantalum system in Figure 6-5. Selected crystallographic and geometric parameters for **2** are presented in Tables 6-1 and 6-2.

In the dimeric structure of **1**, two tantalum atoms each adopt a distorted octahedral geometry with four bonds to oxygen atoms and two bonds to chlorine atoms. Statistically, the bond lengths to the oxygen atoms on the outer rings are equivalent, 1.923(2) and

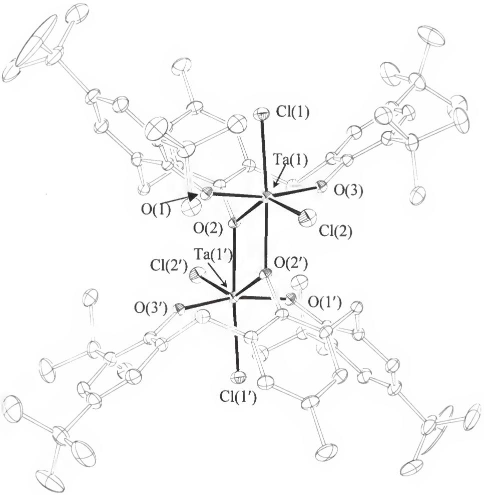

Figure 6-5. ORTEP diagram of **1** showing 30% probability ellipsoids and the atom labelling scheme. Selected bond distances and angles are presented in Table 6-1, and 6-2. Prime and unprimed atoms are related by an inversion center.

Table 6-1. Crystallographic and selected parameters for $L'_2Ta_2Cl_4$ (**1**), $L'_2Nb_2Cl_4$ (**2**), and $L'TaCl_2(py)$ (**3**)

Compound	**1**•$3CHCl_3$	**2**•$3CHCl_3$	**3**•$2(CH_2Cl_2)(C_5H_{12})$
Crystal data			
Formula	$C_{80}\,H_{104}\,Cl_{22}\,O_6\,Ta_2$	$C_{80}\,H_{104}\,Cl_{22}\,O_6\,Nb_2$	$C_{49}\,H_{58}\,C_{l6}\,N\,O_3\,Ta$
Formula weight	2303.43	2127.35	1464.87
Crystal system	Monoclinic	Monoclinic	Monoclinic
Space group	*P2₁/n*	*P2₁/n*	*P2₁/c*
a (Å)	14.4843(6)	14.5164(7)	9.326(2)
b (Å)	24.338(1)	24.288(1)	35.79(1)
c (Å)	14.9144(6)	14.9204(7)	15.535(3)
β (°)	109.728(1)	109.868(1)	96.09(2)
V(Å^3)	4949.1(4)	4947.5(4)	5155(2)
Z	2	2	4
T (K)	173(2)	173(2)	173(2)
R (%)^a	3.46	6.12	5.27
wR^2 (%)^b	8.79	16.84	6.54

^{a} $R = \Sigma\,|\,|F_o| - |F_c|\,|\,/\,\Sigma\,|F_o|$.

^{b} $wR^2 = \{\,\Sigma\,[\,w(F_o^2 - F_c^2)^2\,]\,/\,\Sigma\,[\,w(F_o^2)^2\,]\,\}^{1/2}$.

Table 6-2. Selected bond distances (Å) and angles (°) for $L'_2Ta_2Cl_4$ (**1**), $L'_2Nb_2Cl_4$ (**2**), and $L'TaCl_2(py)$ (**3**).

Compound			
1•$3CHCl_3$			
Ta(1)-O(1)	1.904(2)	Ta(1)-Cl(1)	2.3405(9)
Ta(1)-O(2)	2.066(2)	Ta(1)-Cl(2)	2.305(1)
Ta(1)-O(3)	1.923(2)	Ta(1)-O(2′)	2.181(2)
O(1)-Ta(1)-O(3)	166.9(1)	O(3)-Ta(1)-O(2)	89.9(1)
O(1)-Ta(1)-O(2)	90.2(1)	O(3)-Ta(1)-O(2′)	94.77(9)
O(1)-Ta(1)-O(2′)	97.10(9)	O(3)-Ta(1)-Cl(2)	93.23(8)
O(1)-Ta(1)-Cl(2)	94.22(8)	O(3)-Ta(1)-Cl(1)	83.04(7)
O(1)-Ta(1)-Cl(1)	84.64(8)	O(2′)-Ta(1)-Cl(2)	80.08(6)
O(2)-Ta(1)-O(2′)	64.6(1)	O(2′)-Ta(1)-Cl(1)	174.46(6)
O(2)-Ta(1)-Cl(1)	110.18(7)	Cl(2)-Ta(1)-Cl(1)	105.08(4)
O(2)-Ta(1)-Cl(2)	144.73(7)	Ta(1)-O(2)-Ta(1′)	115.3(1)
2•$3CHCl_3$			
Nb(1)-O(1)	1.904(3)	Nb(1)-Cl(1)	2.351(1)
Nb(1)-O(2)	2.064(2)	Nb(1)-Cl(2)	2.312(1)
Nb(1)-O(3)	1.919(2)	Nb(1)-O(2′)	2.217(2)
O(1)-Nb(1)-O(3)	166.6(1)	O(3)-Nb(1)-O(2)	90.3(1)
O(1)-Nb(1)-O(2)	90.6(1)	O(3)-Nb(1)-O(2′)	95.1(1)
O(1)-Nb(1)-O(2′)	97.2(1)	O(3)-Nb(1)-Cl(2)	93.20(8)
O(1)-Nb(1)-Cl(2)	93.92(8)	O(3)-Nb(1)-Cl(1)	82.72(8)
O(1)-Nb(1)-Cl(1)	84.56(8)	O(2′)-Nb(1)-Cl(2)	78.86(7)
O(2)-Nb(1)-O(2′)	64.7(1)	O(2′)-Nb(1)-Cl(1)	175.52(7)
O(2)-Nb(1)-Cl(2)	143.64(7)	Cl(2)-Nb(1)-Cl(1)	105.13(4)
O(2)-Nb(1)-Cl(1)	111.21(7)	Nb(1)-O(2)-Nb(1′)	115.2(1)

Table 6-2 continued.

3•2(CH_2Cl_2)			
Ta(1)-O(1)	1.910(5)	Ta(1)-N(1)	2.259(6)
Ta(1)-O(2)	1.875(5)	Ta(1)-Cl(1)	2.352(2)
Ta(1)-O(3)	1.937(4)	Ta(1)-Cl(2)	2.377(2)
O(2)-Ta(1)-O(1)	89.4(2)	O(3)-Ta(1)-Cl(1)	99.1(2)
O(2)-Ta(1)-O(3)	84.5(2)	O(1)-Ta(1)-Cl(2)	96.3(2)
O(1)-Ta(1)-O(3)	167.0(2)	O(2)-Ta(1)-Cl(2)	169.8(2)
O(1)-Ta(1)-N(1)	83.6(2)	O(3)-Ta(1)-Cl(2)	88.1(1)
O(2)-Ta(1)-N(1)	88.2(2)	N(1)-Ta(1)-Cl(1)	174.3(2)
O(3)-Ta(1)-N(1)	84.7(2)	N(1)-Ta(1)-Cl(2)	84.1(2)
O(1)-Ta(1)-Cl(1)	93.0(2)	Cl(1)-Ta(1)-Cl(2)	91.71(7)
O(2)-Ta(1)-Cl(1)	96.3(2)		

1.904(2) Å, but the distance to the oxygen atom of the central phenoxide ring is 2.066(2) Å.The significant change in distance from the central phenoxide is due to the bonding interaction with another oxygen atom 2.181(2) Å away from the symmetry related L′ ligand. This interaction suggests that the tantalum is highly electrophilic where the strong donation of electron density from a neighboring ligand is a favorable interaction stabilizing the dimeric structure. The ^{1}H NMR has two distinct peaks generated by the static ^{2}J coupling between the hydrogen atoms in the methyl bridge which suggests that the u-shape is retained in solution Figure 6-6.

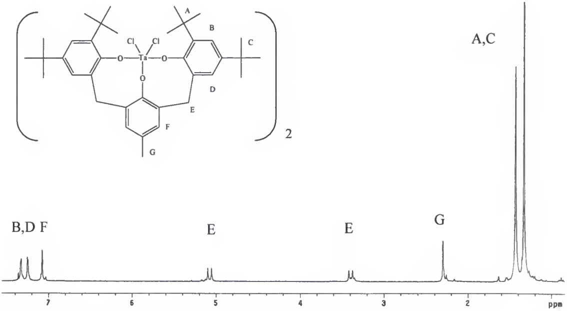

Figure 6-6. ^{1}H NMR (300 Mhz) spectrum of $L'_2Ta_2Cl_2$ (**1**) in $CDCl_3$.

The chlorine atoms occupy two distinct positions with one chloride atom residing in the bowl formed by the ligand, and the other is directed out of the bowl between the two t-butyl groups in the ortho position of the outer phenoxide rings. The chlorine-tantalum bond O(2′)-Ta(1)-Cl(1) has an angle of 174.46(6)Å, and has a bond length

0.039(1)Å longer than the chlorine-metal bond outside the bowl. The u-shape of the ligand imparts considerable steric strain at the metal center, where the second chlorine atom is distorted down out of the bowl at an angle O(2)-Ta(1)-Cl(2) of 144.73(7)°. This distortion deviates greatly from a perfect octahedral where the ideal bond angles of trans substituents are 180°. In a related system, the chlorine atom distances in the compelx $Ta(OC_6H_5Ph_2\text{-}2,6)_3Cl_2$ are 2.347(1) to 2.354(1) Å, similar in length to the metal-chlorine bond residing in the bowl in **1** [75].

The niobium dimer structure is similar to the tantalum analogue, and the metal center again adopts a distorted octahedral geometry with four bonds to oxygen atoms and two bonds to chlorine atoms in distinct sites. The size of the metal is unimportant in determining the geometry of the ligand. The ionic radii of tantalum(V) and niobium(V) in 6 coordinate octahedral geometry are both 78 pm. The u-shape is reatianed and bond lengths and angles are essentially identical to that seen in the tantalum structure.

The interaction of the oxygen atom from the symmetry related ligand is very important in retaining the u-shape of the ligand. This interaction prevents the outer aryloxides from assuming the s-shaped geometry seen in the solid state of the free ligand [79]. By introducing a strong donor ligand such as pyridine, the dimer can be readily broken. The incorporation of pyridine is a surprisingly slow process in methylene chloride solution due to the slight solubility of **1**, and the reaction reguires 4 hours to establish homogeneity in solution. The solid state structure of **3** reveals some interesting structural changes compared to the dimer, Figure 6-7. The central phenoxide oxygen-metal bond distance has shortened to 1.875(5) Å while the outer aryloxide oxygen-metal bond distances have opened up slightly to 1.910(5) and 1.937(4) Å, respectively. The distorted octahedral has now relaxed to more of a true octahedral structure coinciding with a release of steric strain by the ligand as one outer aryl oxide drops down to impart more of an s-shaped geometry to the overall ligand. The more relaxed shape of the ligand allows the metal to assert a stronger interaction with the bridging central phenoxide. The chlorine metal bond distances are statistically identical. The metal-chlorine bond length for Cl(1), the chlorine previously residing in the bowl, is statistically the same at 2.377(2)Å. The metal-chlorine distance for Cl(2), however has increased to 2.377(2)Å, which differs from the length in **1** by 0.072(2)Å. The strong donor properties of pyridine has allowed an outer aryloxide to release strain. The relaxation of the aryloxide results in a distorted s-shape where the geometry is intermediary between the u and s-shapes. The

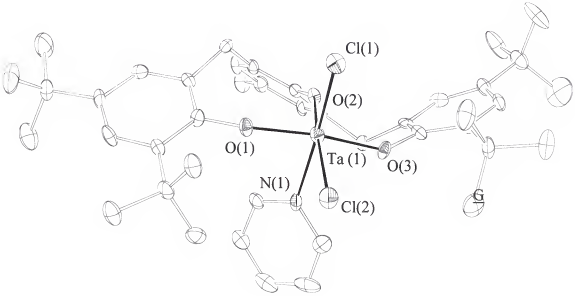

Figure 6-7. ORTEP diagram of **6** showing 30% probability ellipsoids and the atom labelling scheme. Selected bond distances and angles are presented in Table 6-1, and 6-2.

solid state structure of **3** is supported by NMR spectroscopy where the distorted s-shape is retained in solution, Figure 6-8. The linker methyl protons now split into 4 distinct doublets ranging from 2.97 ppm to 5.15 ppm. The *t*-butyl groups are also split into four independent signals, which is quite different from the two peaks found in the dichloride and free ligand. This change in geometry could play an important role in the alkylation of **1** and **2** with bulky alkyls. The steric demand of bulky alkyls may force the bowl to open up to the more accessible s-shape. In a related system, the complex *trans-mer-*[$TaCl_2(OC_6H_3Pr^i{}_2$-2,6$)_3(PMe_2Ph)$] the donor phosphine ligand binds between the chlorides forcing them into axial positions with the aryloxides and phospine occupying meridinal positions [80]. The metal-chlorine bond distances of the *trans* chlorine atoms are identical to those found in **3** and the oxygen-metal bond distances are similar at 1.913(2), 1.868(2), and 1.894(2) Å. In the same study, Rothwell and co-workers have determined that the 2:1 aryloxide inequivalency that should be present in NMR spectroscopy is not found and has been determined as the exchange of the aryloxide ligand on the NMR time scale. It is important to note that **3** does not suffer from the same effect of ligand loss.

Wigley and co-workers have studied the quinoline binding mode of tantalum aryloxide catalysts where the binding mode of the donor substrate such as quinoline correlates well with the oxidation state of the metal [83]. Selective hydrogenation and aromatic disruption by d^2-$Ta(OAr)_nCl_n$ moieties takes place. The propensity for **1** and **2** to interact with donors such as pyridine would be a good model for studying the binding properties of HDN catalysts.

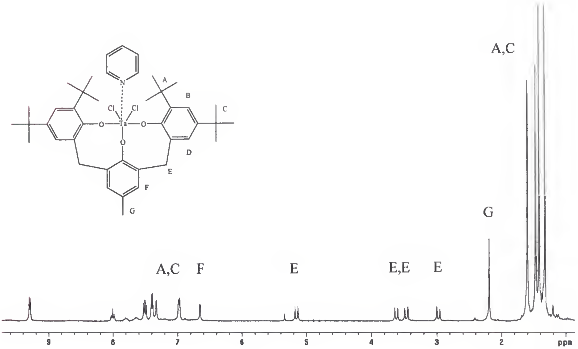

Figure 6-8. ^{1}H NMR (300 MHz) spectrum of L'TaCl$_2$(py) (**3**) in CD$_2$Cl$_2$.

Synthesis of Ta, Nb Dimethyl Complexes

The chlorine atoms of the dichloride complexes can be readily substituted by alkyl groups. Methyllithium was used in the first attempt to exchange the chlorine atoms for methyl groups. The synthesis proved to be unsuccessful, even at low temperatures with only decomposition occurring. To avoid decomposition a milder reagent, dimethyl zinc was used and, upon addition to **1** or **2** dissolved in toluene, this reagent reacts immediately producing the corresponding dimethyl complex. The limited solubility of both dimethyl complexes restricted our use of solvents for recrystallization to chloroform. Large crystals of **4** and **5** can be isolated from saturated solutions of chloroform but these crystals lose solvent very rapidly upon removal from the bulk solvent.

The interesting aspects of these complexes are the observed signals generated by the protons of the corresponding methyl directly bound to the metal center. There are key features in ^{1}H NMR spectroscopy of these compounds that allow us to surmise that the dimeric structure seen for **1** and **2** is retained in the dimethyl complexes, Figure 6-9. The NMR spectra of the dimethyl complexes **4** and **5** are essentially identical with static ^{2}J coupling of the protons of the linker arm methylenes. This implies that the u-shape has been retained in solution, which is not unreasonable considering that the size difference between a chlorine atom and a methyl group is fairly small. More importantly, is the observation that the methyl groups appear to be in completely different environments. The methyl signals for **4** are broad singlets with chemical shifts of –0.42 ppm and 1.09 ppm corresponding to a difference of 1.51 ppm. This is large difference in the environment of the methyl groups suggests that the u-shape must be the geometry of the complex in solution. If the s-shape was present, the linker methyl hydrogens would be equivalent, resulting in a singlet and the methyl groups directly bound to the metal would be equivalent through symmetry also resulting in a singlet. The niobium complex exhibits similar chemical shifts for the methyl groups at 0.00 ppm and 1.62 ppm, a difference of 1.62 ppm. Clearly both complexes contain methyl groups that have distinct environments. A solid state structure of **4** and **5** would be useful to resolve the fundamental differences in the NMR chemical shifts of the two complexes, and to unambiguously determine whether the dimer is kept intact, or the u-shape is retained in a monomeric form not yet seen.

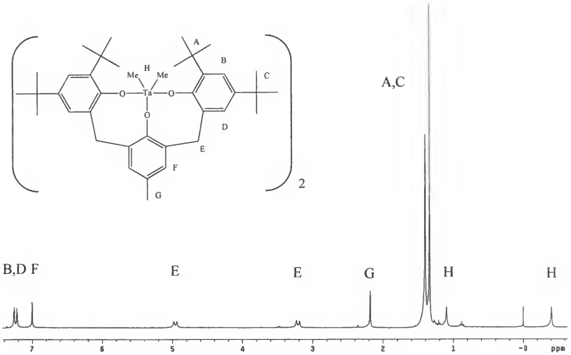

Figure 6-9. ^{1}H NMR (300 MHz) spectrum of $L'_2Ta_2Me_4$ (**4**) in $CDCl_3$.

Synthesis of Tantalum Benzyl Complex

Initial attempts at alkylation of **1** with $(C_6H_5CH_2)_2Zn$ resulted in no reaction at room temperature, but the Gringard reagent $[(C_6H_5CH_2)MgCl]$ resulted in immediate reactivity upon addition to a suspension of **1** in methylene chloride. The choice of solvent is crucial to the success of this reaction. The use of solvents other than methylene chloride resulted in decomposition with no recoverable product. The reaction in methylene chloride, however, takes 4 hours at which time the magnesium salts are removed by addition of dioxane followed by filtration. The yellow solution is then stripped of methylene chloride under vacuum. The resulting yellow solid can be recrystallized from saturated solutions of ether or methylene chloride. The solid state structure was obtained from crystals taken from the slow diffusion of pentane into methylene chloride and is depicted in Figure 6-10. Crystallographic and geometric parameters are presented in Tables 6-3 and 6-4.

In this structure the dimer has been broken assuming a distorted trigonal bi-pyramidal structure with a O(3)-Ta(1)-O(1) angle of 171.5(2)° and O(2)-Ta(1)-O(1) and O(3)-Ta-O(2) angles of 91.6(2) and 93.8(2)° respectively. This is a significant change from a true trigonal bi-pyramidal structur where the equatorial groups assume position at 120°. The ipso interaction of the metal with C(7) is short at 2.689(5) Å and helps compensate for the loss of the oxygen donor from the dimeric structure maintaining the u-shape geometry of the ligand. The benzyl groups occupy two distinct environments. One group is situated in the bowl and the benzyl ring is canted in toward the center. The other benzyl group resides below the bowl and the benzyl ring points down and away from the ligand and both methylene groups bend away from the ligand at a C(201)-Ta(1)-C(101) abgle of 118.8(2)°. The solution NMR of the complex exhibits two distinct singlets at 2.74 and 3.74 ppm indicative of the distinct environments occupied by the benzyl groups. The tantalum-carbon distances in the methylene of the benzyl group are statistically different. The Ta(1)-C(101) distance of 2.190(6) Å and the Ta(1)-C(201) distance of 2.153(6) Å differ by 0.037(6) Å. This difference in bond length is similar to that seen in the dichlorides where the ligand imparts steric strain on the metal center.

A tribenzyl complex [$Ta(OC_6H_5Me_2\text{-}2,6)_2(CH_2Ph)_3$] has longer metal-carbon bond lengths of 2.204(7) Å. The triganol bi-pyramidal structure for this complex assumes a less distorted structure where meridinal angles between benzyl groups are 127.8(3), 115(3) and 116.2(3) °. And the angle between axial groups is 165.5(2)°. In this complex

Table 6-3. Crystallographic and selected parameters for L′Ta(CH_2Ph)$_2$ (**6**).

Compound	**6**•CH_2Cl_2
Crystal data	
Formula	$C_{52}H_{64}Cl_2O_3Ta$
Formula weight	988.88
Crystal system	Monoclinic
Space group	$P2_1/c$
a (Å)	17.304(1)
b (Å)	23.863(1)
c (Å)	11.7911(7)
β (°)	102.224(1)
V(Å^3)	4758.5(5)
Z	4
T (K)	173(2)
R (%)[a]	5.36
wR^2 (%)[b]	12.04

[a] $R = \Sigma \mid |F_o| - |F_c| \mid / \Sigma |F_o|$.

[b] $wR^2 = \{ \Sigma [w(F_o^2 - F_c^2)^2] / \Sigma [w(F_o^2)^2] \}^{½}$.

Table 6-4. Selected bond distances (Å) and angles (°) for L'Ta(CH_2Ph)$_2$ (**6**).

Compound			
	6•CH_2Cl_2		
Ta(1)-O(1)	1.932(4)	Ta(1)-C(101)	2.190(6)
Ta(1)-O(2)	1.925(4)	Ta(1)-C(201)	2.153(6)
Ta(1)-O(3)	1.918(4)	Ta(1)-C(7)	2.689(5)
O(2)-Ta(1)-O(1)	91.6(2)	O(3)-Ta(1)-C(101)	87.8(2)
O(3)-Ta(1)-O(1)	171.5(2)	O(1)-Ta(1)-C(201)	91.0(2)
O(3)-Ta(1)-O(2)	93.8(2)	O(2)-Ta(1)-C(201)	117.0(2)
O(1)-Ta(1)-C(101)	83.8(2)	O(3)-Ta(1)-C(201)	92.3(2)
O(2)-Ta(1)-C(101)	124.1(2)	C(201)-Ta(1)-C(101)	118.8(2)

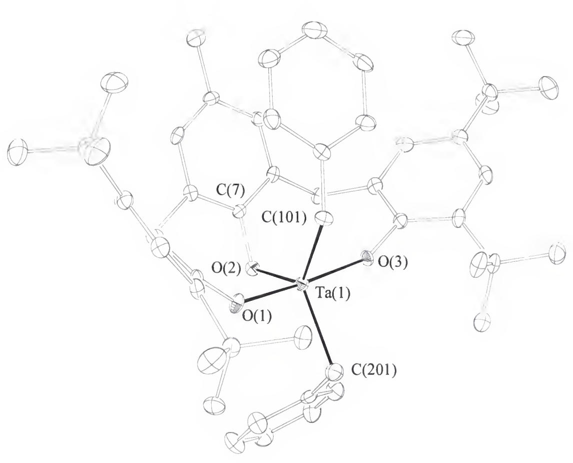

Figure 6-10. ORTEP diagram of L'Ta(CH_2Ph)$_2$ (**6**) showing 30% probability ellipsoids and the atom labelling scheme. Selected bond distances and angles are presented in Table 6-3, and 6-4.

the benzyl groups exert steric strain upon the aryloxides forcing them to bend away from the metal center, which is converse to that seen for **3**. To our knowledge, Rothwell has not described niobium or analogs of similar complexes.

Floriani and coworkers have synthesized similar complex [Ta{*p*-tBu-calix[4]-(OMe)(O)$_3$}(CH$_2$Ph)$_2$] but a solid state structure was not obtained [. The lack of a structure is due to the thermal instability of the compound out of solution. Inserting CO or t-BuNC into the metal carbon bond can isolate an insertion complex.

The syntheses of niobium di-benzyl complexes have been carried out and at this time reproducibility has been a major concern. The lack of examples in the literature lends credence to the difficulty in synthesizing stable benzyl complexes of niobium. Because of the sterics induced by the ligand on the highly reactive metal center, reductive elimination could take place. The increased reactivity of the niobium analog is not uncommon and accounts for the disparity in complexes known for tantalum versus niobium [3]. Because of the adverse side reactions, the reduction of the niobium atom is being studied in order to design complexes with increased stability.

Conclusions

The potential for selective reactivity for these sterically encumbered complexes cannot be understated. The investigation of the di-chloride complexes and the substitution of alkyls have led to the interesting observation that the geometry of the ligand influences the site occupied by alkyl groups. The u-shape of the ligand, if it can be retained, can lead to reactivity that is selective toward a single binding site. The dichloride complexes were instrumental in providing valuable information as to the nature of the ligand shape and it is clear that the ligand in the u-shape imparts a significant degree of steric strain upon the metal center. To our knowledge, very few complexes similar to complex **3** have been structurally characterized. This complex is stable even though the geometry about the metal center is highly distorted. The structure of **3** also suggests that the preference to bind at one site possible and leads to many avenues of study, such as insertion reactions where isocyanides can be mono-inserted into a metal carbon bond. Other interesting reactions for future study are the generation of mixed alkyls. The possibility of generating mixed alkyl complexes may lead to interesting catalytic reactions such as the ring opening metathesis of bulky substrates. Future work with isocyanides will prove useful in determining whether or not a mono-insertion product can be favored over di-insertion.

LIST OF REFERENCES

1. Lowe, J. P. *Quantum Chemistry, Sec. Ed.*, Academic Press Inc., New York, 1993.

2. Morrison, R. T. and Boyd, R. N. *Organic Chemistry, Thir. Ed.*, Allyn and Bacon Inc., Boston, 1973.

3. Collman, J. P.; Hegedus, L. S.; Norton, J. R.; Finke, R. G. *Principles and Applications of Organotransition Metal Chemistry*, University Science Books, Mill Valley, California, 1987.

4. Bone, W. A.; Coward, H. F. *J. Chem. Soc.*, **1908**, *93*, 1197.

5. Crabtree, R. H. *Chem. Rev.*, **1995**, *95*, 987.

6. Gesser, H. D.; Hunter, N. R. *Chem. Rev.*, **1985**, *85*, 235.

7. Tajima, N.; Tsuneda, T.; Toyama, F.; Hirao, K. *J. Am. Chem. Soc.*, **1998**, *120*, 8222

8. Eilers, J.; Posthuma, S. A.; Sie, S. T. *Catal. Lett.*, **1990**, *7*, 253.

9. Sheldon, R. A.; Kochi, J. K. *Metal Catalyzed Oxidations of Organic Compounds* Academic Press Inc., New York, **`1981**.

10. (a) Fusi, A.; Ugo, R.; Fox, F.; Pasini, A.; Cenini, S. *J. Organometal. Chem.*, **1970**, *26*, 412. (b) Booth, B.L.; Haszeldine, R. N.; Neuss, G. R. H. *J. Chem. Soc. Chem. Commun.*, **1972**, 1074.

11. Shilov, A. E. *Activation of Saturated Hydrocarbons by Transition Metal Complexes*, D. Reidel Publishing Co., Boston, 1984.

12. Austin, G. T. *Shreve's Chemical Process Indusries*, McGraw Hill Book Co., New York, 1975.

13. (a) Kochi, J. K. *Accts. Chem. Rsch.*, **1974**, *7*, 351. (b) Kochi, J. K. *Science*, **1967**, *155*, 415.

14. (a) Drago, R. S. *Coord. Chem. Rev.* **1992**, *117*, 185. (b) Drago, R. S.; Beer, R. H. *Inorg. Chim. Acta* **1992**, *198*, 359.

15. (a) Bailey, C. L.; Drago, R. S. *Coord. Chem. Rev.* **1987**, *87*, 321 refs. therein. (b) Nishinaga, A. *Chem. Lett.* **1975**, *18*, 1408.

16. (a) Balch, A. L.; Chan, R. S.; Cheng, G. N.; LaMar, B.; Latos, L. *J. Am. Chem. Soc.* **1984**, *106*, 7779. (b) Groves, T. J.; Quinn, R. *J. Am. Chem. Soc.* **1985**, *107*, 5790. (c) Fenton,H. J. H. *J. Am. Chem. Soc.* **1984**, *65*, 899.

17. (a) Sheldon, R. A.; Patai, S. (ed.) *The Chemistry of Functional Groups, Peroxides*, Wiley, New York, **1983**. (b) Parshall, G. W. *Homogeneous Catalysis*, Wiley, New York, **1980**. (c) Sheldon, R. A. *Recuil*, **1973**, *92*, 253. (d) Chong, A. O.; Sharpless, K. B. *J. Org. Chem.* **1977**, *42*, 1587.

18. (a) Bäckvall, J. E.; Akermark, B.; Ljunggren, S. S. *J. Am. Chem. Soc.* **1979**, *101*, 2411 (b) Bäckvall, J. E.; Hopkins, R. B.; Grennberg, H.; Mader, M. M.; Awasthi, A. K. *J. Am. Chem. Soc.*, **1990**, *112*, 5160.

19. (a) Hunter, N. R.; Gesser, H. D.; Morton. L. A. Yarlogadda, P. S. *Appl. Catal.* **1990**, *45*, 57. (b) Gesser, H. D.; Hunter, N. R.; Prakash, C. B. *Chem. Rev.* **1985**, *85*, 235. (c) Wolf, E. E. (ed) *Methane Conversion by Oxidative Processes* Van Nostrand Reinhold, New York, **1991**.

20. (a) Hogan, T.; Sen, A. *J. Am. Chem. Soc.* **1997**, *119*, 2624. (b) Lin, M.; Hogan, T.; Sen, A *J. Am. Chem. Soc.* **1997**, *119*, 6048. (c) Basickes, N.; Hogan, T.; Sen, A. *J. Am. Chem. Soc.* **1996**, *118*, 13111. (d)Lin. M.; Hogan, T.; Sen, A. *J. Am. Chem. Soc.* **1996**, *118*, 4574. (e) Sen, A.; Benvenuto, M. A.; Lin. M.; Hutson, A. C.; Basickes, N. *J. Am. Chem. Soc.* **1994**, *116*, 998. (f)Periana, R. A.; Taube, D. J.; Evitt, E. R.; Löffler, D. G.; Wentrcek, P. R.; Voss, G.; Masuda, T. *Science* **1993**, *259*, 340. (g) Periana, R. A.; Taube, D. J.; Gamble, S.; Taube, H.; Satoh, T.; Fujii, H. *Science* **1998**, *280*, 560.

22. Einchem Anic Spa, European Patent, EPA 100, 119, **1984**.

23. (a) Bailey, C. L.; Drago, R. S. *J. Chem. Soc. Chem. Commun.* **1987**, 179.
(b) Hamilton, D. E.; Drago, R. S.; Zombeck, A. *J. Am. Chem. Soc.* **1987**, *109*, 374.
(c) Drago, R. S.; Zuzich, A.; Nyberg, E. D. *J. Am. Chem. Soc.* **1985**, *107*, 2898. (d) Corden, B. B.; Drago, R. S.; Perito, R. P. *J. Am. Chem. Soc.* **1985**, *107*, 2903. (e) Nyberg, E. D.; Pibrich, D. C.; Drago, R. S. *J. Am. Chem. Soc.*, **1983**, *105*, 3538. (f) Beer, R. H.; Jiminez, J.; Drago, R. S. *J. Org. Chem.* **1993**, *58*, 1746.

24. (a) Che, C.; Lau, C.; Lau, T.; Poon, C. *J. Am. Chem. Soc.* **1990,** *112*, 5176. (b) Dobson, J. C.; Meyer, T. J. *Inorg. Chem.* **1988**, *27*, 3283.(c) Moyer, B. A.; Meyer, T. J. *Inorg. Chem.* **1981**, *20*, 436. (d) Dobson, J. C.; Meyer, T. J. *Inorg. Chem.* **1989**, *28*, 2018. (e) Ellis, C. D.; Gilbert, J. A.; Murphy, W. R.; Meyer, T. J. *J. Am. Chem. Soc.* **1983**, *105*, 4842. (f) Che, C.; Yam, V. W. *J. Am. Chem. Soc.* **1987**, *109*, 1262.

25. (a) Riley, D. P. *J. Chem. Soc. Chem. Commun.*, **1983**, 1530. (b) Riley, D. P.; Correa, P. E. *J. Org. Chem.* **1985**, *50*, 1564. (c) Riley, D. P.; Shumate, R. E. *J. Am. Chem. Soc.* **1984**, *106*, 3179. (d) Riley, D. P. *Inorg. Chim. Acta* **1985**, *99*, 5. (e) Cheng, W.; Fung, W.; Che, C. *J. Mol. Cat. A: Chem.* **1991**, *113*, 311. (f) Che, C.; Li, C.; Tang, W.; Yu, W. *J. Chem. Soc. Dalton Trans.* **1992**, 3153. (g) Dobson, J. C.; Seok, W. K.; Meyer, T. J. *Inorg. Chem.* **1986**, *25*, 1514. (h) Thompson, M. S.; Meyer, T. J. *J. Am . Chem. Soc.* **1982**, *104*, 5070. (i) Moyer, B. A.; Meyer, T. J. *Inorg. Chem.* **1981**, *20*, 436. (j) Lever, A. B. P. *Inorg. Chem.* **1990**, *29*, 1271.(k) Machii, K.; Watanabe, Y.; Morishima, I. *J. Am. Chem. Soc.* **1995**, *117*, 6691. (l) Bravo, A.; Bjorsvik, H.; Fontana, F.; Minisci, F.; Serri, A. *J. Org. Chem.* **1996**, *61*, 9409. (m) Muller, J. G.; Acquaye, J. H.; Takeuchi, K. J. *Inorg. Chem.* **1992**, *31*, 4552.

26. (a) Cundari, T. R.; Drago, R. S. *Inorg. Chem.* **1990**, *29*, 3904. (b) *Inorg. Chem.* **1990**, *29*, 2303. (c) König, E.; Ritter, G.; Madeja, K. *J. Inorg. Nucl. Chem.* **1981**, *43*, 2273.

27 Collin, J. P.; Sauvage, J. P. *Inorg. Chem.* **1986**, *25*, 135.

28. Goldstein, A. S.; Drago, R. S. *J. Chem. Soc. Chem. Commun.* **1991**, 21.

29. Robbins, M. H.; Drago, R. S. *J. Chem. Soc. Dalton Trans.* **1996**, 105.

30. Skoog, D. A.; West, D. M.; Holler, F. J. *Fundamentals of Analytical Chemistry*, Harcourt Brace College Publisher, New York, 1993.

31. (a) Liu, K. E.; Johnson, C. C.; Newcomb, M.; Lippard, S. J. *J. Am. Chem. Soc.* **1993**, *115*, 939. (b) Battioni, P.; Renaud, J. P.; Bartoli, J. F.; Reina-Artiles, M.; Fort, M.; Mansuy, D. *J. Am. Chem. Soc.* **1988**, *110*, 8462. (c) Groves, J. T.; Nemo, T. E.; Myers, R. S. *J. Am. Chem. Soc.* **1979**, *101*, 1032. (d) Priestly, N. D.; Floss, H. G.; Froland, W. A.; Lipscomb, J. D.; Williams, P. G.; Morimoto, H. *J. Am. Chem. Soc.* **1992**, *114*, 7561. (e) Bowry, V. W.; Ingold, K. U. *J. Am. Chem. Soc.* **1991**, *113*, 5699.

32. Goldstein, A. S.; Beer, R. H.; Drago, R. S. *J. Am. Chem. Soc.* **1994**, *116*, 2424.

33. Gonzalez, M. A. *Ph.D. Dissertation*, University of Florida **1997**.

34. Shilov, A. E.; Shul'pin, G. B. *Chem. Rev.* **1997**, *97*, 2879.

35. Labinger, J. A. *Fuel Process. Technol.* **1995**, *42*, 325.

36. Olah, G. A.; Molnár, A. *Hydrocarbon Chemistry*, Wiley, New York, 1995.

37. Nizova, G. V.; Süss-Fink, G.; Shul'pin, G. B. *Chem. Commun.* **1997**, 397.

38. *Organic Peroxides*, Ando, W. (Ed.) Wiley-Interscience New York, 1992.

39. Swern, D. in *Organic Peroxides*, Wiley-Interscience: New York, 1971.

40. Hawkins, E. G. E. in *Organic Peroxides,* D. Van Nostrand Company Inc.: New Jersey, 1961.

41. Gordon, B. W. F.; Webster, E.; Drago, R. S.; *J. Catal. In review.*

42. Schneider, H. J.; Muller, W. *J. Org. Chem.* **1985**, *50*, 4609.

43. Grinstaff, M. W.; Hill, M. G.; Labinger, J. A.; Gray, H. B. *Science* **1994**, *264*, 1311.

44. Almateus, A. *unpublished results.*

45. Goldstein, A. S.; Drago R. S. *J. Chem. Soc. Chem. Commun.* **1994**, 116.

46. Courthey, J. L.; Swanborough, K. F. *Rev. Pure Appl. Chem.* **1987**, *47*, 22.

47. Lee, D. G.; Van den Engh, M. *Org. Chem.* **1973**, *58*, 177.

48. Ahn, K. H.; Groves, J. T. *Inorg. Chem.* **1987**, *26*, 3833.

49. Mayo, F. R. *Accts. Chem. Rsch.* **1968**, *1*, 1968.

50. Wang, K.; Meyer, J. M. *J. Am. Chem. Soc.* **1997**, *119*, 1470.

51. Che, C.; Tang, W-T.; Lee, W; Wong, K; Lau, T. *J. Chem. Soc. Dalt. Trans.* **1992**, 1551.

52. Roeker, L.; Meyer, T. J. *J. Am. Chem. Soc.* **1987**, *109*, 746.

53. Frank, K; *unpublished results.*

54. Gutsche C. D., *Calixarenes*, Royal Society of Chemistry, Cambridge, England, 1989.

55. Vicens, J. and Böhmer V., *Calixarenes: A Versatile Class of Macrocyclic Compounds*, Kluwer Academic, Boston, 1991.

56. Böhmer, V. *Angew. Chem., Int. Ed. Engl.*, **1995**, *34*, 713.

57. (a) Wieser, C.; Dieleman, C. B.; Matt, D. *Coord. Chem. Rev.*, **1997**, *165*, 93. (b) Roundhill, D. M. *Prog. Inorg. Chem.,* **1995**, *43*, 533.

58. Castellano, B.; Solari, E.; Floriani, C.; Chiesi-Villa, A.; Rizzoli, C. *Chem. Eur. J.*, **1999**, *5*, 722.

59. Floriani, C. *Chem. Eur. J.*, **1999**, *5*, 19.

60. Giannini, L.; Dovesi, S.; Solari, E.; Floriani, C.; Chiesi-Villa, A., and Rizzoli, C. *Angew. Chem., Int. Ed. Engl.*, **1999**, *39*, 807.

61. (a) Castellano, B.; Solari, E.; Floriani, N. Re, Chiesi-Villa, A. and Rizzoli, C. *Organometallics*, **1998**, *17*, 2328. (b) Castellano, B.; Zanotti-Gerosa, A.; Solari, E.; Floriani, C. *Organometallics*, **1996**, *15*, 4894. (c) Zanotti-Gerosa, A, Solari, E.; Giannini, L.; Floriani, C.; Chiesi-Villa, A.; Rizzoli, C. *J. Am. Chem. Soc.*, **1998**, *120*, 437.

62. Zanotti-Gerosa, A.; Solari, E; Giannini, L; C. Floriani, N. Re, Chiesi-Villa, A.; Rizzoli, C. *Inorg. Chim. Acta.*, **1998**, *270*, 298.

63. Koebner, M. *Z. Angew. Chem.*, **1933**, *46*, 251.

64. Gordon, B. W. F. and Scott, M. J. *accepted Inorg. Chim. Acta.*.

65. Dubberley, S. R.; Blake, A. J.; Mountford, P. *Chem. Commun.* **1997** 1603.

66. Davidson, M. G.; Howard, J. A. K.; Lamb, S.; Lehmann, C. W. *Chem. Commun.* **1997** 1607.

67. Bock, H.; John, A.; Näther, C.; Havlas, Z. *J. Am. Chem. Soc.*, **1995**, *117*, 9367.

68. Vilardo, J. S.; Fanwick, P. E.; Rothwell, I. P. *Polyhedron*, **1998**, *17*, 769 and references therein.

69. Czado, W.; Muller, U. *Z. Krist. New. Cryst. St.*, **1999**, *214*, 63.

70. Kunert, M.; Dinjus, E.; Nauck, M.; Sieler, J. *Chem. Ber. Recl.*, **1997**, *130,* 1461.

71. Matilainen, L.; Leskela, M.; Klinga, M. *J. Chem. Soc., Chem. Comm.* **1995** 421.

72. Gatto, V. J. Patent 5,068,388, Ethyl Corporation, US, **1990**.

73. Sapse, A. M.; Schleyer, P. R. *Lithium Chemistry*, Wiley, New York, 1995.

74. Schade, C.; Schleyer, P. R. *Adv. Organomet. Chem.*, **1987**, *27*, 169.

75. Clark, J. R.; Fanwick, P. E.; Rothwell, I. P. *J. Chem. Soc. Chem. Commun.*, **1995**, 553.

76. Lockwood, M. A.; Clark, J. R.; Parkin, B. C.; Rothwell, I. P. *Chem Commun.*, **1996**, 1973.

77. Chisholm, M. H.; Rothwell, I. P. *Polyhedron*, **1995**, *14*, 3175.

78. (a) Chamberlain, L. R.; Rothwell, I. P. *J. Chem. Soc. Dalt. Trans.,* **1987**, 155. (b) Yu, J. S.; Potyen, M. C.; Clark, J. R.; Visciglio, V. M.; Fanwick, P. E.; Rothwell, I. P. *Organometallics*, **1996**, *15*, 4443 references therein. (c) Chamberlain, L. R.; Rothwell, I. P.; Huffman, J. C. *J. Am. Chem. Soc.* **1986**, *108*, 1502.

79. Schrock, R. R.; Messerle, L. W.; Wood. C. D.; Guggenberger, L. J. *J. Am. Chem. Soc.*, **1978**, *100*, 3793.

80. Clark, J. R.; Pulvirenti, A. L.; Fanwick, P. E.; Sigalas, M.; Eisenstein, O.; Rothwell, I. P. *Inorg. Chem.*, **1997**, *36*, 3623.

80. Gordon, B. W. F.; Scott, M. J. *Inorg. Chim. Acta, accepted.*

81. Fowles, G. W.; Rice, D. A.; Wilkins, J. D. and references therein, *J. Chem. Soc. Dalton. Trans.*, **1973**, 961.

82. Schrock, R. R. *J. Organometall. Chem.*, **1976**, *122*, 209.

83. Allen, K. D.; Bruck, M. A.; Gray, S. D.; Kingsborough, R. P.; Smith, D. P.; Weller, K. J.; Wigley, D. E., *Polyhedron*, **1995**, *14*, 3315.

BIOGRAPHICAL SKETCH

Benjamin Willis Franklin Gordon was born on October 25 1971 in Flagstaff, Arizona to Frank and Suzanne Gordon and is the last son in a family of five siblings. Benjamin's parents live in Camp Verde, Arizona in a house built by Frank and Suzanne where they tend daily to their paradise in the valley. After graduating from Coconino High School, Benjamin attended Northern Arizona University where he helped finance his schooling by becoming a Jack of All Trades. As an apprenticed mason, he worked on countless projects ranging from constructing house foundations to installing ceramic tile. After two years, he quit his job as a mason and worked for his father building houses as part of a two-man crew. Ben felt that the period spent building houses from foundation to finish was one of the most influential and interesting times in his life. He had an insatiable appetite for every aspect of construction and feels that he will someday pick up a hammer and trowel again.

Ben graduated from college in 1995 with a B.S. degree in chemistry after switching wildly between majors. He intended to receive a degree in computer science but was eventually sidetracked by the creative aspects of chemistry. He then went on to attend the University of Florida to receive his Ph.D. degree in chemistry. While under the supervision of Dr. Russell S. Drago, Ben applied aspects of homogeneous oxidation chemistry to a variety of systems and, after Dr. Drago's untimely death, finished his studies under the supervision of Dr. Michael J. Scott by synthesizing and characterizing several metal complexes of aryloxide ligands.

To date, Ben's future plans are a mystery. His enigmatic pursuit of different challenges has spurred him on possibly to pursue a career in information technology. He has also entertained the idea of pursuing a career as a professional wrestler. When asked recently what option he was favoring, he replied "I'm thinking about taking a cup of soda upside my head."

I certify that I have read this study and that in my opinion it conforms to acceptable standards of scholarly presentation and is fully adequate, in scope and quality, as a dissertation for the degree of Doctor of Philosophy.

Michael J. Scott, Chairman
Assistant Professor of Chemistry

I certify that I have read this study and that in my opinion it conforms to acceptable standards of scholarly presentation and is fully adequate, in scope and quality, as a dissertation for the degree of Doctor of Philosophy.

David E. Richardson
Professor of Chemistry

I certify that I have read this study and that in my opinion it conforms to acceptable standards of scholarly presentation and is fully adequate, in scope and quality, as a dissertation for the degree of Doctor of Philosophy.

Daniel R. Talham
Associate Professor of Chemistry

I certify that I have read this study and that in my opinion it conforms to acceptable standards of scholarly presentation and is fully adequate, in scope and quality, as a dissertation for the degree of Doctor of Philosophy.

William Weltner Jr
Professor of Chemistry

I certify that I have read this study and that in my opinion it conforms to acceptable standards of scholarly presentation and is fully adequate, in scope and quality, as a dissertation for the degree of Doctor of Philosophy.

Jonathan Bowman Martin
Assistant Professor of Geology

This dissertation was submitted to the Graduate Faculty of the Department of Chemistry in the College of Liberal Arts and Sciences and to the Graduate School and was accepted as partial fulfillment of the requirements for the degree of Doctor of Philosophy.

August 1999

Dean, Graduate School